UNIVERSITÀ DEGLI STUDI DI MILANO
FACOLTÀ DI SCIENZE E TECNOLOGIE

Department of Chemistry

Doctorate course in Chemistry - XXX Cycle

Drug-conjugates for Self-assembled Nanoparticles in Anticancer Treatment

Ph. D. Thesis of
Gaia FUMAGALLI
R10926

Tutor: Prof. Daniele Passarella

Academic Year: 2016/2017

Alla mia famiglia

Replace fear of the unknown
with curiosity

Table of contents

Abstract 11

1. Nanotechnology and cancer 13
  1.1 Nanomedicine 15
    Limitation of traditional chemotherapy 15
    Nanotechnology in drug delivery 16
  1.2 Nanoparticles 20
  1.3 Self-assembled Nanoparticles 23
  1.4 Nanoparticles characterization 24
    Particle size 24
    Surface charge 25
  1.5 Nanoparticles Preparation 26

2. Squalene-based Nanoparticles 29
  2.1 Disulphide containing linker 31
  2.2 Fluorescent hetero-nanoparticles 33
    Paclitaxel 34
    Synthesis of the conjugates 36
    Nanoparticles preparation 38
    Nanoparticles characterization 39
    Fluorescence emission 40
    In vitro evaluation: cell internalization 44
    In vitro evaluation: cytotoxic activity 45
  2.3 Cyclopamine-Paclitaxel hetero-nanoparticles 48
    Stem cells and cancer 48
    CSCs as targets in cancer treatment 49
    Hedgehog Signalling Pathway 49
    Cyclopamine 52
  2.3.1 Cyclopamine nanoparticles 54
    Synthesis of the conjugates 54
    Nanoparticles characterization 55

    In vitro evaluation....................56
  2.3.2 Cyclopamine-Paclitaxel hetero-nanoparticles....................58
    Nanoparticles Characterization....................58
    In vitro evaluation....................60
  2.3.3 Cyclopamine-Paclitaxel-Tetramethylrhodamine hetero-nanoparticles....................62
    Synthesis of the conjugate....................62
    Nanoparticles characterization....................63
    In vitro evaluation....................63
  2.4 Cyclopamine-Doxorubicin hetero-nanoparticles....................66
    Doxorubicin....................66
    Nanoparticles characterization....................67
    In vitro evaluation....................69
    In vitro evaluation: cell internalization....................69
    In vitro evaluation: cellular system with an activated Hedgehog pathway....................70
    In vivo evaluation....................74
Experimental Procedures....................77
3. 4-(1,2-diphenylbut-1-en-1-yl) aniline based nanoparticles....................97
    Aloin....................100
    Podophyllotoxin....................101
    Synthesis of the conjugates....................102
    Nanoparticles characterization....................105
    In vitro evaluation....................107
Experimental Procedures....................109
4. Design and Synthesis of a new Self-immolative Linker....................121
    Self-immolative linkers....................123
    Colchicine....................127
    Synthesis of the conjugates....................132
    Lipase-induced drug release....................136
    Nanoparticles characterization....................137
Experimental Procedures....................139
5. Dual-drug conjugates....................163

Epothilone A 165

Camptothecin 167

Synthesis of the conjugates 169

Nanoparticles characterization 171

Experimental Procedures 173

6. Conclusions 181

Acknowledgements 185

Bibliography 187

Abstract

This dissertation is an overview on the functionalization of known anticancer compounds in order to form different drug-conjugates able to self-assemble in water to form nanoparticles. This approach is useful to improve the drug delivery properties and pharmacokinetic profile of anticancer drugs.

All the described conjugates, except for the ones illustrated in chapter 5, have the same general structure: the anticancer drug is connected to the self-assembly inducer trough a linker (**Figure 1**).

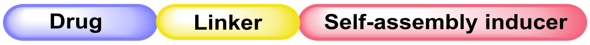

Figure 1. General structure of the conjugates.

Chapter 1 regards a general introduction about nanomedicine, the advantages of the use of nanotechnology-based systems in cancer treatment and the benefits of nano-formulated drugs in the improvement of drug-delivery. Furthermore, nanoparticles are presented with a focus on their classification, characterization and preparation techniques.

Chapter 2 regards the preparation of different types of self-assembled nanoparticles using various anticancer compounds and dyes but with the same lipophilic tail as self-assembling inducer: squalene. Different natural anticancer compounds such as paclitaxel, cyclopamine and doxorubicin and dyes, as fluorescein and tetramethylrhodamine, were functionalized to obtain squalene-based conjugates. Both hetero-nanoparticles composed by two drug-conjugates and drug- and dye-conjugates were prepared and tested.

Chapter 3 is focused on the importance of the self-assembly inducer and describes the preparation of new conjugates containing an active moiety as self-assembly inducer. In particular, in this section, is described the preparation of conjugates composed by aloin or podophyllotoxin as active compounds and 4-(1,2-diphenylbut-1-en-1-yl) aniline, an analog of the know anticancer compound tamoxifen, as self-assembly inducer.

Chapter 4 highlights the influence of the linker between the active compound and the self-assembly inducer to obtain an effective release of the free drug. In particular, it is described the synthesis of a new self-immolative linker able to trigger the drug release in particular conditions, specifically in the presence of a lipase. This linker was used for the preparation of two conjugates containing the known anticancer compound N-desacetylthiocolchicine.

Chapter 5 concerns the preparation of dual drug-conjugates able to form nanoparticles without the presence of a self-assembly inducer. These conjugates have a symmetrical structure: two molecules of the same drug are linked by a chain able to guarantee the drug release in particular conditions (**Figure 2**). The natural anticancer compounds involved in the preparation of this type of conjugates are paclitaxel, epothilone A, podophyllotoxin and camptothecin and the linker used contain a disulfide moiety able to be cleaved in cellular environment.

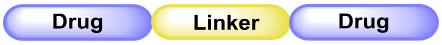

Figure 2. General structure of the conjugates.

1. Nanotechnology and cancer

1.1 Nanomedicine

In the last decades, nanotechnology systems have been extensively studied and remarkable progresses have been made in the field of imaging and cancer therapy.[1] Currently the most advanced area of nanomedicine is the development of nanoparticles for drug delivery because nanotechnology-based systems offer the possibility to improve a personalized treatment of disease.[2]

Nanomedicine are defined as systems that incorporate nanoparticles (1-100 nm) containing adsorbed, encapsulated, dispersed, or conjugated drugs or imaging agents.

The numerous benefits to overcome the limitations of conventional formulations and the promising progresses both in cancer diagnosis and treatment make nanomedicine being enthusiastically evaluated and deeply studied. Indeed, Food and Drug Administration (FDA) have recently approved many nanodrug products and they are now on the market (**Table 1**).

Limitation of traditional chemotherapy

Many anticancer drugs commonly used in clinical practice often show, in addition to a high cytotoxic activity, some toxic side effects. These side effects sometimes force treatment delay and dose reduction. Furthermore, traditional chemotherapeutic agents remain in the circulation for short periods making the therapy ineffective. The therapeutic window of drugs can be limited by the lack of selectivity against cancer cells and their ability to reach the site of action is partially compromised by a poor solubility that make them unable to penetrate biological barriers.[3] In addition, metabolization and degradation phenomena contribute to decrease the drug concentration at the biological target.[4] Drug accumulation inside the tumor is also prevented by the action of P-glycoprotein, a multidrug resistance protein overexpressed on the membrane of cancer cells, which act as efflux pump.[5]

Drug delivery systems	**Stage of development**	**Examples of application**	**References**
Liposomes	Marketed	Amphotericin B	[6]
		Daunorubicin	[7]
		Doxorubicin	[8]
Micelles			
Phospholipid	Preclinical	Paclitaxel	[9]
		Camptothecin	[10]
		Diazepam	[11]
Pluronic®	Clinical	Doxorubicin	[12]
	Preclinical	Paclitaxel	[13]
		Tamoxifen	[14]
		Etoposide	[15]
Poly (L-aminoacid)	Clinical	Doxorubicin	[16,17]
	In vitro	Antisense oligonucleotides	[18]
Polyester	Preclinical	Paclitaxel	[19]
		Doxorubicin	[20,21]
Nanoemulsions	Preclinical	Amphotericin B	[22]
		Paclitaxel	[23]
		Dexamethasone	[24]
		Benzathine penicillin G	[25]
Nanoparticulate systems			
Drug nanocrystals	Preclinical	Amphotericin B	[26]
		Etoposide, camptothecin, paclitaxel	[27]
Polymer-based nanoparticles	Preclinical	Tamoxifen	[28]
		Cyclosporin-A	[29]
		Theophylline	[30]
Lipid-based nanoparticles	Preclinical	Doxoribicin	[31]
		Camptothecin	[32]
Albumin nanoparticles	Marketed	Paclitaxel	[33]
	In vitro	DNA and antisense oligonucleotides	[34,35]
Nanogels	Preclinical	Oligonucleotides	[36]
Dendrimers	Preclinical	Indometacin	[37]
	In vitro	5-fluorouracil	[38]
		Antisense oligonucleotides	[39]

Table 1. Nanoscale systems for drug delivery.

Nanotechnology in drug delivery

The use of nanocarriers as drug delivery system for anticancer drugs can improve their overall pharmacological properties: increasing in biodistribution and pharmacokinetic will result in improved efficacy of the drug.[40,41] Nanobased systems have been also shown to improve the stability of a wide range of anticancer compounds as oligonucleotides, peptides or small molecules. Nanocarriers are often developed exploiting safe and biocompatible materials in order to replace existing vehicles that may cause side effects.[42] Furthermore, side effects are reduced as a consequence of preferential accumulation at tumor sites that have permeable vasculature. The dose required for efficacy is then reduced thanks to selective targeting and decreased clearance.[43,44] In addition, nanoformulated drugs can increase water solubility of hydrophobic chemotherapeutic agents allowing an efficient membrane permeation.[45] The main advantages of nanocarrier formulation in medicine are reported in **Figure 3**.

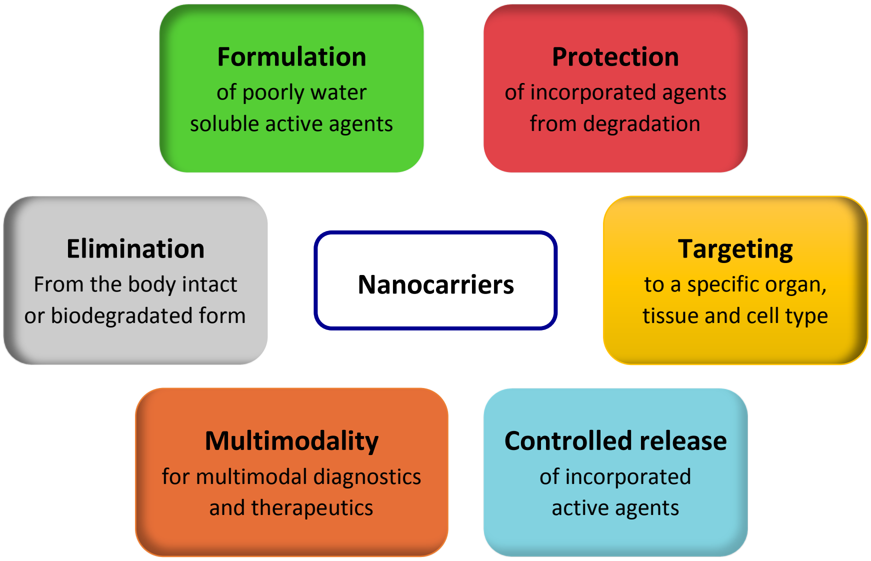
Formulation
of poorly water soluble active agents
Protection
of incorporated agents from degradation
Elimination
From the body intact or biodegradated form
Nanocarriers
Targeting
to a specific organ, tissue and cell type
Multimodality
for multimodal diagnostics and therapeutics
Controlled release
of incorporated active agents

Figure 3. Advantages of nanocarrier formulation in medicine.

Tumor targeting

One of the main advantages of nanotechnology for cancer treatment is tumor targeting. The ability of nanomedicine to selectively target cancer cells and to differentiate tumor and healthy tissues is due to two fundamental processes: passive and active targeting.

Passive targeting exploits the enhanced permeability and retention (EPR) effect[46,47] to reach a higher concentration of nanoparticles in the tumor, while active targeting takes advantage of selective molecular recognition of antigens, usually proteins, which are often overexpressed on cancer cells surface in order to selectively target tumor.[48]

These two different processes of tumor cell targeting can be applied both independently or combined to get an increased outcome.[49]

Passive targeting

Passive targeting occurs due to nanoparticles extravasation in tumor tissue where the microvasculature is leaky. This feature of tumor vasculature is due to increased angiogenesis of the tumor and to the fact that cancer cells are not responsive to signaling for orderly vasculogenesis.[50]

Most of solid tumors shows a vascular pore cutoff size of 100-780 nm,[51,52] while healthy tissue vasculature is impermeable to carriers larger than 2-4 nm.[53] Therefore, nanoparticles are able to increase drug concentration in target sites, by extravasation, and to significantly reduce drug accumulation and toxicity to healthy tissues. Moreover, nanoparticles circulating time in tumor tissue is longer respect to normal tissue because of reduced lymphatic clearance.[54]

Active targeting

In case of active targeting, nanodrugs are designed in order to preferentially interact with cancer cells. Indeed, tumor tissues have some unique features that discriminate them from normal cells. In particular, some receptors are overexpressed on the surface of cancerous cells and they can be used as targets.

Active targeting is based on molecular recognition. Nanoparticles are functionalized with targeting agents and interact with tumor cells either by ligand-receptor interaction or antibody-antigen recognition.[55,56,57] After recognition, nanoparticles are internalized in the cells, by receptor-mediated endocytosis or phagocytosis, allowing the drug to show its biological activity.[58]

A wide variety of receptors, such as folate ligand,[59,60] transferrin,[61,62] death receptor (DR) complexes,[63] epidermal growth factor receptor (EGFR),[64] as well as tumor-specific antigens have been exploited to selectively target tumor tissues.

Besides, nanoparticles have been functionalized with small molecules, monoclonal antibodies[65] and nucleic acid aptamers[66] to achieve active targeting by molecular recognition. Ligands can be attached to nanoparticles by covalent or non-covalent coupling. Non-covalent binding by physical association of targeting ligands to the nanocarrier has the advantage of eliminating the use of hard reaction conditions. However, there are potential problems, such as low and weak binding and poor control of the reactions.

1.2 Nanoparticles

Following the IUPAC definition, we can define a nanoparticle as:

"a particle of any shape with dimensions in the $1x10^{-9}$ and $1x10^{-7}$ m range. [...] Note 2: The basis of the 100- nm limit is the fact that novel properties that differentiate particles from the bulk material typically develop at a critical length scale of under 100 nm.
Note 3: Because other phenomena (transparency or turbidity, ultrafiltration, stable dispersion, etc.) that extend the upper limit are occasionally considered, the use of the prefix nano is accepted for dimensions smaller than 500 nm.[67]

Several types of nanoparticles are currently used for biological application and biomedical research (**Figure 4**).[68]

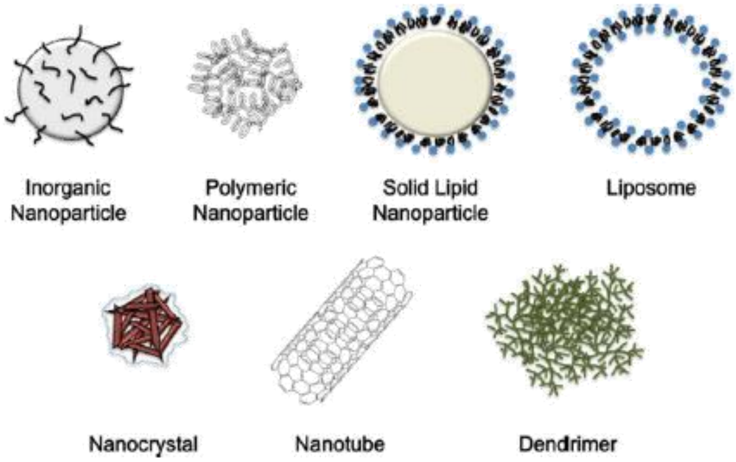

Figure 4. Different types of nanoparticles.

- **Inorganic nanoparticles:** they are typically composed by inorganic material such as alumina, silica, metals, metal oxides and sulfides and they vary in size, shape and porosity. Porous inorganic nanoparticles provide a physical encasement to protect the molecular payload from degradation. They can also be engineered to evade the reticuloendothelial system by varying size and surface composition.

Many inorganic nanoparticles are currently used for biological applications: semiconductor quantum dots are commercially available as a viable alternative to fluorescently labelled particles while iron oxide nanoparticles have been approved for human use in magnetic resonance imaging applications as contrast enhancers.[69]

- **Polymeric nanoparticles:** they are composed by polymers such as poly(ethylene glycol) (PEG), polylactic acid, polyglycolic acid, poly(methylmethacrilate), poly (butyl)cyano acrilate, polylactide (PLA) and poly(-lactide-co-glycolide) (PLGA). They are usually biodegradable and biocompatible and they offer a good potential for surface modification via chemical transformations. Polymerica nanoparticles are suitable for delivery of a wide range of therapeutic agents. The US FDA has approved biodegradable polymeric nanoparticles, such as PLA and PLGA, for human use.

- **Solid lipid nanoparticles:** they are lipid-based colloidal systems characterized by a relatively rigid core consisting of hydrophobic lipids that are solid at room and body temperatures, surrounded by a monolayer of phospholipids. They are less toxic than polymeric or inorganic nanoparticles because of their ease of biodegradation.

- **Liposomes:** they are concentric bilayered vesicles with an aqueous nucleus surrounded by a phospholipid membrane. Their amphiphilic nature, ease of surface modification, and good biocompatibility make them a good solution to increase the circulating half-life of proteins and peptides. Liposomes can adhere to cellular membranes to deliver a drug payload or transfer it by endocytosis.

- **Nanocrystals:** they are aggregates of molecules that can be combined into a crystalline form of the drug surrounded by a thin coating of surfactant. The hydrophilic layer aids in the biological distribution and bioavailability, and prevents aggregation of the crystalline drug material. These factors combine to increase the efficiency of overall drug delivery. Drawbacks are the requirement to crystalize the drug and the limited stability of nanocrystals.

- **Nanotubes:** they are self-assembling sheets of atoms arranged in tubes and characterized by a large internal volume. The external surface can be easily functionalized. While they are potentially promising for pharmaceutical applications, human tolerance of these compounds remains unknown.

- **Dendrimers:** they are polymer-based macromolecules formed from monomeric or oligomeric units, such that each layer of branching units doubles or triples the number of peripheral groups. The void area within a dendrimer, the extent of its branching, its ease of modification and preparation, and size control offer great potential for drug delivery. For example, water-soluble dendrimers may be designed with internal hydrophobicity, suitable for the incorporation of a hydrophobic drug. However, dendrimers require further improvement in cytotoxicity profiles, biocompatibility, and biodistribution.

1.3 Self-assembled Nanoparticles

A small but interesting niche inside anticancer nanotechnology is represented by nanosystems spontaneously obtained by self-assembly of conjugates composed of drugs linked to a proper chemical entity.[70] The self-assembly of drug conjugates into NPs is a process that involves the formation of an ordered structure by spontaneous organization of building blocks as a consequence of specific local interactions. Assembly can be obtained with different methods and conditions but the key role of the amphilicity of the components is often fundamental. In recent years, the use of drug conjugates to obtain NPs has gained considerable attention.[71,72,73] These conjugates are usually obtained by a covalent coupling of the drug to biocompatible lipid moieties and the resulting molecules are able to form NPs by self-assembly. Self-assembly is a process that is mediated by noncovalent interactions between molecules via ionic bonds, H-bonding, hydrophobic interactions and van der Waals interactions. Different organic molecules, such as biocompatible polymeric chains or endogenous molecules (terpenes or polysaccharides), have been used as self-assembly inducers by covalent linkage to drugs. The drug and the self-assembly inducer can be directly attached or can be connected by a linker, which can be stable in serum but able to release the drug intracellularly.

1.4 Nanoparticles characterization

Nanoparticles characterization is based on three main parameters: size, morphology and surface charge. These properties affect the physical stability and the *in vivo* distribution of the nanoparticles.

Particle size

The size of nanoparticles, including mean diameter and size distribution, influences their physical properties as well as biodistribution and retention in the body. It can be determined with different techniques.

- **Dinamic Light Scattering (DLS):** it is used to determine the size of Brownian nanoparticles in colloidal suspensions in the nano and submicron ranges. In this technique, a solution of spherical particles in Brownian motion causes a Doppler shift when exposed against shining monochromatic light (laser). This monochromatic light exposure hits the moving particle and it results in changing the wavelength of the incoming light. The extent of this change in wavelength determines the size of the particle.[74]

- **Scanning Electron Microscopy (SEM):** it determines the size, shape and surface morphology with direct visualization of the nanoparticles. The sample is analysed by scanning with a focused beam of electrons and secondary electrons emitted from the sample surface determine the surface characteristic of the sample. Average mean size evaluated by SEM is comparable with results obtained by DLS.[75]

- **Transmission Electron Microscopy (TEM):** it can provide imaging, diffraction and spectroscopic information of the nanoparticle. The surface characteristic of the sample are obtained by scanning the sample with a beam of electrons and analysing the transmitted beam.[75]

- **Atomic Force Microscopy (AFM):** it is based on a physical scanning of samples at sub-micron level using a probe tip of atomic scale. This technique offers a ultra-high resolution in particle size measurement, with reported resolution on the order of fractions of a nanometre.[76]

Surface charge

Surface charge determines the interaction of nanoparticles with each others, with the biological environment as well as their electrostatic interaction with bioactive compounds. The stability of colloidal systems is usually analysed through the zeta potential of nanoparticles. Zeta potential is an indirect measure of the surface charge and it can be evaluated by analysing the potential difference between the outer Helmholtz plane and the surface of shear. High zeta potential (either positive or negative) are advantageous to ensure stability and avoid aggregation of the particles during storage.[77]

1.5 Nanoparticles Preparation

A number of approaches have evolved for the preparation of nanoparticles, mainly relying on the composition, size, and shape of the nanoparticles to be prepared. Some common methods are discussed in detail below.

- **Solvent Evaporation Method:** this method involves two steps. The first is the dissolution of the polymer/drug mixture in an organic solvent (as dichloromethane, chloroform or ethyl acetate) and the emulsification of the solution into an aqueous phase containing surfactant or emulsifying agents. The second step is the evaporation of the organic layer either by continuous stirring or by reducing the pressure, inducing polymer precipitation as nanospheres. Size range of nanoparticles was found to be influenced by the concentration and type of stabilizer, the polymer concentration and the homogenizer speed. Ultrasonication or high-speed homogenization may be often employed in order to produce small particle size.[78] The nanoparticles are collected by ultracentrifugation and washed with distilled water to remove stabilizer residue or any free drug and lyophilized for storage.[79]

- **Salting Out Method:** this method involves the separation of a water-miscible solvent from aqueous solution via a salting-out effect.[80] The polymer and the drug are dissolved in an organic solvent, which is subsequently emulsified into an aqueous gel containing the salting out agent (electrolytes, such as magnesium chloride and calcium chloride, or non- electrolytes such as sucrose) and a colloidal stabilizer. This leads to the formation of oil/water emulsion which is further diluted with a certain volume of water or aqueous solution to enhance the diffusion of solvent into the aqueous phase, inducing the formation of nanospheres. Parameters such as stirring rate, internal/external phase ratio, concentration of polymers in the organic phase, type of electrolyte, concentration and type of stabilizer in the aqueous phase can be varied in this process.[81]

- **Solvent Displacement/Precipitation Method:** in this method, the molecule is dissolved in a semi-polar water miscible solvent, such as acetone or ethanol, and the solution is then poured or injected in an aqueous solution, either in the presence or absence of surfactant, under magnetic stirring. Nanoparticles are formed immediately by the rapid solvent diffusion, then the organic solvent is removed from the suspension under reduced pressure.[82]

- **Polymerization Method:** this technique involves the polymerization of monomers to form nanoparticles in an aqueous solution. Ultracentrifugation can be used to purify nanoparticle suspension by removing various stabilizers and surfactants employed for polymerization, followed by the re-suspension of particles in an isotonic surfactant-free medium.

- **Production of Nanoparticles Using Supercritical Fluid Technology:** Among the various processing techniques involving supercritical fluids, supercritical anti-solvent (SAS) and rapid expansion of critical solution (RESS) are the most common. In the SAS technique, a liquid solvent, commonly methanol, is selected in order to be completely miscible with the supercritical fluid (CO_2). The solute is dissolved in the organic layer and the extraction by the supercritical fluid leads to the instantaneous precipitation of the solute, since it is insoluble in the supercritical fluid, resulting in the formation of nanoparticles. In RESS method, the solute is dissolved in a supercritical fluid, such as supercritical methanol, and then the solution is rapidly expanded into a lower pressure region. This dramatically affects the solvent power of supercritical fluid, which is decreased, and the solute eventually precipitates.

2. Squalene-based Nanoparticles

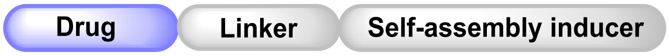
Drug
Linker
Self-assembly inducer

2.1 Disulphide containing linker

The concept of lipid-drug conjugates has gained considerable attention in recent years, and these conjugates are usually obtained by a covalent coupling of the drug to biocompatible lipid moieties. Among them, squalene, a natural precursor of many steroids, showed the ability, when linked to biologically active compounds, to achieve a spontaneous formation of nanoassemblies in water. Thus, squalene protects the drugs from environment damaging factors and, in some cases, also improves their pharmacokinetic profile by decreasing the toxicity of the associated drugs with an increase in their therapeutic index. This novel approach progressively extended its field of application from anticancer agents (gemcitabine, paclitaxel, cisplatin, doxorubicin)[83,84,85,86,87,88] to antibiotics and from antiviral agents (penicillin, AZT, acyclovir)[89,90] to nucleotides (siRNA).[91,92] Furthermore, the ability to spontaneously nanoassemble allowed the preparation of nanoparticles containing both therapeutic and diagnostic agents.[93,94] One of the key points in the realization of potent and efficient squalene prodrug resides in the release of the free drug; thus, the role of the linkage between the drug and the squalene moiety is crucial.

In the last years our research group investigated the possibility to improve the biological activity of anticancer compounds by the preparation of squalene-incorporating derivatives with the use of a disulfide-containing linker to secure the drug release. It was prepared a novel class of disulfide-containing squalene conjugates (**Scheme 1**).

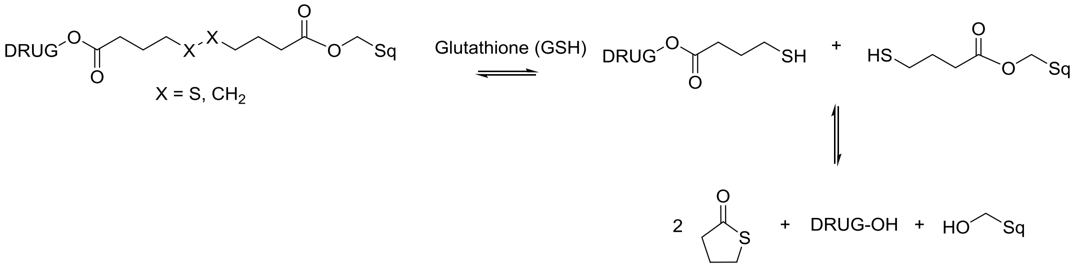

Scheme 1. Supposed pathway for drug release of disulfide-containing squalene conjugates.

The presence of the squalene tail induces spontaneous self-assembly in water, while the disulfide bond induces drug release in the intracellular environment. Four known anticancer compounds were selected: paclitaxel, podophyllotoxin, camptothecin and epothilone A (**Figure 5**). These compounds are known to interact with tubulins (paclitaxel, podophyllotoxin and epothilone A) and with topoisomerase I (camptothecin), but they all suffer from many drawbacks, primarily due to the side effects associated with their low water solubility. The introduction of a lipophilic tail overcomes the problem by favouring the formation of nanoassemblies, more capable of membrane permeation.

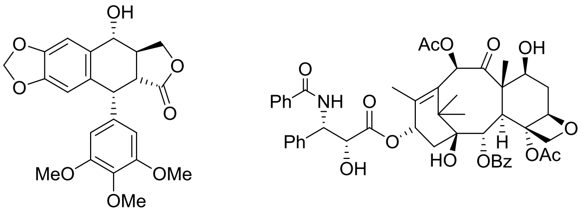

Podophyllotoxin (PODO) *Paclitaxel (PTX)*

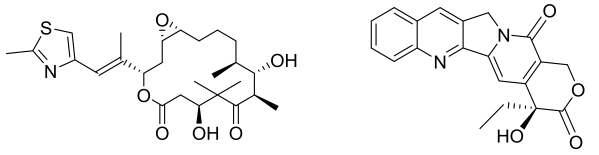

Epothilone A (EPO) *Camptothecin (CPT)*

Figure 5. Structures of podophyllotoxin, paclitaxel, epothilone A and camptothecin.

All the obtained compounds were effectively able to self-assemble in water to form nanoparticles and they were also able to release the parent drug *in vitro*. Disulfide-containing paclitaxel squalene derivative showed a similar biological activity when compared to the parental drug. Immunofluorescence assay showed that this squalene conjugate enters A549 cells and stain microtubule bundles.

The results described herein paved the way for different classes of squalene-based releasable nanoassemblies.[95]

2.2 Fluorescent hetero-nanoparticles

The recent advances in nanotechnology and nanomaterials have been integrated into analytical chemistry for the design of large numbers of fluorescent chemical and biological probes. In recent years instead of using single organic dye probes, these organic fluorophores were encapsulated in a particle matrix. These particles are much brighter than the dyes alone because one particle contains several dyes molecules. In addition, these dyes are more photostable because the entrapment enhances the stability and biocompatibility of the fluorophores. The small size of the nanoparticles allows a high signal-to-noise ratio response and signal amplification, therefore improving the analytical sensitivity and the response time. More importantly, their molecular size minimizes physical perturbation of living cells. Generally, fluorescent nanoparticles show superior optical properties, which facilitate their application for single molecule imaging and long-term tracking of biological molecules *in vivo.*[96]

The need to trace the delivery of the nanoassemblies and to demonstrate the internalization of the drugs prompted us to prepare fluorescent hetero-nanoassemblies by mixing a paclitaxel–squalene conjugate (PTX-Sq) and a fluorescein–squalene conjugate (FITC-Sq) (**Figure 6**).[97]

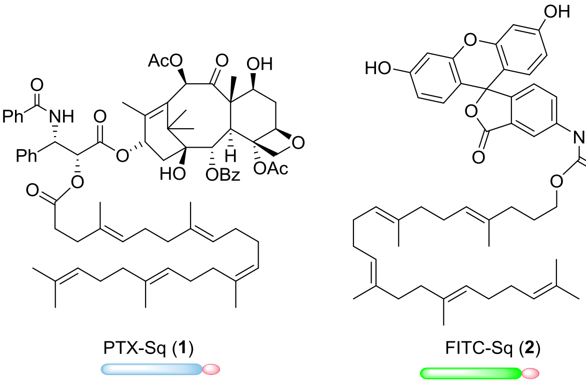

PTX-Sq (**1**)

FITC-Sq (**2**)

Figure 6. Structures of the paclitaxel- and fluorescein-squalene conjugates.

Paclitaxel

Paclitaxel (PTX), a tetracyclic diterpenoid, was first isolated in 1971 from the Western Yew *Taxus Brevifolia* by Wani, Wall and co-workers, who established its structure by X-ray crystallographic methods[98] (**Figure 7**).

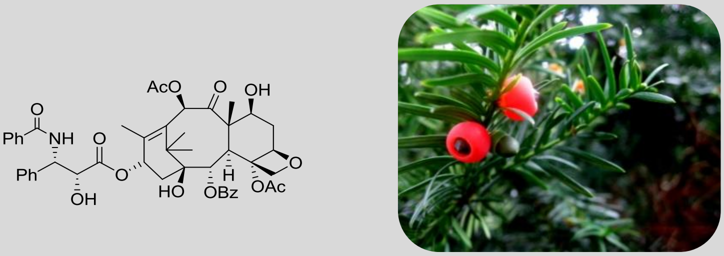

Figure 7. Paclitaxel (PTX) and *Taxus Brevifolia*.

Different from most anticancer drugs, PTX acts as a microtubule-stabilizing drug, which inhibits cellular growth by preventing cytoskeletal microtubule depolymerisation to free tubulin and disrupting the balance between polymerization and depolymerisation, and thus leads to cessation of the cell cycle with arrest at the G2/M phase.[99]

Despite its promising cytotoxic activity, many limitations in its clinical use are related to its low water solubility. For this reason, paclitaxel is usually formulated in adjuvant Cremophor EL, that anyway has been reported to cause serious side effects, including hypersensitivity reactions, nephrotoxicity, cardiotoxicity and neurotoxicity.[100]

Furthermore, significant side effects are also induced due to paclitaxel nonspecific, indiscriminate biodistribution in the body after administration.

Therefore, many kinds of PTX analogues have been prepared,[101] on the base of SAR studies, in order to improve water solubility while maintaining the activity.

Different approaches, obtained from SAR studies, for the preparation of paclitaxel analogues can be summarized as in **Figure 8**:[102,103]

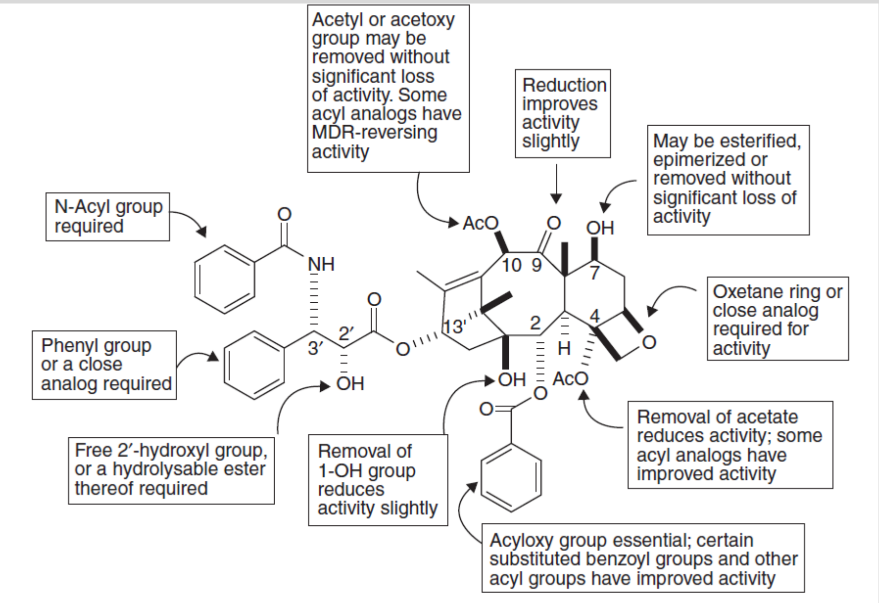
Acetyl or acetoxy group may be removed without significant loss of activity. Some acyl analogs have MDR-reversing activity
Reduction improves activity slightly
May be esterified, epimerized or removed without significant loss of activity
N-Acyl group required
Oxetane ring or close analog required for activity
Phenyl group or a close analog required
Free 2′-hydroxyl group, or a hydrolysable ester thereof required
Removal of 1-OH group reduces activity slightly
Removal of acetate reduces activity; some acyl analogs have improved activity
Acyloxy group essential; certain substituted benzoyl groups and other acyl groups have improved activity
AcO
O
OH
NH
O
10
9
7
13′
2
4
2′
3′
H
OH
OH
AcO
O

Figure 8. SAR studies for paclitaxel.

Another strategy is to find a different formulation to avoid the use of Cremophor EL, and also in this direction many efforts have been made and some good results have been obtained, such as those related to albumin-bound paclitaxel (Abraxane®).[104,105,106]

Synthesis of the conjugates

To obtain the conjugate **2** (FITC-Sq), the first step was the preparation of the 1,1’,2-tris-norsqualene alcohol **7**. In particular, it was obtained starting from squalene (**1**), as described in **Scheme 2**. The crucial reaction is the formation of monobromohydrine **4** that was converted into 2,3-epoxide **5** by simple treatment with K_2CO_3. The oxidative cleavage of the epoxide furnished 1,1’,2-tris-norsqualene aldehyde **6**[107] and the subsequent $NaBH_4$ reduction secured the alcohol **7**.

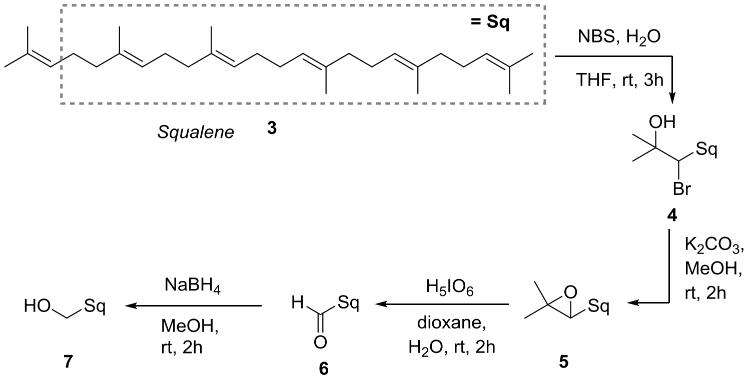
= Sq
Squalene
3
NBS, H2O
THF, rt, 3h
OH
Sq
Br
4
K2CO3,
MeOH,
rt, 2h
O
Sq
5
H5IO6
dioxane,
H2O, rt, 2h
H
Sq
O
6
NaBH4
MeOH,
rt, 2h
HO
Sq
7

Scheme 2. Synthetic pathway for the preparation of 1,1’,2-tris-norsqualene alcohol.

The reaction of 1,1’,2-tris-norsqualene alcohol **7** with fluorescein isothiocyanate (FITC) in the presence of sodium hydride gave the stable compound **2** (**Scheme 3**).

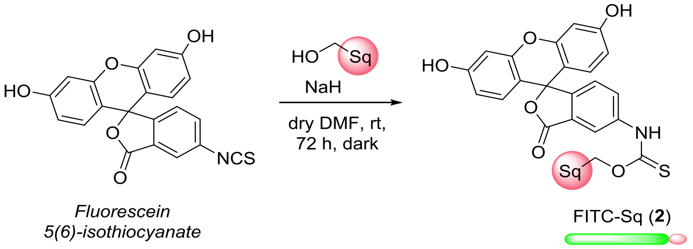
HO
O
OH
O
O
NCS
Fluorescein
5(6)-isothiocyanate
HO
Sq
NaH
dry DMF, rt,
72 h, dark
HO
O
OH
O
O
NH
Sq
O
S
FITC-Sq (2)

Scheme 3. Synthesis of the conjugate FITC-Sq (**2**).

As paclitaxel conjugate, we planned to use the recently described squalenoyl–paclitaxel **1** that was recognized as being able to act as a prodrug and to self-assemble.[83] PTX-Sq (**1**) was prepared following a procedure described by Dosio and co-workers. Compound **6** was oxidized to the corresponding carboxylic acid **8** by treatment with $H_2SO_4/Na_2Cr_2O_7$ and then condensed to paclitaxel using EDC·HCl/DMAP as activating system (**Scheme 4**).

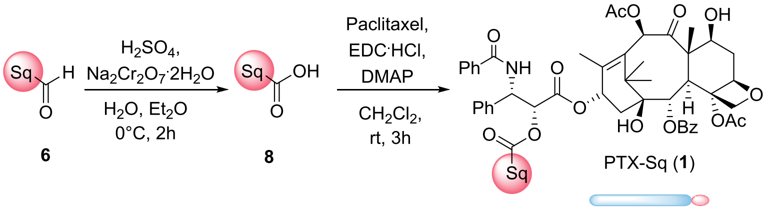
Sq
H
O
6
H_2SO_4,
$Na_2Cr_2O_7 \cdot 2H_2O$
H_2O, Et_2O
0°C, 2h
Sq
OH
O
8
Paclitaxel,
EDC·HCl,
DMAP
CH_2Cl_2,
rt, 3h
Ph
NH
O
Ph
O
O
O
O
Sq
AcO
O
OH
O
HO
OBz
H
OAc
PTX-Sq (1)

Scheme 4. Synthesis of the conjugate PTX-Sq (**1**).

Nanoparticles preparation

To verify the ability of compound **2** (FITC-Sq) to form nanoassemblies and of compounds **1** and **2** to form hetero-nanoparticles (**Figure 9**), five different nanosuspensions were prepared by the solvent displacement method (**Figure 10Figure 10**).[108]

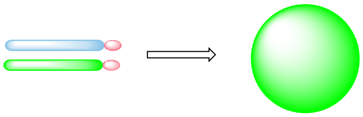

Figure 9. Schematic representation of hetero-nanoparticles formation.

A) FITC-Sq (2 mg/mL);

B) PTX-Sq (2 mg/mL): FITC-Sq = 10 : 1;

C) PTX-Sq (2 mg/mL): FITC-Sq = 20 : 1;

D) PTX-Sq (2 mg/mL): FITC-Sq = 30 : 1;

E) PTX-Sq (2 mg/mL).

In the case of suspensions B, C and D, the final concentration (2 mg/mL) is referred to PTX-Sq, while the amount of FITC-Sq was calculated considering the molar ratios PTX-Sq: FITC-Sq (10:1, 20:1, 30:1).

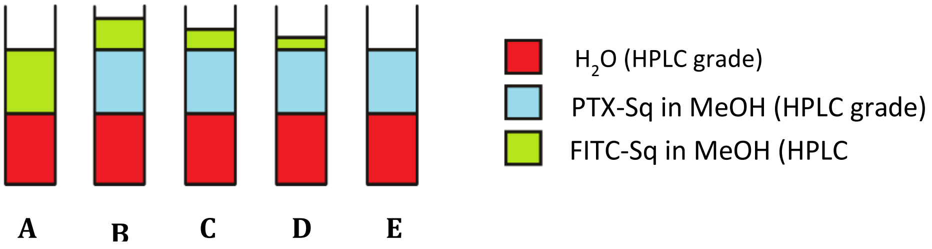

Figure 10. Schematic representation of the five mixtures.

Nanoparticles characterization

Measurement of the mean diameter and polydispersity index by using dynamic light scattering (DLS) confirmed the presence of self-assemblies (**Table 2**). It was evident that by decreasing the amount of fluorescein–squalene conjugate **2**, the mean diameter increased toward the value of the pure paclitaxel–squalene conjugate **1**.

Unfortunately, we were not able to obtain a precise measure for Z potential of most of the suspensions, but values very different one from the other (all the measurements were always repeated thrice). This could be due to intrinsic factors of our nanoparticles or to a malfunctioning of the instrument we used.

	Compound	**Mean Diameter (nm)**	**Polydispersity Index**	**Z potential (mV)**
A	**FITC-Sq**	196.4	0.232	-19.91
B	**PTX-Sq: FITC-Sq 10:1**	149.4	0.147	n.d.
C	**PTX-Sq: FITC-Sq 20:1**	171.9	0.179	n.d.
D	**PTX-Sq: FITC-Sq 30:1**	225.4	0.190	n.d.
E	**PTX-Sq**	231.6	0.270	n.d.

Table 2. Mean diameter, polydispersity index and Z potential of the five mixtures.

Fluorescence emission

To verify the relevance of the amount of fluorescein derivative and the pertinence of the nature of the samples (solutions or nanosuspensions), we measured the fluorescence emission of different mixtures deriving from nanoparticles or from simple dissolution, using a spectrofluorometer FP-750 (Jasco).

For a better measurement nanoparticle samples were diluted with water (HPLC grade) and pure FITC-Sq was dissolved in MeOH (HPLC grade) in order to have the main component of the mixture at a fixed concentration. The results we obtained are summarized in the following graphs.

- *Graph A*: FITC-Sq at different concentrations (samples as nanoparticles). Samples with higher amounts of FITC-Sq possess a higher fluorescence emission.

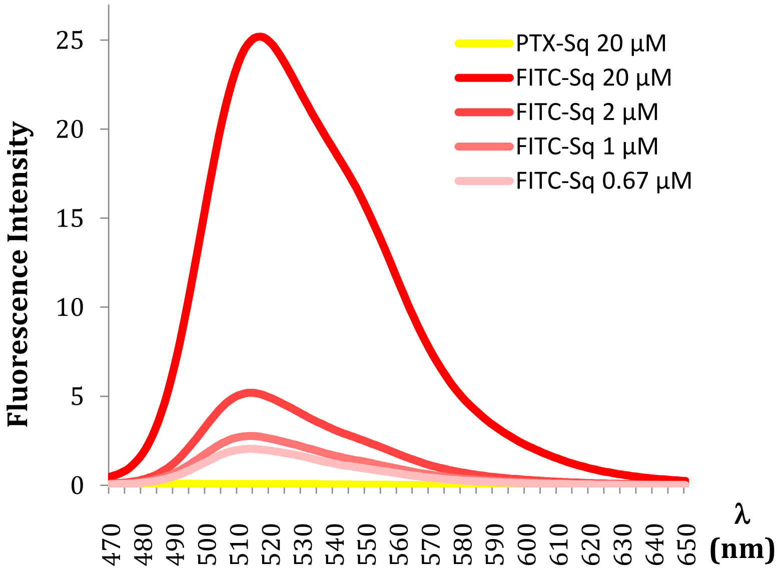

- *Graph B*: PTX-Sq at a fixed concentration (20 µM) with different amounts of FITC-Sq compared to FITC-Sq 20 µM (samples as nanoparticles). Also in this case, samples with higher amounts of FITC-Sq possess a higher fluorescence emission.

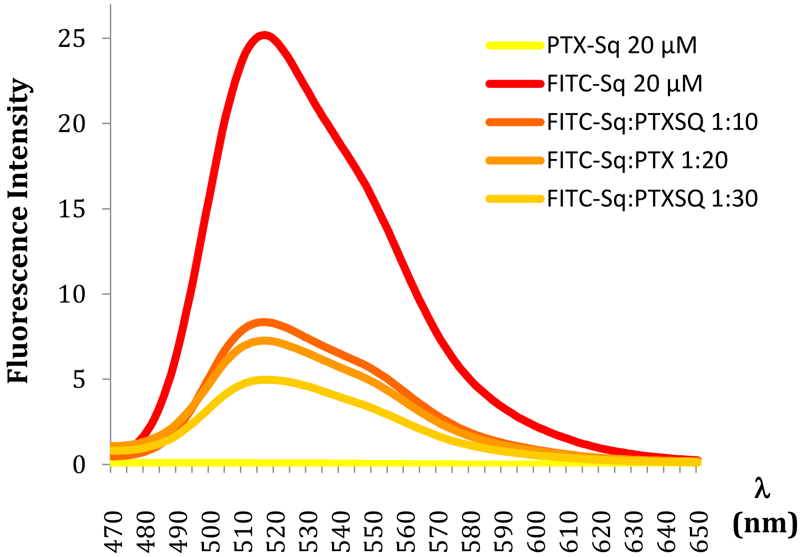

- *Graphs C, D and E*: samples with different amounts of FITC-Sq (as nanoparticles) were compared to samples containing the same amounts of FITC-Sq but in solution. Noteworthy, the samples of nanosuspensions displayed a higher emission of fluorescence than the corresponding solutions and, at each value of FITC-Sq concentration, the mixture of PTX-Sq and FITC-Sq displayed a higher emission than FITC-Sq alone.

  This can be explained by the fact that the more hydrophobic the environment is, the higher the emission: thus, a nanosuspension results to be a more hydrophobic environment than a methanolic solution even if the sample is diluted with water. Moreover, the presence of PTX-Sq in a 10:1 ratio respect to FITC-Sq further increase the hydrophobicity of the system.

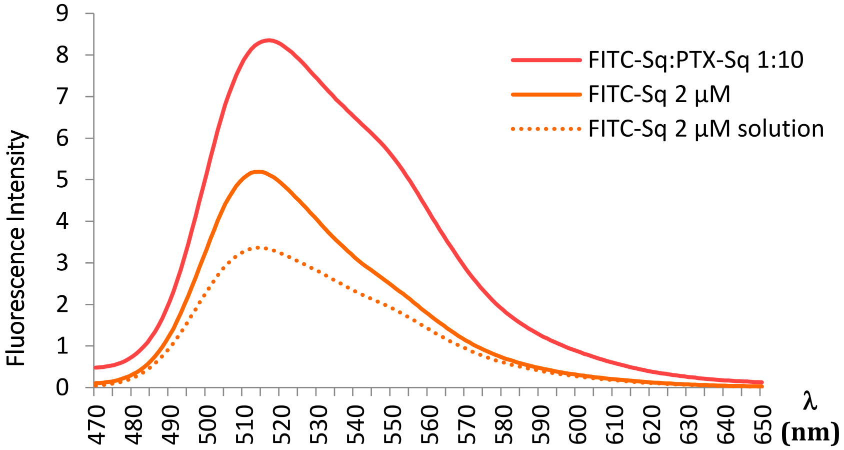

Graph C: Fixed FITC-Sq concentration: 2 µM

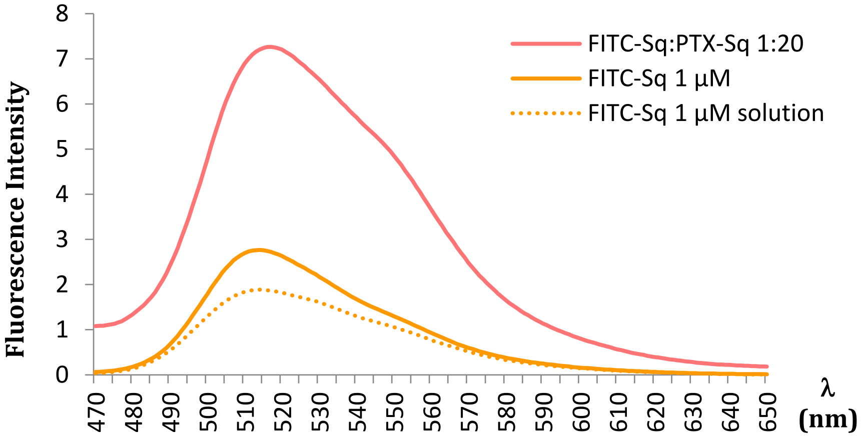

Graph D: Fixed FITC-Sq concentration: 1 µM

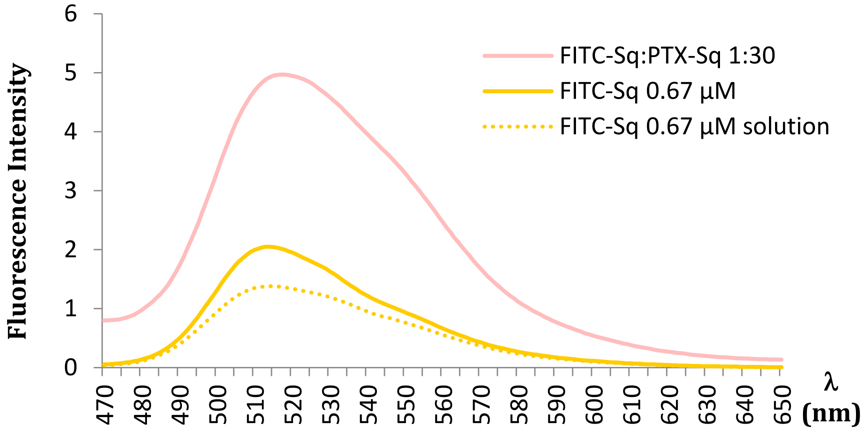

Graph E: Fixed FITC-Sq concentration: 0.67 μM

In vitro evaluation: cell internalization

To verify the capability of nanoassemblies to enter the cell, A549 cells were incubated with suspensions of hetero-nanoparticles **1**/**2** at two different molar ratios (10:1 and 30:1). **Figure 11**Figure 11 shows that after different incubation times (10, 30, and 60 min), fluorescent entities accumulate in the perinuclear region.

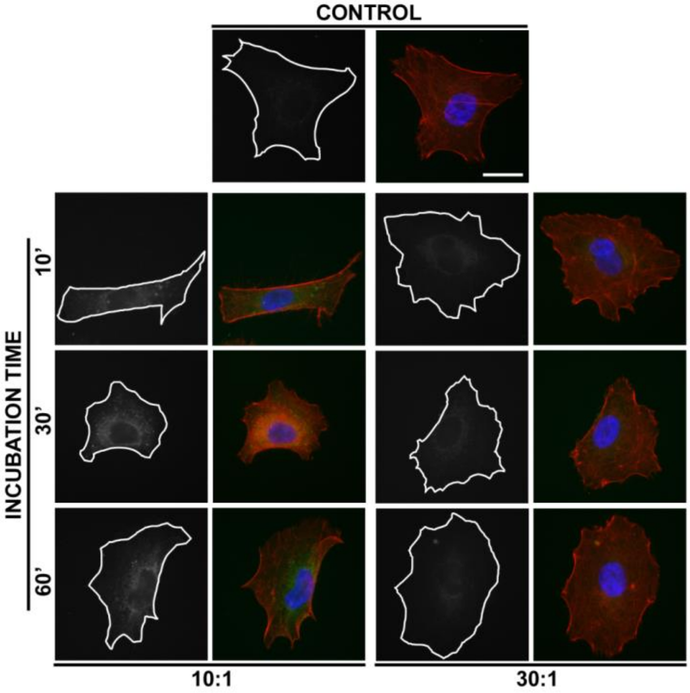

Figure 11. Right columns show actin filaments (red) and nuclei (blue), whereas white lines in the left columns mark the cell boundaries. Top row (Control) shows A549 cell that were not incubated with PTX-Sq/FITC-Sq co-nanoassemblies. Scale bar = 20 µm.

We also took advantage of live cell imaging to directly visualize moving nanoparticles and, as reported in **Figure 12**, it is possible to recognize cells that contain fluorescent spherical spots whose perceptible diameter (< 450 nm) is consistent with that of the reported mean diameter (see **Table 2**). Thereby showing that the fluorescence inside the cells is really due to the nanoassemblies and not to diffused compound **2**.

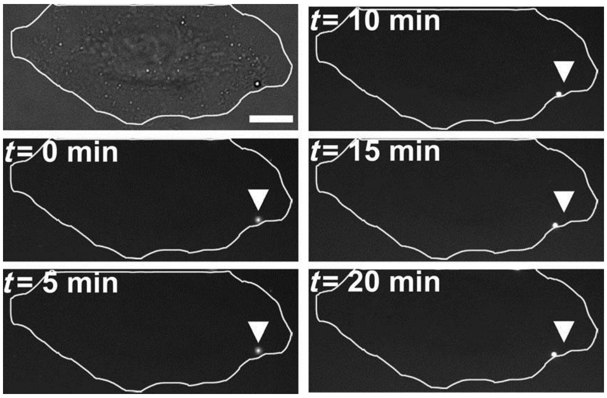

Figure 12. Frames from a time-lapse series of A549 cells exposed to nanoassemblies 1/2. The incubation time is shown on each frame; white lines mark the cell boundaries and the arrowheads indicate the initial position of the fluorescent particle. Image on the top left shows the phase contrast channel. Scale bar = 5 mm.

In vitro evaluation: cytotoxic activity

After proving that nanoassemblies **1**/**2** are able to cross the cell membrane, we wondered if the contained paclitaxel retains its antitubulin effect. Microscopy analyses (**Figure 13**) reveal that control cells are spread with a well-organized microtubule network, whereas cells treated with either paclitaxel or nanoassemblies of **1**/**2** become smaller and roundish, as if to signify they were dying and detaching from the plate.

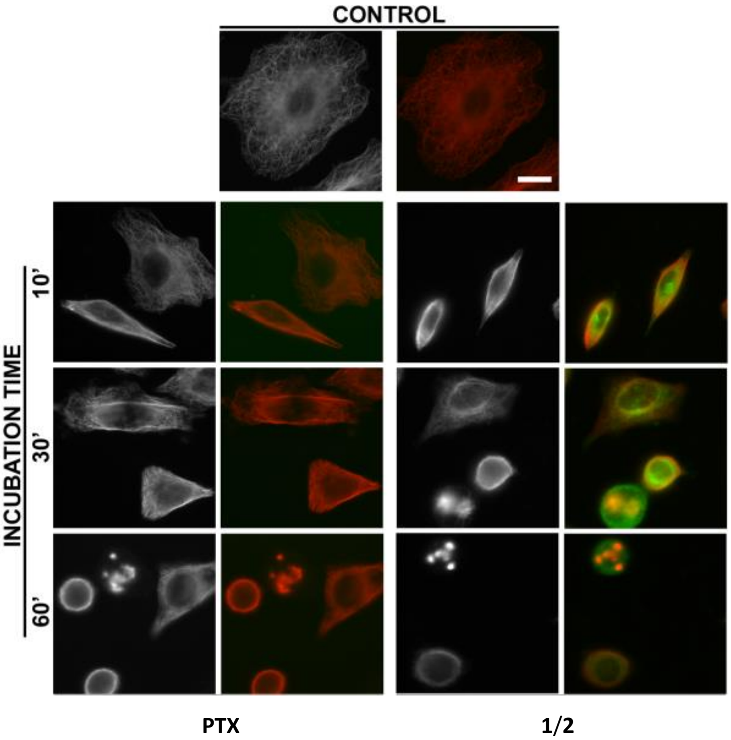

Figure 13. A549 cells were treated for 10, 30, and 60 min with paclitaxel (PTX) or nanoassemblies 1/2. Left column shows the a tubulin staining, whereas the right column shows both a tubulin (red) and fluorescent compound (green). Top row displays untreated cells (CONTROL). Scale bar = 20 mm.

Furthermore, both microtubule bundles and tubulin accumulation are noticeable, meaning that the observed changes in cell shape are a result of aberrant organization of the microtubule cytoskeleton. To further certain that paclitaxel in the nanoassemblies target microtubules, we removed the unassembled pool of tubulin, as previously described.[109] As highlighted by the arrowheads, paclitaxel decorates microtubule bundles (**Figure 14**).

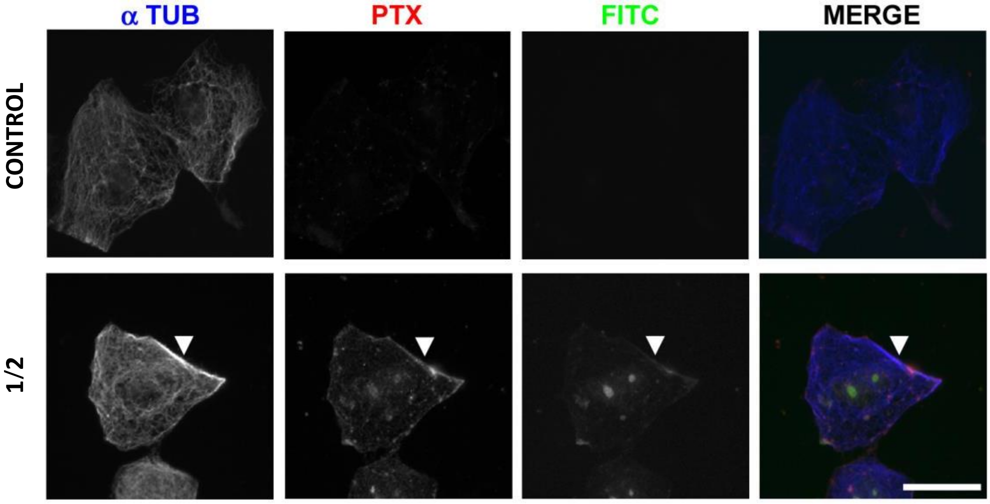

Figure 14. Untreated A549 cells (CONTROL) or A549 treated 60 minutes with nanoassemblies 1/2 were extracted and immune-stained for α tubulin (α TUB, blue) and paclitaxel (PTX, red); fluorescent compound is shown in green. Arrowheads indicate a microtubule bundle. Scale bar = 20 µm.

Therefore, we conclude that nanoassemblies **1**/**2** cross the cell membrane and act on the microtubule cytoskeleton by inducing typical taxol-like effects.

We suppose that the internalization of nanoassemblies **1**/**2** has occurred even though the alternative possible pathway envisages efflux through the cellular membrane of the partially disassembled compounds after the approach of the nanoparticles to the cell. This second possibility does not affect the relevance of creating self-assembled hetero-nanoparticles.

The self-assembly ability of lipid–drug conjugates is advantageous for the preparation of fluorescent hetero-nanoparticles that can help follow the dynamic of the delivery. The easy formation of nanoparticles by simple mixing of the lipid–drug conjugates makes this strategy simple to apply for different types of drugs and biological targets.

2.3 Cyclopamine-Paclitaxel hetero-nanoparticles

Tumors are heterogeneous, composed of distinct types of cells including cancer stem cells (CSCs), which exhibit high clonogenic capacity and the ability to reform parental tumors upon transplantation. Existing anticancer therapies are in most cases palliative rather than curative, not being able to prevent re- lapse. One possible explanation is that current treatments target the more differentiated tumor cells resulting in tumor regression; they do not target CSCs, and subsequently there is a relapse of the disease. Indeed, resistance to therapy has been shown for several types of CSCs. Therefore, a combination of agents against both CSCs and bulk tumor cells may offer improved therapeutic benefits.[110] In this field, the use of a combination of paclitaxel, a known microtubule stabilizer, and cyclopamine, a natural alkaloid acting as Hedgehog signalling pathway (Hh) inhibitor, has been reported for the treatment of some prostate cancer cells resulting in decreased proliferation and increased apoptosis.[111,112]

Stem cells and cancer

Normal adult multipotent stem cells are usually able to self-renew, producing at least one progeny cell with a similar developmental capacity and many evidences indicate that this cell population, through initial genetic or epigenetic alterations, can become responsible for the development of several tumors through a progressive establishment of a CSC population.

The CSCs model suggests that tumor progression, metastasis and recurrence after therapy can be driven by a rare subset of tumor cells that have the capacity to self-renew, while the bulk of the tumor does not have this capacity.

For these reasons, the deregulation of the self-renewal process may be a key event in carcinogenesis, and while self-renewal can drive tumorigenesis, the differentiation process may contribute to tumor phenotypic heterogeneity.

CSCs as targets in cancer treatment

It is well known that several cancers are peculiarly resistant to conventional radio- and chemotherapy that typically kill the majority of cancer cells. This clinical response may reflect the targeting of the bulk of non-stem cell population.

On the other hand, there are several specific key intracellular signaling pathways implicated in CSCs self-renewal and proliferation processes that appear to be promising therapeutic targets.

An ideal therapeutic strategy might be to sensitize CSCs to chemo- and radiotherapy by inhibiting their stem properties and then by promoting a direct cytotoxicity. Since the CSCs population is driven by embryonic signaling pathways, the targeting of these pathways could result in a better outcome of the therapy: in this direction, many drugs for the inhibition of embryonic signaling pathways are currently under development.

Hedgehog Signalling Pathway: a new biological target for the design of new anticancer compounds

Some of the most characterized signalling pathways controlling self-renewal and differentiation in adult stem cells, such as Wnt/b-catenin, Hedgehog, Notch and TGF-b/BMP pathways, are frequently modulated in cancer by epigenetic mechanisms.

Hedgehog (Hh) is a key signaling pathway for the regulation of embryonic development and tissue repair, mainly through the control of stem and progenitor cells (e.g. neural stem cells) and for the control of a number of genes involved in cell fate determination and stemness features. When hyperactivated by genetic and/or epigenetic alterations, Hh pathway promotes tumorigenesis in several tissues by subverting the regulation of stemness-determining genes overexpressed in that type of cancer.

Normal Hh signalling

Binding of Hh to its receptor Patched (Ptch-1) activates the transmembrane protein Smoothened (SMO), which subsequently activates the Gli family of transcription factors, leading to activation of target genes (**Figure 15**):

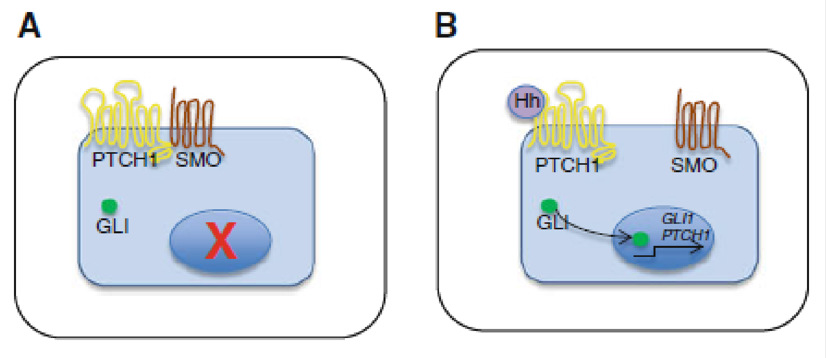

Figure 15. Normal Hedgehog signalling pathway.

Hedgehog signaling in cancer

Aberrant Hh signaling occurs in some cases because of a ligand-independent activation of SMO due to a mutation in PTCH1 or in SMO (**Figure 16**), but it generally happens through ligand-dependent mechanisms. Increased Hh ligand expression leads to increased Hh signaling in the activated target cell. This can theoretically occur through either an autocrine mechanism where the malignant cells both secrete and respond to Hh ligand, or through a paracrine mechanism where the secreting cell and recipient target cell are different. Even if the autocrine mechanism has been reported for multiple tumor types, the currently overall favored mechanism is the paracrine model, based partly on evidence that tumor cells do not appear to respond to Hh ligand themselves.[113]
One proposed explanation has been that tumor cells lack the primary cilium necessary for canonical Hh signaling through PTCH1 and SMO.

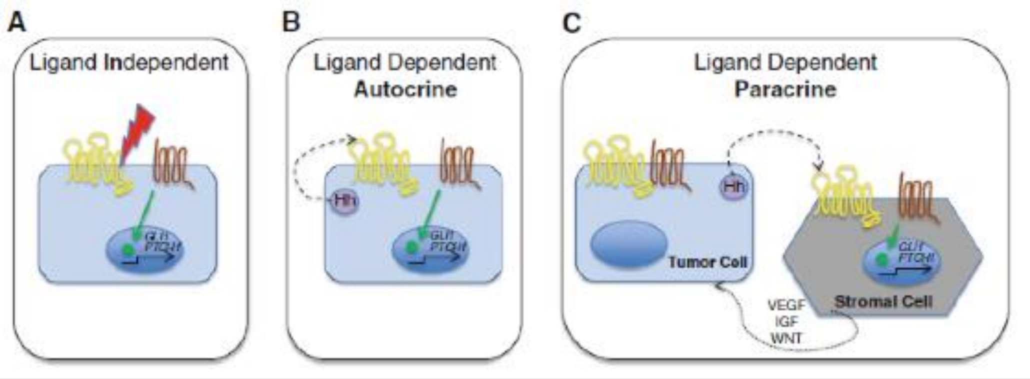
A
Ligand Independent
B
Ligand Dependent
Autocrine
Hh
GLI1
PTCH1
C
Ligand Dependent
Paracrine
Hh
Tumor Cell
Stromal Cell
GLI1
PTCH1
VEGF
IGF
WNT

Figure 16. Hedgehog signalling pathway in cancer.

Hedgehog inhibitors

On the base of the acquired knowledge concerning the signaling steps of the Hh signaling pathway, it is possible to identify different potential ways to inhibit this pathway in cancer. To date, the best-characterized approach is to target the SMO receptor with small molecule inhibitors, and many of such inhibitors are under clinical trial investigation.

Alternatively, preventing SMO from converting from the inactive to the active form should also achieve the same result.

The limitation with these two approaches is that they will fail if activation occurs by alteration of the signaling pathway downstream of SMO.

Drugs that can interfere with the Hh signaling pathway downstream of SMO are therefore also of potential therapeutic benefit.

We decided to examine self-assembled hetero-nanoparticles that incorporate two different drugs: paclitaxel and cyclopamine (**Figure 17**).[114] A ternary combination obtained by further addition of a tetramethylrhodamine–squalene conjugate generated fluorescent nanoparticles that could be used to observe the cellular internalization by confocal microscopy and super-resolution dSTORM (direct stochastic optical reconstruction microscopy).[115]

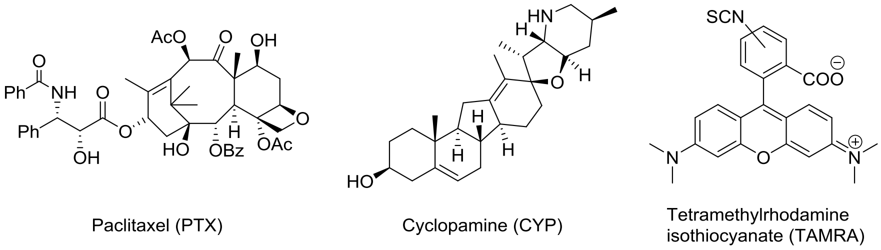
Paclitaxel (PTX)
Cyclopamine (CYP)
Tetramethylrhodamine isothiocyanate (TAMRA)

Figure 17. Structures of the drugs paclitaxel and cyclopamine and of the dye tetramethylrhodamine.

Cyclopamine

The *Veratrum* alkaloid known as cyclopamine (CYP) was the first agent that was found capable of disrupting the Hh signalling pathway.

Cyclopamine belongs to the family of jervine alkaloids, which constitute the majority of *Veratrum* secondary metabolites. The association of *Veratrum Californicum* (**Figure 18**) to sheep congenital deformities during the 1950s raised the possibility that jervine alkaloids could be potent teratogens. Later studies confirmed that jervine and cyclopamine (**Figure 19**) given during gestation can directly induce cephalic defects in lambs, including cyclopia.

Figure 18. *Veratrum Californicum*.

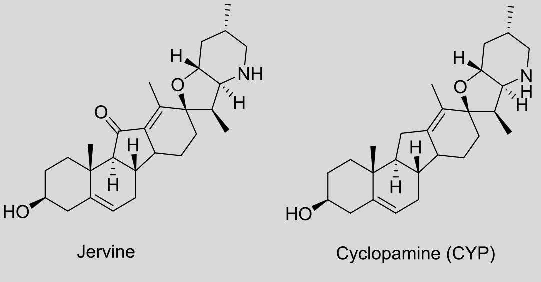
Jervine
Cyclopamine (CYP)

Figure 19. Structure of jervine and cyclopamine.

Cyclopamine[116] was shown to be a potent antagonist of the Hh pathway, directly acting on the protein Smo, and has been shown to have antitumor activity in several xenograft models.

Despite the attractive pharmacological profile of cyclopamine, its use as a systemic treatment may be limited by its poor aqueous solubility (~5µg/ml) and stability in acid. In fact, cyclopamine readily converts to veratramine as a result of an acid-catalyzed opening of the spirotetrahydrofuran E ring followed by rapid aromatization of the D ring (**Figure 20**). Veratramine, while not acting as Hh antagonist, has been shown to interact with several other receptors and cause hemolysis.

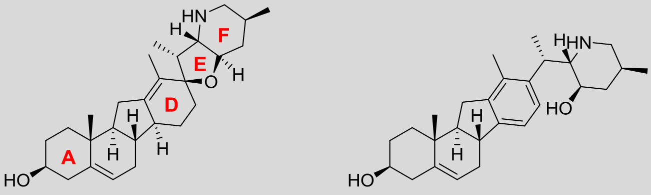

Cyclopamine

Veratramine

Figure 20. Structure of cyclopamine and veratramine.

In order to obtained more stable and soluble hedgehog inhibitors, many efforts have been made for the preparation of cyclopamine analogues.[117,118]

2.3.1 Cyclopamine nanoparticles

Synthesis of the conjugates

We first investigated the synthesis of cyclopamine–squalene conjugates incorporating a disulfide bond. In **Scheme 5** we report a successful synthesis that relies on the protection of the amino group.[119] Condensation of cyclopamine N-Fmoc[120] with dicarboxylic acid monoesters **11** and **12**, respectively synthetized by condensation of 1,1′,2-tris-norsqualene alcohol **7** with 4,4′-dithiodibutyric acid or sebacic acid, in the presence of EDC–DMAP and subsequent removal of the protecting group led to cyclopamine conjugates **13** and **14**.

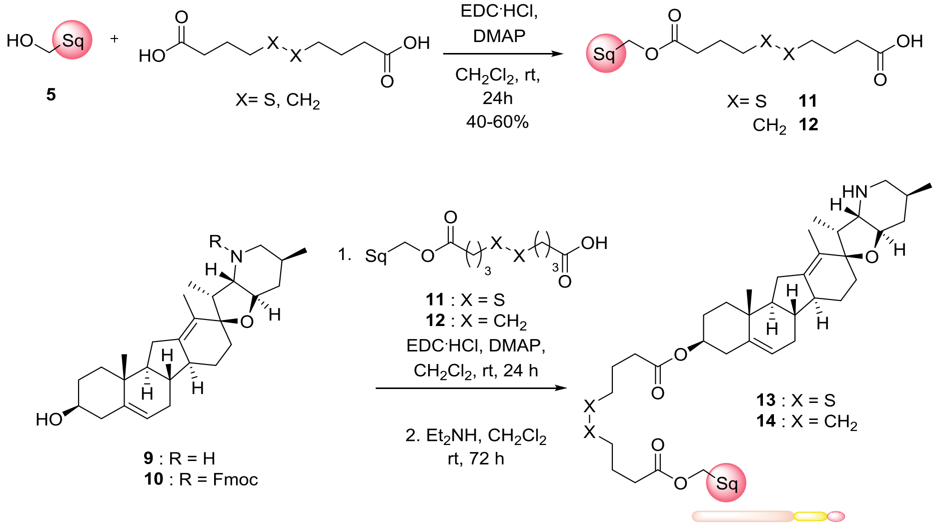
HO Sq
+
5
HO O X X OH O
X= S, CH2
EDC·HCl, DMAP
CH2Cl2, rt, 24h
40-60%
Sq O O X X OH O
X= S 11
CH2 12
R N H H O H H H HO
9 : R = H
10 : R = Fmoc
1. Sq O O ( )3 X X ( )3 OH O
11 : X = S
12 : X = CH2
EDC·HCl, DMAP, CH2Cl2, rt, 24 h
2. Et2NH, CH2Cl2 rt, 72 h
HN H H O H H H O O X X O O Sq
13 : X = S
14 : X = CH2

Scheme 5. Synthesis of the cyclopamine-squalene conjugates.

Nanoparticles characterization

The obtained conjugates were used to form nanoparticles by solvent-displacement method (**Figure 21***Figure 21*) and were characterized by dynamic light scattering (DLS) (**Table 3**).

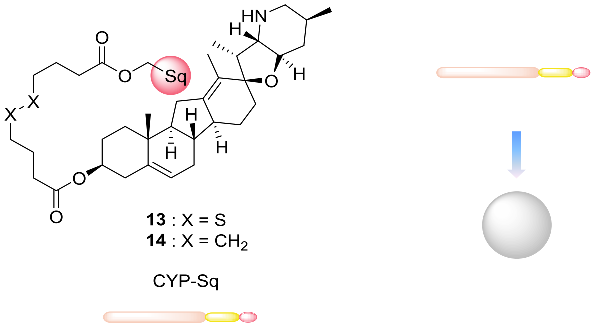

Figure 21. Nanoparticles formation.

Compound	Mean Diameter (nm)	Z potential (mV)
13	105±1	+37.8±3.3
14	240±2	+38.4±4.3

Table 3. Cyclopamine-nanoparticles characterization.

In vitro evaluation

To assess the effect of the compounds **13** and **14** on cancer cell growth, we evaluated their biological effect in U251 glioblastoma cell line taking into account that their resistance is associated also with an increase of glutathione (GSH) level.[121] We found compound **14** to be the more active (**Figure 22**).

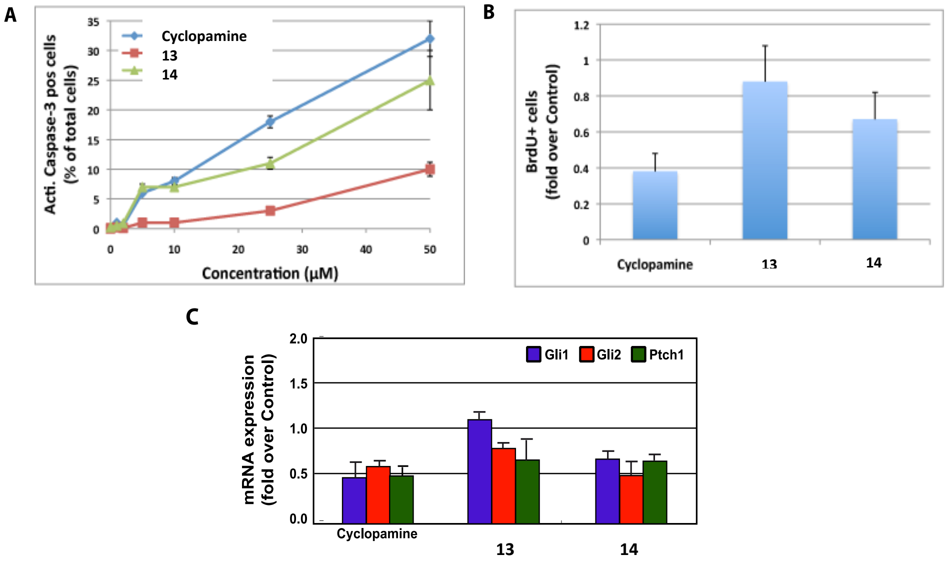

Figure 22. A) Effect on U251 glioblastoma cell line, at the indicated concentrations after 48h of culture; B) Effect on the proliferation of U251 cells, at a concentration of 25 µM after 48h culture; C) Quantitative RT-PCR analysis of the mRNA expression of the main genes of Hh signalling pathway in U251 glioblastoma cells 24h after the addition in culture of indicated compounds at a concentration of 25 µM.

Our results show that the compound **14** inhibited proliferation (**Table 4**) and induced apoptosis at comparable levels to that of cyclopamine, and this effect was indeed mediated by inhibition of the Hh pathway.

Compound	**IC_{50} (µM)**			
	#83	#110	OVCAR5	U251
CYP	> 50	> 50	> 50	30
13	n.a	n.a.	n.a.	68
14	34	40	42	40

Table 4. IC_{50} values determined with different cell lines.

In our proposal, compound **13** releases the drug as a consequence of the cleavage of the disulfide bond by GSH, which is particularly present inside the cancer cells. If the release of cyclopamine is responsible for the activity, the unexpected result seems to suggest a better release in compound **14**. With the aim to evaluate the chemical reactivity induced by the presence or the absence of the disulfide bond, we studied the behaviour of both compounds **13** and **14** in the presence of GSH. With ESI mass spectrometry, we had the possibility of detecting the release of cyclopamine from both of the compounds. In the absence of GSH we observed only the peaks of the conjugate.

2.3.2 Cyclopamine-Paclitaxel hetero-nanoparticles

Given the better activity of compound **14**, we decided to use compound **14** and compound **15** (previously described by our research group)[95] to form hetero-nanoparticles (**Figure 23**). Hetero-nanoparticles having different molar ratios of the two compounds were prepared; the best results were obtained with the most active nanosuspension (molar ratio **14/15** 23 :1).

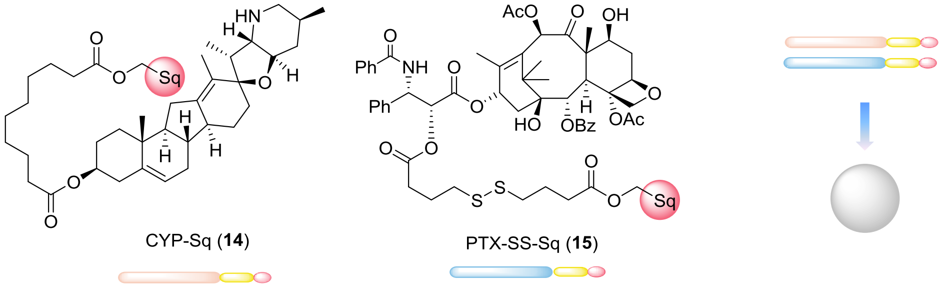

Figure 23. Structures of conjugates **14** and **15**.

Nanoparticles Characterization

Hetero-nanoparticles were prepared by solvent-displacement method and they were characterized using DLS (**Table 5**) and the morphology was evaluated by AFM (**Figure 24**).

Compound	Mean Diameter (nm)	Z potential (mV)
14	240±2	+38.4±4.3
15	437±5	-35.7±0.1
14/15	229±2	+26.4±1.7

Table 5. Diameter and Z potential of the obtained nanoparticles.

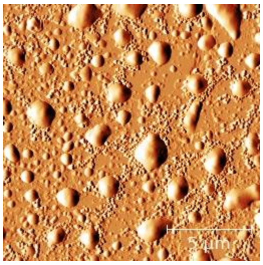

Figure 24. AFM picture showing the morphology of **14**/**15** hetero-nanoparticles (molar ratio 23:1).

In vitro evaluation

Biological evaluation of hetero-nanoparticles (**Table 6**) showed that the activity of the two drugs was maintained and comparable to the activity of nanoassemblies of compounds **14** and **15** in different cellular systems, that is, OVCAR5 (ovarian cancer cell) and #83 and #110 (ovarian tumor-initiating cells).[122]

Compound	IC_{50} (μM)			
	#83	**#110**	**OVCAR5**	**U251**
CYP	> 50	> 50	> 50	30
14	34	40	42	40
15	< 3	< 3	< 3	4
14/15	16	15	32	28

Table 6. IC_{50} values determined with different cell lines.

The induction of apoptosis (**Figure 25**) showed a combined effect. It is worth noting that the IC_{50} value reported for **14/15** NPs refers to sum of the concentrations of the two compounds assembled in the hetero-nanoparticles: this means that for the reported values 23/24 is due to compound **14** and 1/24 to compound **15**. As an example, the IC_{50} obtained for **14/15** in U251 cells corresponds to a concentration of compound **15** equal to 1.2 mm and to a concentration of compound **14** equal to 26.8 mm, both lower than the IC_{50} obtained for the corresponding homo-nanoparticles.

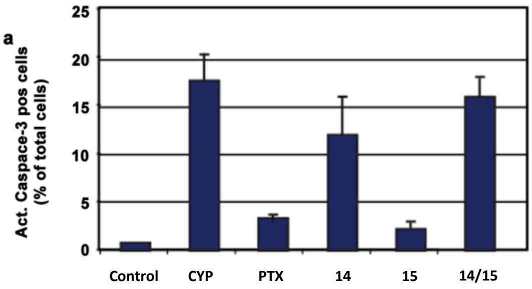

Figure 25. Apoptosis of the U251 glioblastoma cell line, 24h upon addition of the mentioned compounds; CYP (Cyclopamine): 2.07 µM; PTX (Paclitaxel): 0.094 µM; **14**: 2.07 µM; **15**: 0.094 µM; **14**/**15** (NP): 2.07 µM / 0.094 µM.

2.3.3 Cyclopamine-Paclitaxel-Tetramethylrhodamine hetero-nanoparticles

Next, we aimed to monitor the ability of the hetero-nanoparticles to pass through the cell membrane in biological media. In order to apply fluorescence microscopy, we assembled hetero-NPs that incorporated a squalene–tetramethylrhodamine (TAMRA) conjugate (**16**). TAMRA was chosen as a fluorescent dye because it is used in super-resolution localization microscopy techniques such as dSTORM (direct stochastic optical reconstruction microscopy).[123]

Synthesis of the conjugate

The fluorescent squalene conjugate was synthesized by reaction of tetramethylrhodamine isothiocyanate with compound **7** in the presence of sodium hydride (**Scheme 6**).

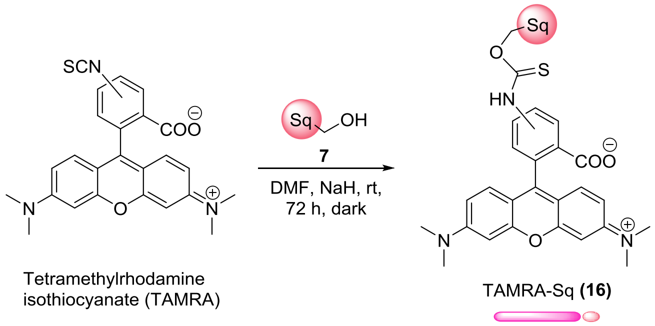
SCN
COO
N
O
N
Tetramethylrhodamine isothiocyanate (TAMRA)
Sq
OH
7
DMF, NaH, rt, 72 h, dark
Sq
O
S
HN
COO
N
O
N
TAMRA-Sq (16)

Scheme 6. Synthesis of the fluorescent squalene conjugate TAMRA-Sq.

Nanoparticles characterization

The fluorescent hetero-nanoparticles were obtained by the solvent-displacement method by mixing compounds **14**, **15** and **16** in a 23:1:15 molar ratio; we confirmed by DLS the formation of the nanoparticles (mean diameter: 224±2 nm, zeta potential: + 43.5±3.4 mV).

In vitro evaluation

Breast cancer MCF-7 cells were treated with the fluorescent hetero-nanoparticles for 20 min and imaged by multiple fluorescence microscopy methods. Three-dimensional confocal microscopy (**Figure 26**) allowed the identification of the fluorescent nanoparticles in the cytoplasm of the cells, providing evidence that the nanoparticles are capable of permeating the cellular membrane.

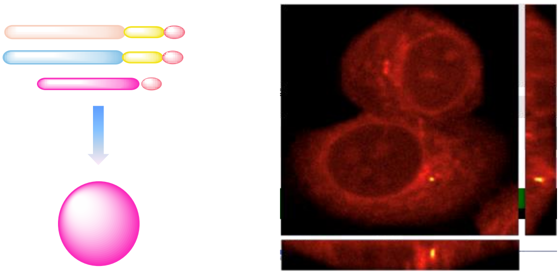

Figure 26. Cellular imaging of three-component **14**/**15**/**16** hetero-NPs. Confocal imaging of cells treated for 20 min with fluorescent hetero-nanoparticles. Displayed are the orthogonal projection of the three-dimensional stack for two MCF-7 cells. The bottom cell shows a bright fluorescent dot (a putative hetero-NP) in the cytoplasmplasm close to the nucleus.

However, to provide an estimation of the size of the nanoparticles, the resolution of conventional microscopy is not sufficient. We therefore applied super-resolution microscopy (dSTORM)[124] to quantify the diameter of the bright particles detected inside the cells. **Figure 27** shows images of the cells recorded after 1.5 h of incubation. The enlarged detail of the nanoparticle served to quantify its diameter: 156 nm. The diameter is in good agreement with our previous measurements by DLS (224±2 nm).

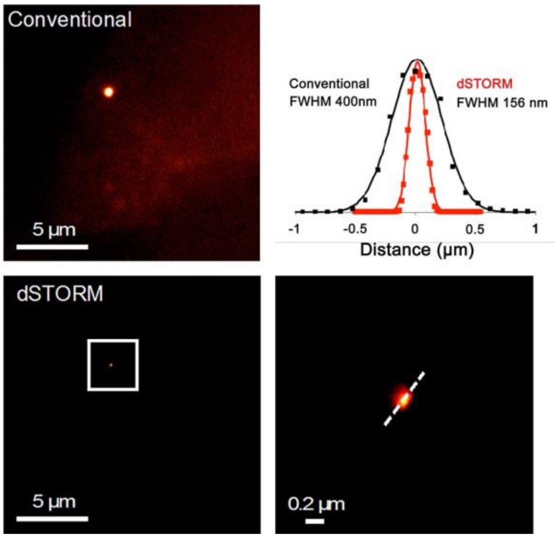

Figure 27. Cellular imaging of three-component hetero-NPs. Results obtained from application of super-resolution dSTORM: shown are the conventional widefield image (top left) and the super-resolution image (bottom left) of the same cell together with a enlarged detail of the NP (bottom right) and the quantification of the diameter of the shown NP in the conventional and the super-resolution image (top right). FWHM = full width at half maximum.

In order to monitor the behaviour of the internalized nanoparticles, we performed dStorm imaging at different incubation times. In this way we confirmed (**Table 7**) a progressive increase in the variability of the nanoparticle diameter—as indicated by the increase in the coefficient of variation—which might be an indication of their tendency to disassemble.

Time after incubation (h)	Mean Diameter (nm)	Coefficient of variation	Number of cells
0.5	147±17	0.12	10
1	140±31	0.22	10
1.5	178±63	0.36	12

Table 7. Mean diameter of three-component hetero-NPs (**14**/**15**/**16** = 23:1:15) at different times after the incubation.

We have demonstrated the possibility of forming hetero-nanoparticles containing two different drugs and we also established that the two drugs that do not influence each other's activity. We confirmed the possibility of following the internalization mechanism by the addition of a third dye-based compound using super-resolution microscopy.

The functionalization of different known drugs with a cleavable linker and a proper lipophilic chain that induces self-assembly and the generation of hetero-nanoparticles could be exploited for personalized treatment of different types of diseases, and it may be possible to trace these nanoparticles in the cells by imaging.

2.4 Cyclopamine-Doxorubicin hetero-nanoparticles

Pursuing our interest in self-assembled nanoparticles, we investigated he combination of cyclopamine (CYP) and doxorubicin (DOXO) conjugates (**Figure 28**) with the aim to demonstrate the formation of hetero-NPs that could improve the performance given by the use of the simple parental drugs.[125]

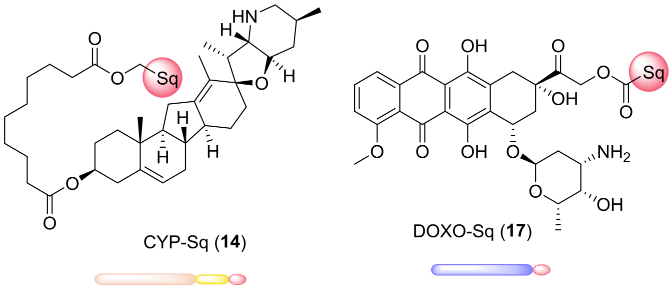
CYP-Sq (**14**)

DOXO-Sq (**17**)

Figure 28. Structure of the CYP and DOXO conjugates.

Specifically, we decided to investigate the combination of cyclopamine-squalene (CYP-Sq) derivative **14**, active on different types of cancer cells as previously cited, with doxorubicin-squalene (DOXO-Sq) **17**, described as able to improve the anticancer efficacy and the therapeutic index of DOXO.[126]

Doxorubicin

Doxorubicin (DOXO), isolated from the bacterium *Streptomyces peucetius var. caesius*, is an anthracycline antibiotic and it is the 14-hydroxylated congener of daunorubicin (**Figure 29**).

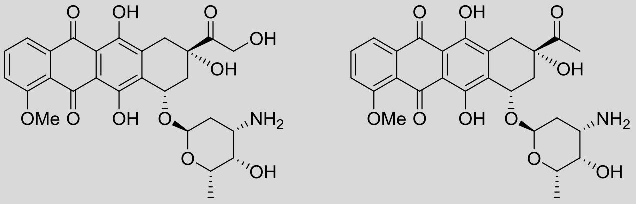
Doxorubicin (DOXO)

Daunorubicin

Figure 29. *Structures of doxorubicin and daunorubicin.*

Doxorubicin intercalates between base pairs in the DNA helix, thereby preventing DNA replication and ultimately inhibiting protein synthesis. Additionally, doxorubicin inhibits topoisomerase II which results in an increased and stabilized cleavable enzyme-DNA linked complex during DNA replication and subsequently prevents the ligation of the nucleotide strand after double-strand breakage. Doxorubicin also forms oxygen free radicals resulting in cytotoxicity secondary to lipid peroxidation of cell membrane lipids; the formation of oxygen free radicals also contributes to the toxicity of the anthracycline antibiotics, namely the cardiac and cutaneous vascular effects.

Doxorubicin is one of the leading anticancer drugs in clinical oncology with a broad spectrum of activity against various solid and hematologic neoplastic diseases. The effectiveness of doxorubicin is impeded by acute and subacute side effects, mainly dose-limiting irreversible cardiotoxicity and myelosuppression.[127] In an attempt to reduce the side-effects of doxorubicin and to improve its anticancer efficacy, various nanocarriers of doxorubicin and daunorubicin have been developed, including micelles, dendrimers, solid-lipid, and polymer nanoparticles.[128,129,130,131,132]

Nanoparticles characterization

Hetero-NPs were obtained by mixing two squalene conjugates, CYP-Sq (**14**) and DOXO-Sq (**17**), prepared according to the previously described approaches[126]. All NPs were prepared by solvent-displacement method, using THF as organic solvent and without adding any surfactant.

Five different nanosuspensions were prepared:

- NP0: CYP-SQ (10 µM)
- NP1: CYP-SQ/DOXO-SQ 1:1 (10 µM, 10 µM)
- NP2: CYP-SQ/DOXO-SQ 5:1 (10 µM, 2 µM)
- NP3: CYP-SQ/DOXO-SQ 10:1 (10 µM, 1 µM)
- NP4: DOXO-SQ (10 µM)

14 and **17** were co-nanoprecipitated at 1:1, 5:1, 10:1 molar ratios (**Table 8**, NP1, NP2 and

NP3 respectively) with a constant concentration of **14**, giving a suspension of narrow monodispersed NPs. **14** and **17** were also separately nanoprecipitated to obtain NPs of CYP-Sq or DOXO-Sq alone (**Table 8**, NP0 and NP4).

All the formulations were characterized in terms of mean diameter and zeta potential of the NPs. As showed in **Table 8**, CYP-Sq and DOXO-Sq alone spontaneously self- assembled in water forming NPs; however, DOXO-Sq NPs displayed a larger mean diameter of about 400 nm. When DOXO-Sq was formulated with an equimolar amount of CYP-Sq (NP1), the mean size drastically reduced from 400 to about 130 nm; in these conditions DOXO-SQ probably took a different supramolecular organization and mutual interactions between the two squalene conjugates caused the formation of smaller nanoparticles. The addition of DOXO-Sq in various molar ratios did not influence the mean size of CYP-SQ NPs. The zeta potential of all NPs is highly positive; for NPs containing DOXO-Sq it is higher than the one of CYP-Sq-containing NPs. After 4-weeks storage at 4°C in water, no appreciable NPs size and/or zeta potential changes were detected by DLS for all formulations and no NPs aggregation was observed. After dilution with fetal bovine serum, NP1 did not show aggregation, even after 24 h at 4°C. On the contrary, the incubation in PBS 10 mM resulted in an increase of the NP1 mean diameter up to about 400 nm (700 nm after 24 h).

	Mean Diameter (nm)	**Polydispersity index**	**Z potential (mV)**
NP0	127.8±0.723	0.106	+44.1±2.048
NP1	126.9±1.108	0.102	+61.6±4.18
NP2	129.4±1.589	0.109	+50.9±0.404
NP3	127.7±0.734	0.106	+56.8±2.66
NP4	395.4±6.739	0.122	+58.1±0.643

Table 8. Nanoparticles characterization.

In vitro evaluation

With the aim to confirm the maintenance of the biological activity of the parental drugs, and in particular of DOXO, the obtained NPs and the relative single conjugates **14** and **17** were evaluated on 4 ovarian cancer cell lines (A2780, IGROV, OVCAR432 and OVCAR433) with similar results. **Figure 30** reports the results obtained in IGROV cells. As illustrated in **Figure 30**, NP1 was the most active NP formulation with a cytotoxic activity similar to CYP:DOXO (1:1) and to DOXO (10µM). In all these cell lines CYP was not very active, likely to the fact that these cells do not have an activated Hedgehog pathway.

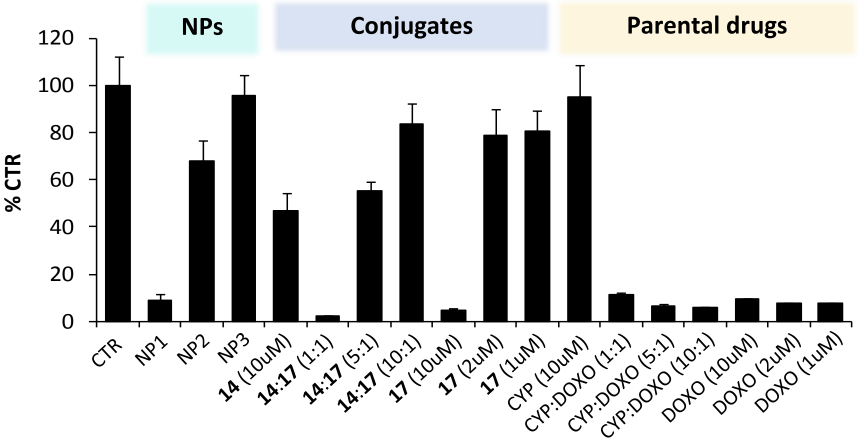

Figure 30. Cytotoxic activity of the different NP formulation and single or combined treatment agents in IGROV ovarian cancer cell line. Concentration of the samples: NP1: [CYP-SQ]=[DOXO-SQ]= 10 µM; NP2: [CYP-SQ]=10 µM, [DOXO-SQ]=2 µM; NP3: [CYP-SQ]=10 µM, [DOXO-SQ]=1 µM; **14**:**17** (1:1): [CYP-SQ]=[DOXO-SQ]=10 µM; **14**:**17**(5:1): [CYP-SQ]=10 µM, [DOXO-SQ]=2 µM; **14**:**17**(10:1): [CYP-SQ]=10 µM, [DOXO-SQ]=1 µM; CYP:DOXO (1:1): [CYP]=[DOXO]=10 µM, CYP:DOXO (5:1): [CYP]=10 µM, [DOXO]=2 µM, CYP:DOXO (10:1): [CYP]=10 µM, [DOXO]=1 µM.

In vitro evaluation: cell internalization

As the best cytotoxic activity was observed with NP1 formulation, we next verified the dynamic of its internalization into ovarian cancer cells. To this aim, we applied confocal microscopy on cultured IGROV cells at different time points (i.e. 1.5, 4 and 24 h) following incubation with hetero-nanoparticles NP1 (**Figure 31**). Longer incubation with the NPs resulted in the increase of the intracellular fluorescence in the 560-660 nm band, corresponding to the emission of DOXO. Interestingly at the latest point (24 h), DOXO is observed in the cell nucleus, suggesting that the active compound can be released from the hetero-NPs to reach the nuclear compartment.

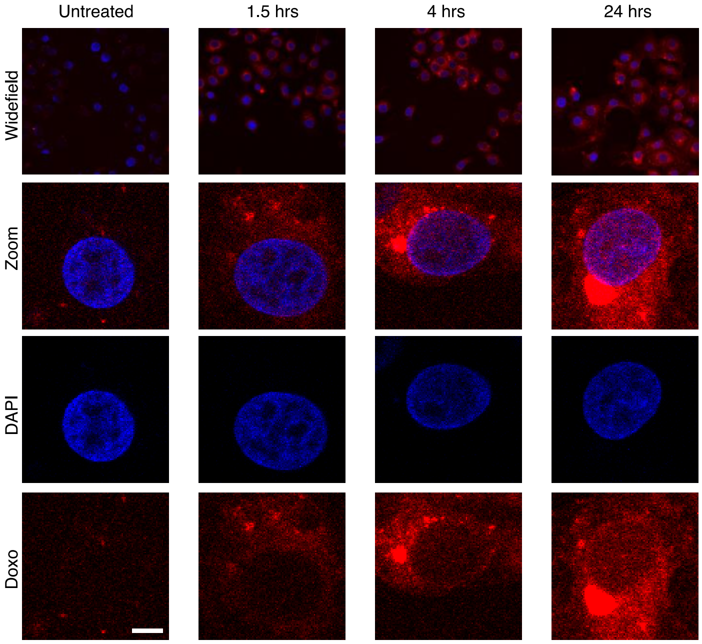

Figure 31. Confocal microscopy on cultured IGROV cells at different times (i.e. 1.5, 4 and 24 h) following incubation with hetero-nanoparticles NP1.

In vitro evaluation: cellular system with an activated Hedgehog pathway

We next investigated in details the effect of the NPs in a cellular system with an activated Hedgehog pathway. Specifically, we used the human epidermoid carcinoma cell line A431, which carries a single point mutation in exon 23 of both alleles of Patched1 gene, resulting in a proline to leucine substitution and subsequent constitutive activation of the Hedgehog pathway.[133] In a similar experimental setting, we studied the inhibition of proliferation and the apoptosis induction upon addition of CYP, DOXO and distinct ratios of CYP:DOXO, conjugate **14**, conjugate **17** and distinct ratios of **14** and **17**, free or assembled in NPs.

DOXO alone at 10 µM (**Figure 32 A**) was able to inhibit proliferation of more than 50%, and the addition of CYP further enhanced the cytostatic effect. The combination of **14** and **17** in 1:1 molar ratio also resulted in inhibition of proliferation, although to a lesser extent. Interestingly, when NP1 was used, cell proliferation is essentially entirely blocked. The same trend appears when investigating cell death, with CYP and derivative **14** not causing significant apoptosis, DOXO and derivative **17**, alone or in combination with CYP or derivative **14** inducing apoptosis in 30-60% of the cells, while when assembled in NP1, practically all cells are dead (**Figure 32 B**). Notably, while apoptosis is only observed at the 1:1 ratio of CYP:DOXO or of derivatives **14** and **17**, inhibition of proliferation could be observed also at the ratio 5:1, potentially indicating that either lower concentration of DOXO or derivative **17** is necessary for the cytostatic function, or that apoptosis is a later stage event in this system.

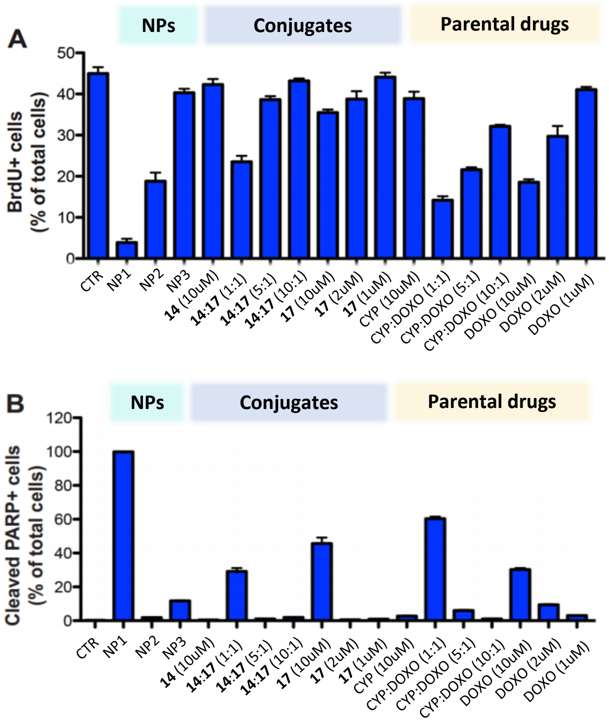

Figure 32. Effect on proliferation (A) and viability (B) in the A431 cancer cell line of cyclopamine, doxorubicin (reported as Parental drugs), compounds 1 and 2 not nanoprecipitated (reported as Conjugates) and nanoprecipitated compounds 1 and 2 (reported as NP). Concentration of the samples: NP1 (nanoprecipitated CYP-Sq = DOXO-Sq = 10 µM); NP2 (nanoprecipitated CYP-Sq = 10 µM, DOXO-Sq = 2 µM; NP3 (nanoprecipitated CYP-Sq = 10 µM, DOXO-Sq = 1 µM; **14**:**17** (1:1): CYP-Sq = DOXO-Sq = 10 µM; **14**:**17** (5:1): CYP-Sq = 10 µM, DOXO-Sq = 2 µM; **14**:**17** (10:1): CYP-Sq = 10 µM, DOXO-Sq = 1 µM; CYP:DOXO (1:1): CYP = DOXO = 10 µM, CYP:DOXO (5:1): CYP = 10 µM, DOXO = 2 µM, CYP:DOXO (10:1): CYP = 10 µM, DOXO = 1 µM. Statistical significance (Student's t test) compared to Control: ns, $p>0.01$; *, $p < 0.01$; **, $p<0.001$; ***, $p<0.0001$.

Given the strong cytostatic and cytotoxic effect of the 10 µM equimolar concentration of CYP:DOXO and **14** and **17**, free or assembled in NP1, we sought to investigate the dose response of A431 cells to these formulations, so as to define the lowest concentration required for a toxic effect. As shown in **Figure 33**, NP1 has a significant cytotoxic and cytostatic effect already at 2.5 µM, while the free drugs require at least 3-fold higher concentration to induce apoptosis. Small differences in the percentage of proliferating cells treated with 10 µM of compounds in the sets of experiments presented in the **Figure 32 A** and **Figure 33 A** are a result of difference in confluence, since the first set of experiments was performed in 6-well plates and the latter in 24-well plates. Our results show that the combination of the compounds **14** and **17** assembled in NP1 exhibit strong cytotoxic and cytostatic effect on cells requiring Hedgehog signalling even at low concentrations.

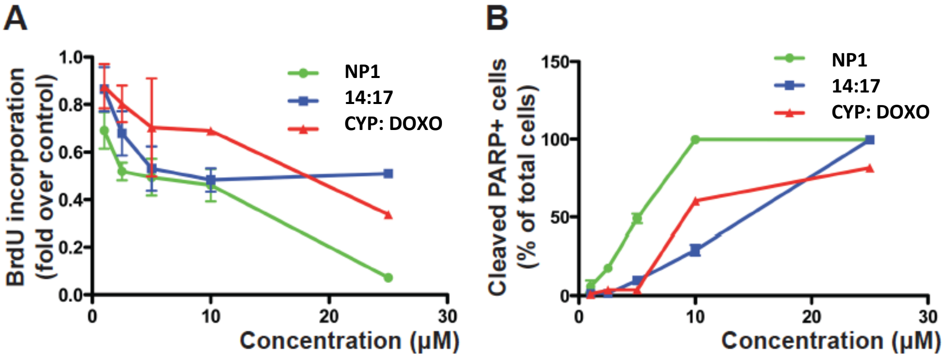

Figure 33. Dose response of equimolar concentrations of CYP and DOXO as parental drugs (CYP:DOXO), conjugates (**14**:**17**) or assembled in nanoparticles (NP1). The effect on proliferation (A) and their cytotoxic potential (B) is estimated by FACS analysis of BrdU incorporation and cleaved PARP immunostaining respectively. Concentration of the samples: NP1: [CYP-SQ]=[DOXO-SQ]= 10 μM; **14**:**17**(1:1): [CYP-SQ]=[DOXO-SQ]=10 μM; CYP:DOXO (1:1): [CYP]=[DOXO]=10 μM.

In vivo evaluation

Given the very promising results obtained by the *in vitro* experiments using cell lines, we sought to investigate whether these results could also be observed *in vivo*, now investigating both the antitumor activity and the toxicity of the formulation. We used a xenograft model, injecting A431 cells into the flank of immunosuppressed mice. When tumours reached 3 mm in diameter, mice were administered intraperitoneally twice weekly equimolar concentrations (4 mg/kg of derivative **14** and 5mg/kg of derivative **17**) of **14**, **17** and **14** /**17** free or assembled in NP1, or solely the vehicle. Strikingly, when the derivative **17** is injected as a free drug, alone or together with **14**, it induces very high toxicity and the mice die or have to be sacrificed due to weight loss and general health deterioration less than a week after treatment initiation (**Figure 34 A**). The derivative **14** alone is not toxic, but does not have an effect on tumour growth. Although, when the same concentration of **14**/**17** is administered as self- assembled NPs, there is no toxicity and there is a significant delay in tumour growth compared to the control mice **(Figure 34 B**).

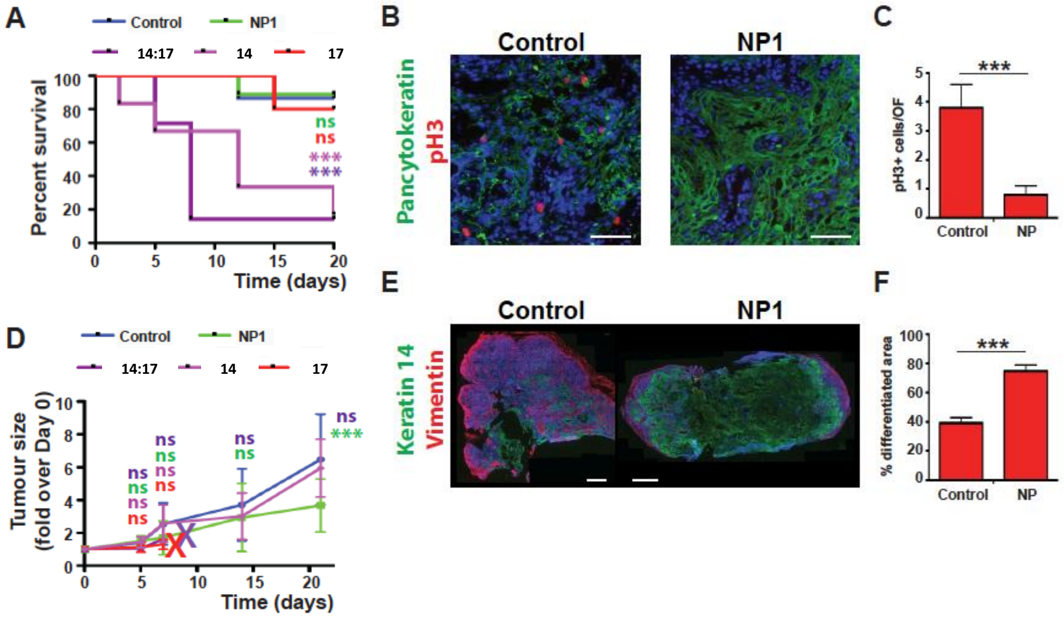

Figure 34. *In vivo* effect of equimolar concentration of CYP and DOXO conjugates, alone or in combination, or assembled in nanoparticles (NP1). (A) Kaplan Meier survival plot of mice upon treatment-administration, as indicated, twice weekly. Note that conjugate **17** alone or in combination with conjugate **14** exhibits high toxicity. (B) Representative immunofluorescence images of tumours from mice treated with NP1 or vehicle, stained for pH3 labelling cells undergoing mitosis. Note the inhibition of proliferation upon treatment with NP1. The antibodies are colour-coded. (C) Histogram illustrating the quantification of proliferating cells in mice treated with NP1 or vehicle, as illustrated in (B). Results are expressed as pH3+ cells per optical field. (D) Follow up of tumour size over time, upon treatment as described in (A). 20 random images per tumour form 3 separate tumours were counted. (E) Representative mosaic immunofluorescent images of tumours from mice treated with NP1 or vehicle, stained with Keratin 14 indicating differentiated cancer cells and vimentin labelling tumour-associated fibroblasts and cells undergone epithelial-mesenchymal transition. Note the striking difference in the differentiation of the tumours. The antibodies are colour-coded. (F) Histogram illustrating the quantification of differentiated areas in tumours from mice treated with NP1 or vehicle, based on the expression of Keratin 14. 20 random images per tumour form 3 separate tumours were counted. Concentration of the samples: NP1: CYP-SQ = DOXO-SQ = 10 μM; **14**:**17**(1:1): CYP-SQ = DOXO-SQ =10 μM; **14** = 10 μM; **17** = 10 μM. Statistical significance (Student's t test): ns, $p>0.01$; ***, $p<0.0001$. Scale bars: Panel B, 100 μm; Panel E, 1000 μm.

Microscopic analysis of tumours from control mice and mice treated with NP1, 3 weeks after treatment, showed that the latter exhibit very strong inhibition of proliferation (**Figure 34 C**, **D**) and a more differentiated phenotype (**Figure 34 E, F**). The latter could have important implications in moderating the metastatic potential, although longer experiments should be performed to investigate this possibility. Therefore, our *in vivo* experiments unambiguously show that self-assembled NPs reduce tumour growth and toxicity of chemotherapy; this could enable the administration of higher doses, thus more effective cancer treatment.

The results obtained demonstrated that the approach of the self-assembled hetero NPs is a promising way to treat different types of cancer cells and it makes possible to modulate the ratio of the combined drugs. Moreover, these results point out the possible application of this approach in the personalized therapy.

Experimental Procedures

General

Thin-layer chromatography (TLC) was performed on Merck precoated 60F254 plates. Reactions were monitored by TLC on silica gel, with detection by Uv light (λ = 254 nm) or by charring with 1% permanganate solution. Flash chromatography was performed using Silica gel (240-400 Mesh, Merck). NMR spectra were recordered with Brucker 300 and 400 MHz spectrometers. Chemical shifts are reported in parts per million (δ) downfield from tetramethylsilane (TMS). EI mass spectra were recorded at an ionizing voltage of 6 kEv on a VG 70-70 EQ. ESI mass spectra were recorded on FT-ICR APEXII. Specific rotations were measured with a P-1030-Jasco polarimeter with 10 cm optical path cells and 1 ml capacity (Na lamp, λ = 589 nm). Microwave assisted reaction were performed with Emrys Creator single-mode (power range 0-400 W from magnetron at 2.45 GHz).

Synthesis of 4

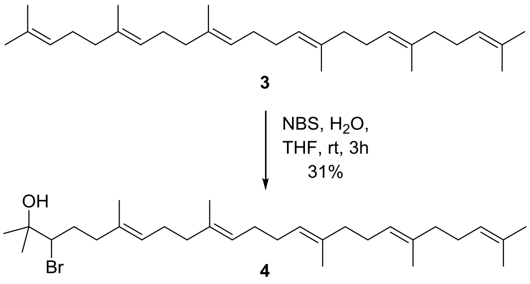

To a solution of squalene (**3**, 4.290 g, 0.010446 mol) in THF (30 mL) H_2O (5 mLl) is added and then THF is dropwise added to obtain a clear solution. N-bromosuccinimide (2.231 g, 0.012535 mol) is portionwise added and the reaction mixture is stirred at room temperature for 3h. The solvent is removed under reduced pressure, brine (100 mL) is added and extracted with AcOEt (5x20 mL). The organic layers are dried over Na_2SO_4 and the solvent is removed under reduced pressure. The crude is purified by flash chromatography (CH_2Cl_2:Hex 1:1) to obtain **4** as a pale-yellow oil (1.652 g, Yield: 31%).

^{1}H-NMR ($CDCl_3$, 400 MHz): δ(ppm)= 5.10-5.25 (m, 5H); 4.01 (dd, *J*=11.3 Hz, *J*=1.9 Hz, 1H), 2.32-2.35 (m, 1H), 1.95-2.17 (m, 18H); 1.77-1.88 (m, 1H), 1.70 (s, 3H), 1.63 (bs, 15H), 1.37 (s, 3H), 1.36 (s, 3H).

^{13}C-NMR ($CDCl_3$, 100 MHz): δ(ppm)= 135.11, 134.89, 132.97, 131.24, 126.03, 124.47, 124.26, 72.44, 71.01, 39.73, 38.18, 32.17, 28.28, 26.68, 25.75, 17.68, 16.03, 15.85.

APCI-MS: m/z 507.3 $[M]^+$.

Synthesis of 5

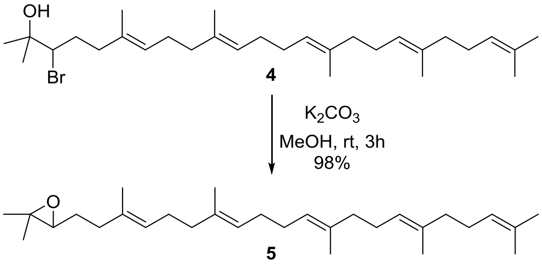

To a solution of **4** (1.652 g, 0.003258 mol) in MeOH (60 mL) K_2CO_3 (0.898 g, 0.006517 mol) is added and the reaction mixture is stirred at room temperature for 2 h, then concentrated under reduced pressure. H_2O (120 mL) is added and extracted with AcOEt (4x30 mL). The organic layers are dried over Na_2SO_4 and the solvent is removed under reduced pressure to obtain **5** as a yellow oil (1.360 g, Yield: 98%) without any further purification.

^{1}H-NMR ($CDCl_3$, 300 MHz): δ(ppm)= 5.06-5.17 (m, 5H), 2.69 (t, *J*=6.1 Hz, 1H), 1.95-2.19 (m, 20H), 1.68 (s, 3H), 1.60 (s, 3H), 1.58 (bs, 12H), 1.28 (s, 3H), 1.24 (s, 3H).

^{13}C-NMR ($CDCl_3$, 100 MHz): δ(ppm)= 135.06, 134.89, 133.96, 131.18, 124.93, 124.26, 64.17, 58.27, 39.72, 36.31, 28.25, 27.46, 25.69, 24.89, 18.72, 17.67, 16.00.

APCI-MS: m/z 427.3 $[M+1]^+$.

Synthesis of 6

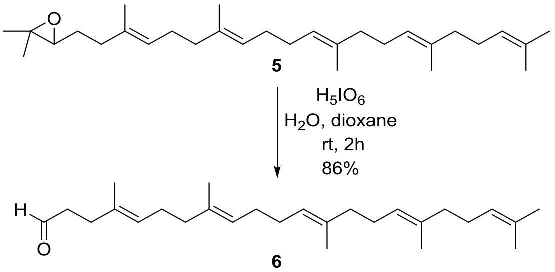

To a solution of H_5IO_6 (1.379 g, 0.006058 mol) in H_2O (5 mL) a solution of **5** (1.434 g, 0.003366 mol) in dioxane (12 mL) is added and the reaction mixture is stirred at room temperature for 2h. H_2O (150 mL) is added and extracted with AcOEt (3x40 mL). The organic layers are washed with brine (100 mL) and H_2O (100 mL), then dried over Na_2SO_4 and concentrated under reduced pressure to obtain **6** as a pale yellow oil (1.111 g, Yield: 86%) without any further purification.

^{1}H-NMR ($CDCl_3$, 300 MHz): δ(ppm)= 9.73 (s, 1H), 5.06-5.13 (m, 5H), 2.49 (t, *J*=7.1 Hz, 2H), 2.30 (t, *J*=7.1 Hz, 2H), 1.97-2.10 (m, 16H), 1.67 (s, 3H), 1.55 (bs, 15H).

^{13}C-NMR ($CDCl_3$, 75 MHz): δ(ppm)= 202.65, 135.11, 134.88, 134.77, 132.86, 131.23, 125.41, 124.52, 124.37, 124.25, 67.06, 42.14, 39.73, 39.51, 31.83, 28.24, 26.73, 26.62, 25.68, 17.66, 16.01.

APCI-MS: m/z 385.3 $[M+1]^+$.

Synthesis of 7

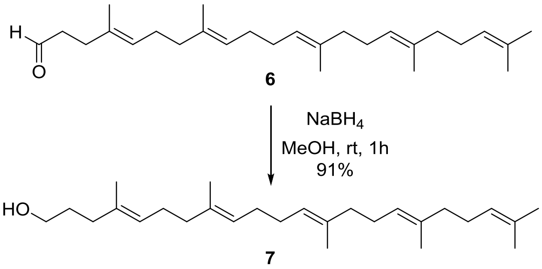

To a solution of **6** (1.111 g, 0.002893 mol) in MeOH (45 mL) $NaBH_4$ (0.055 g, 0.001446 mol) is portionwise added and the reaction mixture is stirred at room temperature for 1 h. HCl 1M is added to quench the unreacted $NaBH_4$. The solvent is the removed under reduced pressure, H_2O (150 mL) is added and extracted with AcOEt (3x40 mL). The organic layers are dried over Na_2SO_4 and concentrated under reduced pressure to obtain **7** as a colorless oil (1.016 g, Yield: 91%) without any further purification.

^{1}H-NMR ($CDCl_3$, 300 MHz): δ(ppm)= 5.08-5.13 (m, 5H), 3.61 (t, *J*=6.3 Hz, 2H), 1.99-2.08 (m, 18H), 1.78-1.85 (m, 2H), 1.67 (s, 3H), 1.59 (s, 15H).

^{13}C-NMR ($CDCl_3$, 75 MHz): δ(ppm)= 135.11, 134.92, 134.54, 131.24, 125.83, 124.42, 124.26, 62.80, 39.72, 35.99, 30.73, 28.24, 26.60, 25.67, 17.66, 15.99.

APCI-MS: m/z 387.3 $[M+1]^+$.

Synthesis of 8

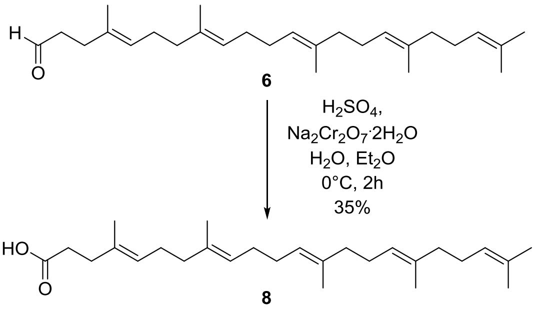

Sodium dichromate dihydrate (6.350 g, 0.021780 mol) was slowly added at 0°C to a solution of sulfuric acid (11.600 mL, 0.217796 mol) in H_2O (110 mL). The resulting solution was then added to a solution of **6** (7.940 g, 0.021778 mol) in Et_2O (160 mL) and stirred at 0 °C for 2 h. The reaction mixture was washed with brine (3 x 1000 mL) until neutral pH, then dried over Na_2SO_4 and evaporated under reduced pressure. The crude material was purified by flash chromatography (petroleum ether/Et_2O 95:5) obtaining **8** as a colorless oil (2.862 g, Yield: 35%).

^{1}H-NMR (Acetone-*d$_6$*, 300 MHz): δ (ppm) = 5.11 (m, 5H), 2.38 (t, *J*=7.1 Hz, 2H), 2.26 (t, *J*=7.1 Hz, 2H), 2.13-1.86 (m, 16H), 1.65-1.59 (m, 15H), 1.26 (s, 3H).

EI-MS: m/z 400 $[M]^+$.

Synthesis of 1

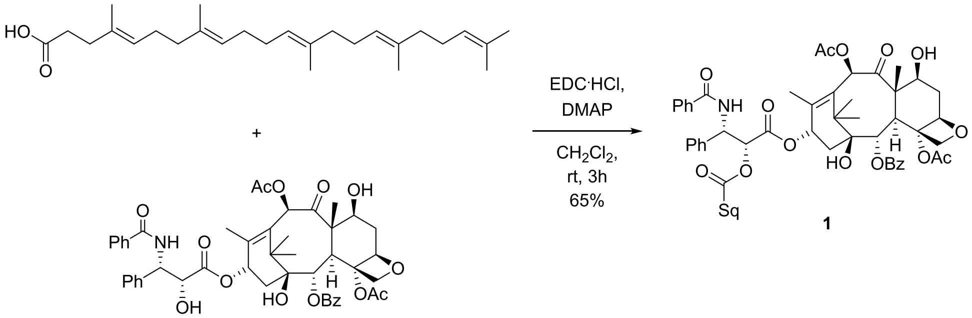

To a solution of paclitaxel (1.200 g, 0.001405 mol) in CH_2Cl_2 (30 mL) EDC·HCl (0.270 g, 0.001405 mol), DMAP (0.120 g, 0.000983 mol) and **8** (0.562 g, 0.001405 mol) were added and the reaction mixture was stirred at room temperature for 3 h. The reaction mixture was then extracted with HCl 0.1 M (3 x 15 mL), the organic layers were dried over Na_2SO_4 and evaporated under reduced pressure. The crude material was then purified by flash chromatography (CH_2Cl_2/AcOEt from 95:5 to 80:20) affording **1** as a white solid (1.128 g, Yield: 65%).

^{1}H NMR ($CDCl_3$, 300 MHz): δ (ppm) = 8.13 (d, *J* = 7.3 Hz, 2H), 7.75 (d, *J* = 6.9 Hz, 2H), 7.62 (t, *J* = 7.1 Hz, 1H), 7.53-7.49 (m, 3H), 7.43-7.35 (m, 7H), 6.91-6.85 (m,1H), 6.35 (s, 1H), 6.24-6.19 (m, 1H), 5.99-5.88 (m, 1H), 5.69-5.65 (m, 1H), 5.53-5.48 (d, 1H), 5.20-5.16 (m, 5H), 4.97-4.90 (m, 1H), 4.44-4.39 (m, 1H), 4.33-4.28 (m, 1H), 4.20-4.16 (m, 1H); 3.85-3.81 (m, 1H), 2.55-2.48 (m, 1H), 2.49 (s, 3H), 2.45-2.38 (m, 2H), 2.30-2.27 (m, 2H), 2.23 (s, 3H), 2.09 (s, 3H), 2.00-1.98 (m, 16H), 1.97-1.95 (m, 1H), 1.75-1.69 (m, 1H), 1.67 (s, 3H), 1.61-1.55 (m, 18H), 1,28-1.23 (m, 1H), 1.21 (s, 3H), 1.13 (s, 3H).

ESI-MS: m/z 1237.2 $[M+H]^+$.

Synthesis of 2

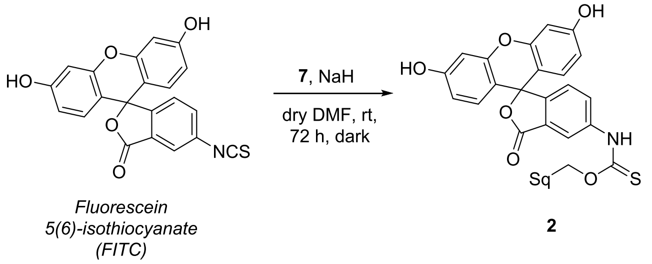
OH
HO
O
NCS
Fluorescein
5(6)-isothiocyanate
(FITC)
7, NaH
dry DMF, rt,
72 h, dark
NH
Sq
S
2

To a solution of **7** (0.040 g, 0.000103 mol) in dry DMF (2 mL) NaH (0.003 g, 0.000103 mol) was added and stirred at room temperature for 3 h. Then FITC (0.041 g, 0.000103 mol) was added and the reaction was stirred in the dark at room temperature for 72 h. Then the volatiles were removed under reduced pressure affording **2** without any further purification.

^{1}H-NMR: ($CDCl_3$, 300 MHz): δ(ppm)= 7.20-6.50 (m, 9H), 5.23-5.00 (m, 5H), 4.55 (bs, 1H), 4.10 (t, *J*=7.1 Hz, 2H), 2.19-1.72 (m, 20H), 1.65 (s, 3H), 1.57 (bs, 15H).

ESI-MS: m/z 775.7 $[M-2]^+$.

Synthesis of 10

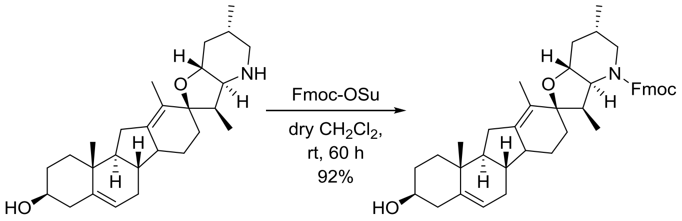

10

To a solution of cyclopamine (0.045 g, 0.000109 mol) in dry CH_2Cl_2 (2 mL) Fmoc-OSu (0.044 g, 0.000131 mol) is added and the reaction mixture is stirred at room temperature for 60 h. The solvent is then removed under reduced pressure and the crude material is purified by flash chromatography (CH_2Cl_2/MeOH 10:0.05) to obtain **10** as a white solid (0.062 g, Yield: 92%).

^{1}H-NMR: ($CDCl_3$, 300 MHz): δ(ppm)= 7.72 (dd, *J*= 7.2, 7.2 Hz, 2H), 7.58 (dd, *J* = 7.2, 2 Hz, 2H), 7.37 (dd, *J*= 16, 7.2 Hz, 2H), 7.30 (ddd, *J*=14.8, 7.2, 1.2 Hz, 2H), 5.37 (br d, *J*= 2.8 Hz, 1H), 4.68 (dd, *J*= 10.8, 5.2 Hz, 1H), 4.57 (dd, *J*= 10.8, 5.6 Hz, 1H), 4.21 (dd, *J*= 5.2, 5.6 Hz, 1H), 3.54 (dd, *J*=12.8, 4.0 Hz, 2H), 3.44 (ddd, *J*= 11.6, 11.6, 4.0 Hz, 1H), 2.95 (dd, *J*= 9.6, 7.2 Hz, 1H), 2.75 (dd, *J*= 12.8, 8.4 Hz, 1H), 2.39-2.35 (m, 1H), 2.30-2.09 (m,5H), 1.75 (s, 3H), 1.85-1.63 (m, 5H), 1.59-1.49 (m, 1H), 1.46-1.39 (m, 4H), 1.35-1.27 (m, 1H), 1.23 (ddd, *J*= 13.2, 3.2, 3.2 Hz, 1H), 1.02-0.88 (m, 2H), 0.93 (d, *J*= 6.8 Hz, 3H), 0.93 (s, 3H), 0.6 (s, 3H).

^{13}C-NMR: ($CDCl_3$, 100 MHz): δ(ppm)= 157.94, 143.97, 143.87, 142.59, 141.69, 141.45, 141.39, 127.65, 127.62, 127.09, 127.06, 126.66, 124.58, 121.79, 119.99, 119.95, 84.76, 72.63, 71.73, 66.58, 52.05, 51.05, 49.19, 47.31, 41.78, 41.57, 41.50, 38.21, 36.56, 35.22, 32.63, 31.35, 31.08, 30.89, 29.00, 28.28, 24.60, 20.26, 18.66, 13.63, 10.23.

ESI-MS: m/z 634.67 $[M+ H]^+$.

$[\alpha]_D^{32}$= -7.5462 (c = 0.067, $CHCl_3$).

Synthesis of 11

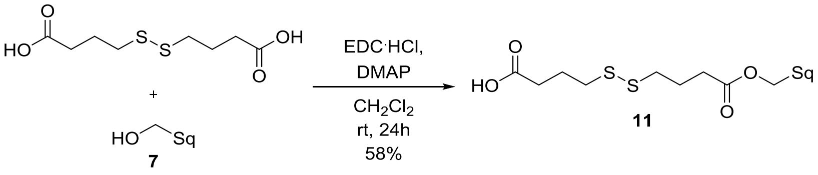

To a solution of **7** (0.660 g, 0.001706 mol) in dry CH$_2$Cl$_2$ (18 mL) 4,4'-dithiodibutyric acid (0.812 g, 0.003411 mmol), EDC·HCl (0.393 g, 0.002047 mol) and DMAP (0.146 g, 0.001194 mmol) are added and the reaction mixture is stirred at room temperature for 24 h. HCl 1M (15 mL) is added and extracted with CH$_2$Cl$_2$ (5x5 mL). The organic layers are dried over Na$_2$SO$_4$ and the solvent is removed under reduced pressure. The crude is purified by flash chromatography (AcOEt/Hex) to obtain **11** as a colourless oil (0.596 g, Yield: 58%).

^{1}H-NMR (CDCl$_3$, 300 MHz): δ(ppm)= 5.12-5.06 (m, 5H), 4.03 (t, *J* = 6.0 Hz, 2H), 2.74-2.68 (m, 4H), 2.51-2.40 (m, 4H), 2.07-1.99 (m, 22H), 1.79-1.71 (m, 2H), 1.68 (s, 3H), 1.59 (s, 15H).

^{13}C-NMR (CDCl$_3$, 75 MHz): δ(ppm)= 178.0, 173.1, 135.1, 134.9, 133.6, 125.1, 124.3, 64.3, 39.7, 37.8, 37.6, 35.8, 32.6, 32.1, 28.2, 26.8, 26.7, 25.7, 24.3, 23.9, 17.7, 16.0, 15.9.

ESI-MS: m/z 606.2 [M-1]$^+$.

Synthesis of 12

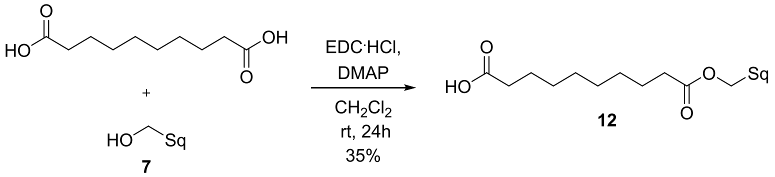

To a solution of **7** (0.100 g, 0.000258 mol) in dry CH_2Cl_2 (2.5 mL) sebacic acid (0.104 g, 0.000517 mol), EDC·HCl (0.060 g, 0.000310 mol) and DMAP (0.022 g, 0.000181 mol) are added and the reaction mixture is stirred at room temperature for 24 h. HCl 1M (15 mL) is added and extracted with CH_2Cl_2 (5x5 mL). The organic layers are dried over Na_2SO_4 and the solvent is removed under reduced pressure. The crude is purified by flash chromatography (AcOEt/Hex 1:3) to obtain **12** as a colourless oil (0.051 g, Yield: 35%).

^{1}H-NMR ($CDCl_3$, 300 MHz): δ(ppm)= 5.13-5.06 (m, 5H), 4.02 (t, *J* = 9.0 Hz, 2H), 2.36-2.25 (m, 4H), 2.08-1.97 (m, 20H), 1.84-1.59 (m, 22H), 1.30 (bs, 8H).

^{13}C-NMR ($CDCl_3$, 75 MHz): δ(ppm)= 178.9, 173.9, 135.1, 134.9, 1337.7, 125.1, 124.3, 64.0, 39.7, 35.8, 34.3, 33.8, 29.7, 29.0, 28.2, 26.9, 26.7, 25.6, 24.9, 24.6, 17.7, 16.0.

ESI-MS: m/z 507.3 $[M-1]^+$.

Synthesis of 13a

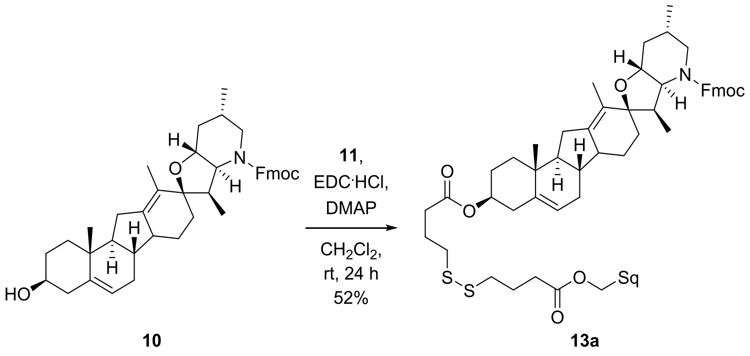

To a solution of **10** (0.030 g, 0.000047 mol) in CH_2Cl_2 (1 mL) **11** (0.029 g, 0.000047 mol), EDC·HCl (0.011 g, 0.000057 mol) and DMAP (0.005 g, 0.000040 mol) are added and the reaction mixture is stirred at room temperature for 24 h. The solvent is then removed under reduced pressure and the crude material is purified by flash chromatography (CH_2Cl_2/Hex 8:2) to obtain **13a** as a colorless oil (0.030 g, Yield: 52%).

^{1}H-NMR: ($CDCl_3$, 300 MHz): δ(ppm)= 7.80-7.68 (m, 2H), 7.60-7.51 (m, 2H), 7.41-7.22 (m, 4H), 5.45-5.35 (m, 1H), 5.20-5.06 (m, 5H), 4.74-4.50 (m, 2H), 4.25-4.00 (m, 4H), 3.70-3.27 (m, 2H), 2.97-2.92 (m, 1H), 2.80-2.69 (m, 4H), 2.45-2.40 (m, 4H), 2.38-0.91 (m, 74H).

ESI-MS: m/z 1246.1 $[M+Na]^+$.

$[\alpha]_D^{31}$ = -4.9062 (c = 0.133, $CHCl_3$).

Synthesis of 14a

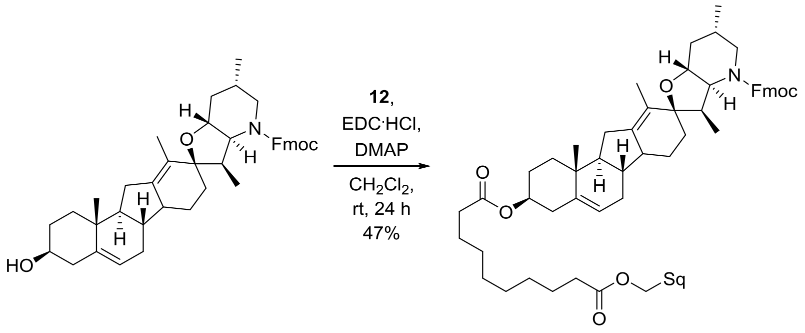

10 **14**

To a solution of **10** (0.031 g, 0.000049 mol) in CH_2Cl_2 (1 mL) **12** (0.028 g, 0.000049 mol), EDC·HCl (0.011 g, 0.000058 mol) and DMAP (0.005 g, 0.000041 mol) are added and the reaction mixture is stirred at room temperature for 24 h. The solvent is then removed under reduced pressure and the crude material is purified by flash chromatography (CH_2Cl_2/Hex) to obtain **14a** as a colourless oil (0.027 g, Yield: 47%).

^{1}H-NMR: ($CDCl_3$, 300 MHz): δ(ppm)= 7.80-7.65 (m, 2H), 7.75-7.50 (m, 2H), 7.50-7.13 (m, 4H), 5.45-5.31 (m, 1H), 5.20-5.00 (m, 5H), 4.70 - 4.50 (m, 2H), 4.25-4.13 (m, 1H), 4.10-3.92 (m, 3H), 3.30-2.75 (m, 2H), 2.-.69 (m, 1H), 2.45-0.67 (m, 88H).

ESI-MS: m/z 1209.3 $[M+Na]^+$.

$[\alpha]_D^{31}$ = -5.5589 (c = 0.133, $CHCl_3$).

Synthesis of 13

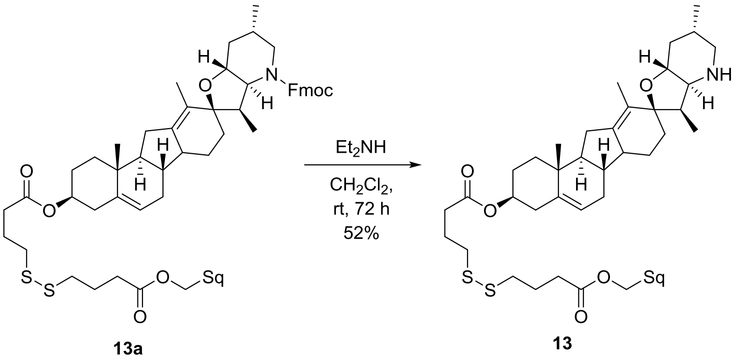

To a solution of **13a** (0.030 g, 0.000024 mol) in CH_2Cl_2 (0.6 mL) diethylamine (0.106 g, 0.001447 mol) was added and the reaction mixture was stirred at room temperature for 72 h. The volatiles were then removed under reduced pressure and the crude material was purified by flash chromatography (from 100% CH_2Cl_2 to AcOEt/MeOH 25:1) to obtain **13** as a colourless oil (0.013 g, Yield: 52%).

^{1}H-NMR: ($CDCl_3$, 300 MHz): δ(ppm)= 5.40-5.35 (m, 1H), 5.20-5.03 (m, 5H), 4.70-4.56 (m, 2H), 4.03 (t, *J*= 7.1Hz, 2H), 3.51-3.32 (m, 2H), 3.25-3.14 (m, 1H), 2.71 (t, *J*=7.1 Hz, 4H), 2.46-2.37 (m, 4H), 2.32-0.81 (m, 76H).

^{13}C-NMR: ($CDCl_3$, 75 MHz, detected signals): δ(ppm)= 172.94, 172.27, 144.25, 142.67, 140.42, 135.10, 134.45, 133.60, 126.95, 125.19, 125.12, 124.38, 124.36, 134.20, 122.78, 86.32, 84.67, 73.92, 69.82, 64.62, 64.30, 51.85, 49.05, 41.51, 39.72, 39.64, 39.59, 39.57, 38.22, 37.84, 37.63, 36.60, 35.76, 33.68, 32.96, 31.03, 29.67, 29.14, 28.90, 28.39, 28.24, 27.51, 26.84, 26.75, 26.64, 26.57, 24.29, 24.21, 24.16, 19.30, 18.55, 18.42, 17.65, 16.02, 15.85, 13.69, 13.09, 10.72.

ESI-MS: m/z 1000.9 $[M+1]^+$.

$[\alpha]_D^{31}$ = -12.0955 (c = 0.660, $CHCl_3$).

Synthesis of 14

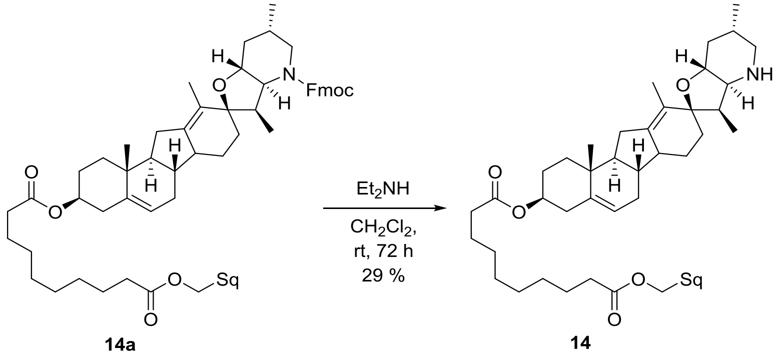

To a solution of **14a** (0.027 g, 0.000023 mol) in CH_2Cl_2 (0.6 mL) diethylamine (0.098 g, 0.001342 mol) was added and the reaction mixture was stirred at room temperature for 72 h. The volatiles were then removed under reduced pressure and the crude material was purified by flash chromatography (from 100% CH_2Cl_2 to AcOEt/MeOH 25:1) to obtain **14** as a colourless oil (0.007 g, Yield: 29%).

^{1}H-NMR: ($CDCl_3$, 300 MHz): δ(ppm)= 5.42-5.38 (m, 1H), 5.20- 5.00 (m, 5H), 4.70-4.50 (m, 2H), 4.02 (t, *J*= 6.4Hz, 2H), 3.40-3.25 (m, 1H), 3.19-3.11 (m, 1H), 2.79-2.68 (m, 1H), 2.62-2.48 (m, 1H), 2.45-0.80 (m, 87H).

^{13}C-NMR: ($CDCl_3$, 75 MHz, detected signals): δ(ppm)= 173.87, 173.20, 144.29, 140.51, 134.96, 133.67, 125.04, 124.37, 124.25, 122.66, 86.34, 73.54, 63.95, 51.86, 49.05, 39.71, 39.64, 35.77, 34.33, 29.06, 28.24, 26.89, 26.63, 24.96, 18.56, 18.41, 17.65, 16.00, 15.83, 13.08.

ESI-MS: m/z 965.0 $[M+1]^+$.

$[\alpha]_D^{31}$ = -17.9880 (c = 0.467, $CHCl_3$).

Synthesis of 15

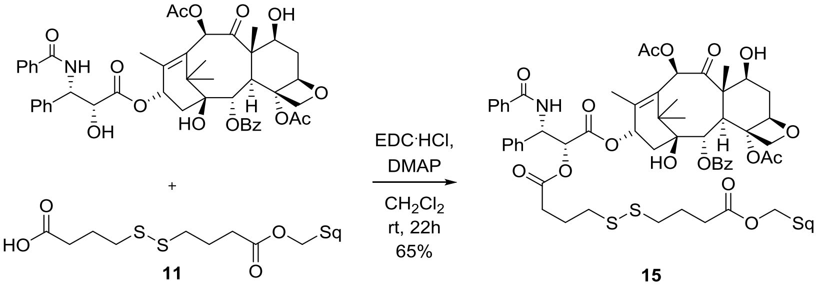

To a solution of **11** (0.024 g, 0.000494 mol), in dry CH$_2$Cl$_2$ (2.5 mL) EDC·HCl (0.013 g, 0.000659 mol) and DMAP (0.003 g, 0.000231 mol) are added. Then paclitaxel (0.020 g, 0.000330 mol) is added and the reaction mixture is stirred at room temperature for 22h. HCl 1M (15 mL) is added and extracted with CH$_2$Cl$_2$ (5x5 mL). The organic layers are dried over Na$_2$SO$_4$ and the solvent is removed under reduced pressure. The crude is purified by flash chromatography (AcOEt/Hex from 1:2 to 1:1) to obtain **15** as a white solid (0.025 g, Yield: 65%).

^{1}H-NMR (CDCl$_3$, 400 MHz): δ(ppm)= 8.17 (d, *J*=7.1Hz, 2H), 7.77 (d, *J*=7.1 Hz, 2H), 7.63 (t, *J*=7.1 Hz, 1H), 7.56-7.51 (m, 3H), 7.47-7.35 (m, 10H), 6.93 (d, *J*=9.3 Hz, 1H), 6.32 (s, 1H), 6.28 (t, *J*=9.0 Hz, 1H), 6.00 (dd, *J*=9.2 Hz, *J*=3.1 Hz, 1H), 5.71 (d, *J*=7.1 Hz, 1H), 5.53 (d, *J*=3.1 Hz, 1H), 5.32 (s, 2H), 5.16-5.10 (m, 5H), 5.00 (d, *J*=7.6 Hz, 1H), 4.50 (dd, *J*=10.9 Hz, *J*=6.6 Hz, 1H), 4.34 (d, *J*=8.4 Hz, 1H), 4.23 (d, *J*=8.4 Hz, 1H), 4.05 (t, *J*=6.7 Hz, 2H), 3.84 (d, *J*=7.0 Hz, 2H), 2.73-2.51 (m, 6H), 2.48 (s, 3H), 2.25 (t, *J*=7.2 Hz, 2H), 2.25 (s, 3H), 2.22-2.15 (m, 2H), 2.13-1.87 (m, 20H), 1.79-1.68 (m, 8H), 1.63 (bs, 18H), 1.26 (s, 3H), 1.16 (bs, 3H).

^{13}C-NMR (CDCl$_3$, 100 MHz, detected signals): δ(ppm)= 204.5, 173.6, 172.6, 171.9, 170.5, 168.7, 167.8, 143.5, 137.7, 135.8, 135.6, 134.4, 134.3, 133.5, 132.7, 130.9, 129.8, 129.4, 129.2, 127.8, 127.2, 125.8, 125.0, 124.9, 85.1, 81.7, 79.9, 77.1, 76.3, 75.8, 74.7, 72.8, 72.5, 65.0, 59.2, 53.4, 46.3, 43.9, 40.4, 38.4, 37.8, 36.5, 36.3, 33.3, 32.7, 29.0, 27.6, 27.5, 27.4, 26.4, 24.9, 24.6, 23.4, 22.8, 21.5, 18.3, 16.7, 16.6, 15.5.

ESI-MS: m/z 1465.8 $[M+Na]^+$.

$[\alpha]_D^{22}$ **=** -46.2300 (c = 0.100, $CHCl_3$).

Synthesis of 16

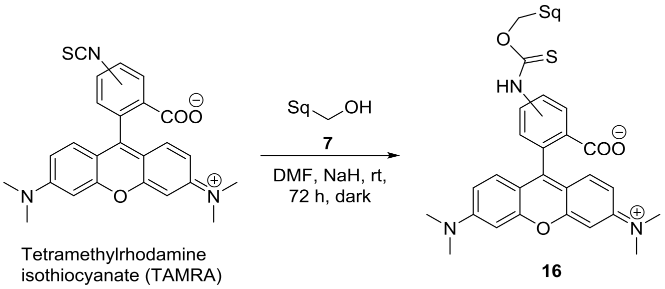
SCN
COO
Tetramethylrhodamine isothiocyanate (TAMRA)
Sq
OH
7
DMF, NaH, rt, 72 h, dark
Sq
O
S
HN
COO
O
N
N
16

To a solution of **7** (13 mg, 0.0337 mmol) in dry DMF was added NaH (0.81 mg, 0.0337 mmol) and the reaction was stirred for 3h. A solution of TAMRA (10 mg, 0.0225 mmol) in dry DMF was then added to the mixture. The reaction was stirred in the dark at room temperature for 72h. The volatiles were then removed under reduced pressure to afford **16** after filtration on silica gel.

ESI-MS: m/z 831 $[M+1]^+$;

MALDI-MS: m/z 830 [M].

3. 4-(1,2-diphenylbut-1-en-1-yl) aniline based nanoparticles

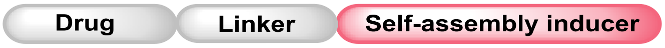
Drug
Linker
Self-assembly inducer

In this scenario, we moved our interest to new self-assembly inducers with particular attention to the ones that possess an antiproliferative activity to make possible the obtainment of self-assembling dual drugs. We considered the use of the hydrophobic moiety of 4-(1,2-diphenylbut-1-en-1-yl)aniline (**Figure 35**), a tamoxifen analogue, which was recently demonstrated to have antiproliferative activity on different human tumor cell lines.[134,135]

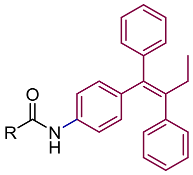

Figure 35. Structure of the self-assembly inducer 4-(1,2-diphenylbut-1-en-1-yl)aniline.

The expected self-assembly ability of this structure could derive from the π-stacking interactions among the aromatic rings of the adjacent molecules, forming a hydrophobic core and exposing the polar moieties toward the aqueous environment.

We prepared five conjugate compounds using aloin or podophyllotoxin as building blocks (**Figure 36**). Aloin was first selected because of its hydrophilic structure in order to test the self-assembly properties of amphiphilic conjugates. Then we moved to podophyllotoxin, a lipophilic antiproliferative compound, to prove the ability of 4-(1,2-diphenylbut-1-en-1-yl)aniline to induce self-assembly also in a totally lipophilic conjugate.[136]

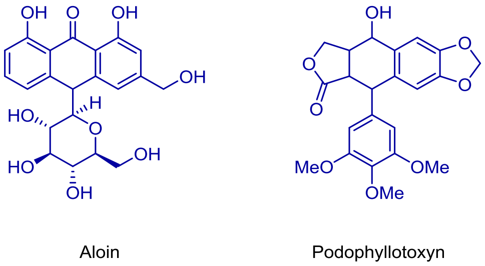

Figure 36. Structures of the active compounds aloin and podophyllotoxin.

Aloin

Aloin is the major anthraquinone of aloe and characterized as the C-glycoside of aloe-emodin. Aloin is extracted from different types of *Aloe* as a mixture of two diasteromers named as aloin A and aloin B. Aloin A and B differ only in the configuration at C-10. (**Figure 37**).

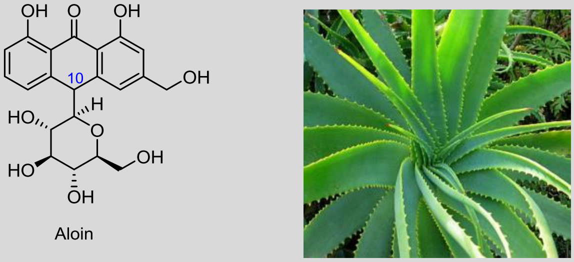

Aloin

Figure 37. Structure of aloin and *Aloe barbadensis*.

Recent studies showed aloin to have a certain antitumor activity against murine tumors (ascites and solid Ehrlich carcinoma),[137] as well as on human breast (T47D) and ovarian tumor cell lines.[138,139] It was also demonstrated that aloin caused a significant dose-dependent elevation in the S-phase fraction of breast and ovarian tumor cells, and the appearance of cells cycling at a higher ploidy level (4G2M). This indicates that aloin did not inhibit DNA synthesis and that cells replicated a full complement of DNA but had difficulty in mitosis. *In vitro* study of aloin on human breast cancer cell lines, without (MCF-7) and with (SKBR-3) erbB-2-topoisomerase IIa co-amplification, showed that aloin at higher concentrations caused a reduction in the proportion of cells undergoing mitosis by induction of apoptosis, inhibition of topoisomerase IIa protein expression, and down-regulation of cyclin B1 protein expression in MCF-7, whereas erbB-2 protein expression was not affected. Topoisomerase IIa protein expression was mildly down-regulated in the SKBR-3 cell line at higher concentrations only.[140]

Furthermore, *in vitro* and *in vivo* studies, reported that repeated treatment of rats with aloin at its maximum tolerated dose, unlike doxorubicin, does not affect the heart function confirmed by biochemical analyses in the serum and tissue and histological examination of cardiomyocytes by light and transmission electron microscopy. The non-cardiotoxic effect of aloin was explained due to its strong antioxidant and scavenging activities for free radicals and reactive oxygen species, as well as iron-chelating potential.[141]

Podophyllotoxin

Podophyllotoxin[142] is a naturally occurring lignan isolated from the genera *Podophyllum* (**Figure 38**). Due to its high toxicity, this compound is currently used only as local antiviral agent: in fact, it was found unsuitable for clinical use as an anticancer agent due to its toxic side effects. However, its semi-synthetic derivative etoposide is an important anticancer drug due to a mechanism of action based on the inhibition of the enzyme topoisomerase II.

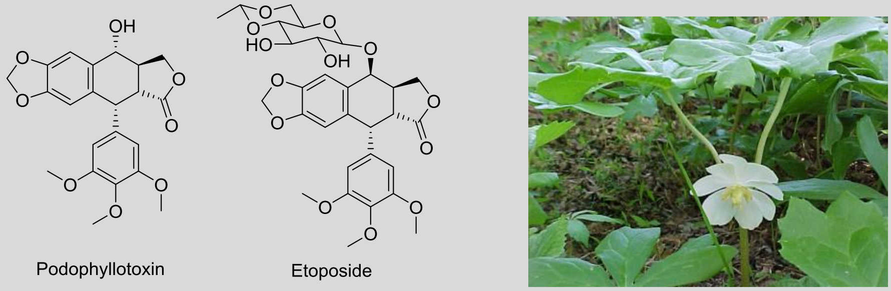

Podophyllotoxin

Etoposide

Figure 38. Podophyllotoxin, etoposide and *Podophyllum Peltatum*.

Podophyllotoxin is able to inhibit the formation of the mitotic spindle: this microtubule disruption causes the cell cycle arrest at the G2/M phase and subsequently induces apoptosis.[143]

In general, the binding behaviour of podophyllotoxin results in the partial unfolding of the secondary structure of β-tubulin at the carboxy terminus and prevents polymerization.[144]

Semi-synthetic podophyllotoxin derivatives, such as etoposide, are recognized as clinically useful drugs against various cancers, including small-cell lung cancer, testicular carcinoma, lymphoma and Kaposi's sarcoma.[145] Even if these derivatives possess a superior pharmacological profile and broader therapeutic uses, the major drawback is the low water solubility that, for example in the case of etoposide, can cause severe allergic reactions.

Synthesis of the conjugates

Four different compounds (**Figure 39**) have been synthesized according to **Scheme 7** and **Scheme 8**.

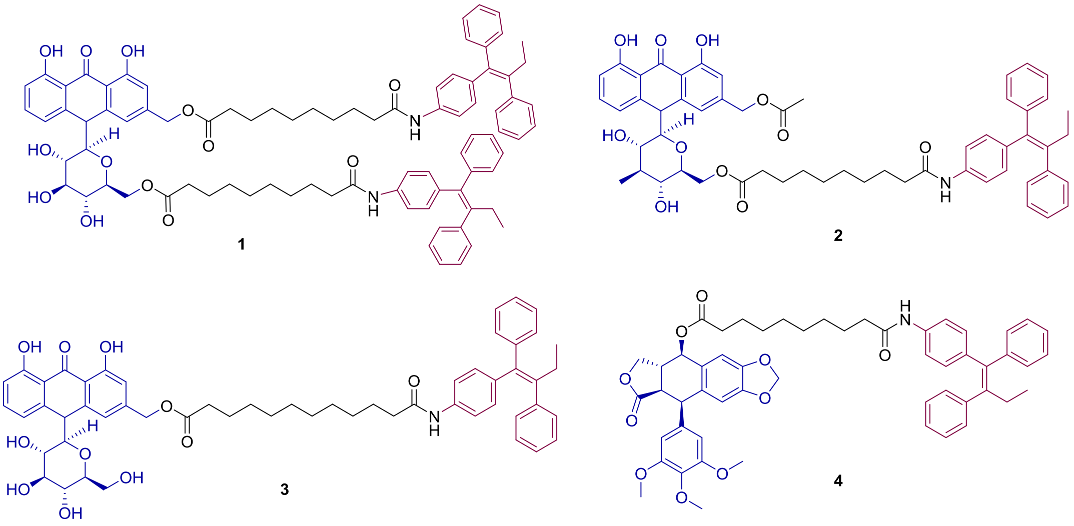

Figure 39. Structures of the four conjugates synthetized.

Aniline **5** was obtained through a McMurry reaction between the commercially available propiophenone and 4-aminobenzophenone. Acid **6**, derived from aniline **5** and sebacic acid (**Scheme 7**), was used for the preparation of compound **1** (as an inseparable mixture of diastereomers at position 10) and **4** via a condensation reaction using a coupling agent.

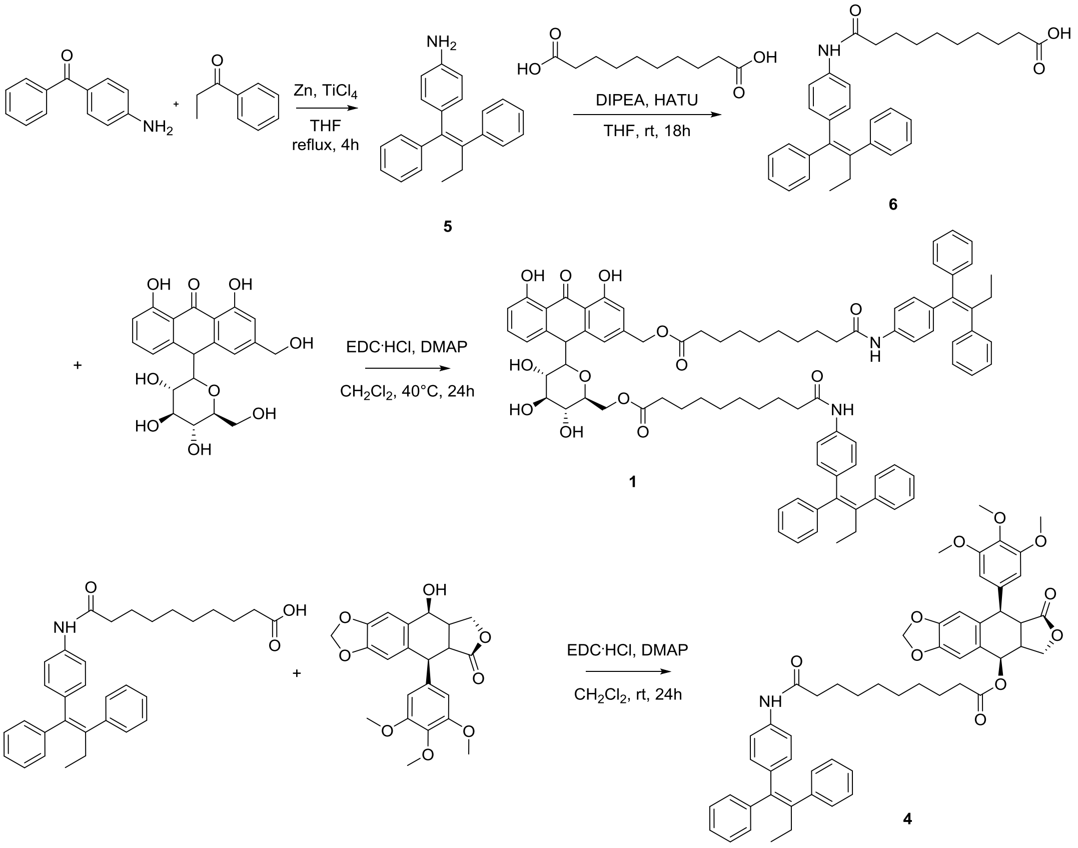
Zn, TiCl4
THF
reflux, 4h
5
DIPEA, HATU
THF, rt, 18h
6
EDC·HCl, DMAP
CH2Cl2, 40°C, 24h
1
EDC·HCl, DMAP
CH2Cl2, rt, 24h
4

Scheme 7. Preparation of conjugates **1** and **4**.

The obtainment of single acylation of aloin resulted tricky and after unsuccessful chemical attempts we considered the use of an enzyme-controlled regioselective reaction.[146] Intermediates **7** and **8** were prepared via enzyme-controlled procedures and subjected to chemical acylation in the presence of EDC or HATU to give **2** and **3**, as inseparable mixtures of diastereomers (**Scheme 8**).

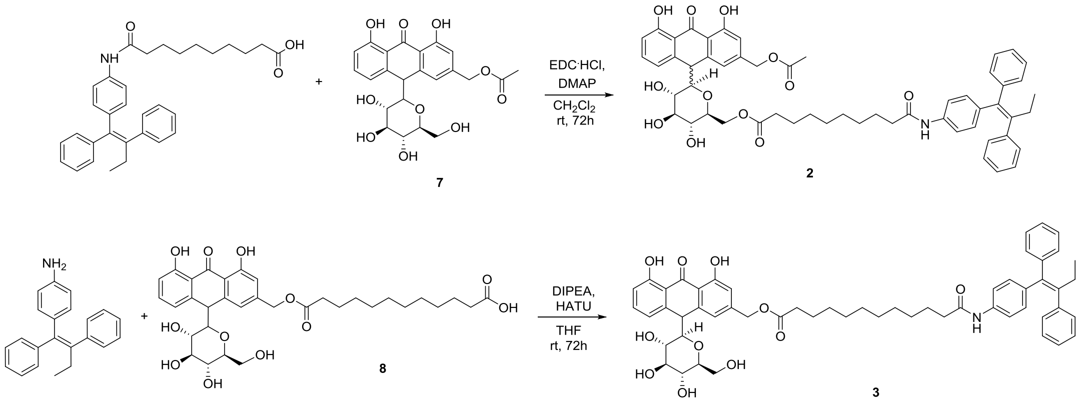
EDC·HCl,
DMAP
CH_2Cl_2
rt, 72h
7
2
DIPEA,
HATU
THF
rt, 72h
8
3

Scheme 8. Preparation of conjugates **3** and **4**.

Nanoparticles characterization

Next, the ability of the obtained compounds to form NPs was investigated. Four different nanosuspensions were prepared by a dropwise addition of an organic solution of the compounds to ultrapure water and by the subsequent removal of the organic solvent under reduced pressure. All the conjugates, except **3**, seemed to self-assemble, and the resulting homogeneous suspensions were characterized by DLS, TEM and nanoparticle tracking analysis (NanoSight).[147]

DLS measurements (**Table 9**) gave a first confirmation of the success of the process: as indicated by the low values of polydispersity index (PDI < 0.2), compounds **1**, **2** and **4** were able to give monodisperse suspensions of NPs, with hydrodynamic diameters in the range of 80–140 nm. These results appear valuable considering that NPs with diameters of about 100 nm were demonstrated to show optimal behaviour in terms of both cellular uptake and elimination properties.

Zeta potential values were negative (<−20.0 mV) for all the nanoassemblies in a range of pH between 4 and 7.4. These values suggest that the electrostatic repulsion contributes to the colloidal stability of the suspension.

Compound	Mean Diameter (nm) DLS	Mean diameter (nm) TEM	Z potential (mV)
1	85.93 ± 2.76	69.30 ± 8.05	-23.9 ± 0.36
2	105.2 ± 10.5	75.72 ± 9.50	-23.0 ± 0.50
4	133.4 ± 9.1	114.3 ± 23.4	-29.8 ± 0.32

Table 9. Size and zeta potential of the nanosuspensions.

TEM images (**Figure 40**) confirmed the uniformity of NP size and showed the NPs to have a spherical shape.

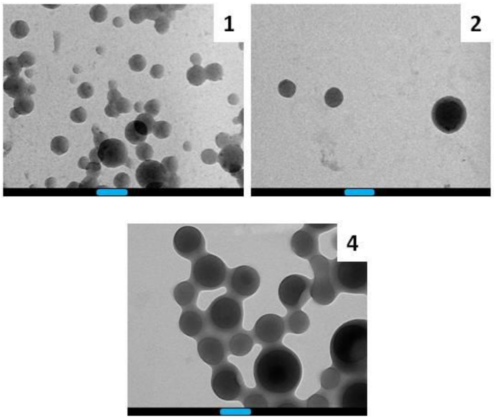

Figure 40. TEM micrographs of nanoparticles formed by self-assembly of compound **1**, compound **2** and compound **4**. All samples were stained with uranyl acetate solution. In all the panels scale bar represents 100 nm.

In order to get more information about the newly formed nanoassemblies, nanoparticle tracking analysis was performed by NanoSight technology (**Table 10**). The direct analysis provided sample concentration in terms of number of NPs per volume unit, which was then exploited, together with the concentration and the molecular weight of the conjugates, to derive the number of molecules self-assembled in one particle.

Compound	**Concentration (NPs mL^{-1})**	**Molecule/NPs**
1	8,73 × 10^{11}	5,11 × 10^{8}
2	4,01 x 10^{11}	1,95 x 10^{9}
4	3,71 x 10^{11}	1,66 x 10^{9}

Table 10. Nanoparticle Tracking Analysis (NTA by NanoSight) quantification of nanoconjugates in suspension. Derived from NTA concentration calculated as: (Cm/Cn) x (1/MW) x NA. Cm: concentration in mass (g mL–1). Cn: concentration in number (number of NPs mL–1). MW: molecular weight of the compound. NA: Avogadro's constant.

In addition, UV-absorbance measurements showed a red shift in the spectra of the nanoformulated compounds, suggesting that π-stacking contributed significantly to the stability of NPs.

In vitro evaluation

The antiproliferative activities of compounds **1**–**4** and of the corresponding NPs were evaluated on two human tumor cell lines, HeLa and HepG2 (**Table 11**).

Compound	**GI$_{50}$ (µM)**	
	HeLa	**HepG2**
Podophyllotoxin	0.0808	0.123
Aloin	> 30	> 30
1	> 30	> 30
1-NP	> 30	> 30
2	12.7	15.9
2-NP	11.9	10.6
3	> 30	> 30
4	0.39	1.17
4-NP	9.75	9.0

Table 11. Cell growth inhibition (GI$_{50}$) of the obtained conjugates (**1**–**4**) and of the corresponding nanoparticles (**1**-, **2**- and **4**-NP) on HeLa (human cervix adenocarcinoma cells) and HepG2 (human hepatocellular carcinoma). GI$_{50}$ values are the concentration of tested agent inducing 50% reduction in cell number compared to control cultures after 72 h of incubation.

In detail, the GI$_{50}$ values indicate for compounds **1** and **2** that the corresponding nanosuspensions (**1**-NP and **2**-NP) maintain the biological profile of the native conjugates. Interestingly, for **2** and **2**-NP the ability to inhibit cell growth is detectable and comparable on both cell lines and it is appreciably higher than the antiproliferative activity of aloin itself. In this connection, a crucial role seems to be played by the increase in lipophilicity due to the conjugation of the aloin with the lipid moiety containing the 4-(1,2-diphenylbut-1-en-1-yl)aniline, that could allow a more efficient cell uptake. This hypothesis is supported by previous studies demonstrating a significant lower absorption percentage of aloin with respect to aloe-emodin, in a Caco-2 cell culture model and in everted gut sac.[148]

As regards conjugate **4**, it exerts the most significant cytotoxic effect, with GI_{50} values in the low micromolar range; nevertheless, the corresponding nanoparticle **4**-NP exhibited a GI_{50} value notably higher, indicating a decrease in the antiproliferative effect. It could be hypothesised that for **4**-NP the disassembling is not very efficient or it occurs slowly as to lead to a lower cellular concentration of the parental drug.

In conclusion we tested the ability of 4-(1,2-diphenylbut-1-en-1- yl)aniline to induce self-assembly on different types of conjugates containing aloin or podophyllotoxin. We demonstrated that conjugates **1**, **2** and **4** are able to self-assemble in spherical NPs, confirming the propensity of 4-(1,2-diphenylbut-1-en-1-yl)aniline to induce self-assembly both when incorporated into amphiphilic and lipophilic conjugates. The obtained nanoformulations showed a diameter of about 100 nm and exhibited negative ζ-potential values from −30 to −20 mV, best suited for future *in vivo* testing. Nevertheless, under our experimental conditions compound **3** did not exhibit the same self-assembling behaviour, underlying the importance of testing the self-assembly properties of each new conjugate. Conjugates **2** and **4** and the corresponding NPs demonstrated a certain antiproliferative activity against different cell lines and in one case (compound **2**) the activity of the conjugate was maintained when nanoformulated. Moreover, both **2** and **2**-NP appeared more active than the native aloin, suggesting a beneficial effect of amphiphilic conjugation resulting from the chemical derivatization and formulation.

The reported results open the possibility to prepare a plethora of 4-(1,2-diphenylbut-1-en-1-yl)aniline based conjugates containing different anticancer drugs as building blocks and suitable linkers to induce drug release after cell internalization.

Experimental Procedures

General

Thin-layer chromatography (TLC) was performed on Merck precoated 60F254 plates. Reactions were monitored by TLC on silica gel, with detection by Uv light (λ = 254 nm) or by charring with 1% permanganate solution. Flash chromatography was performed using Silica gel (240-400 Mesh, Merck). NMR spectra were recordered with Brucker 300 and 400 MHz spectrometers. Chemical shifts are reported in parts per million (δ) downfield from tetramethylsilane (TMS). EI mass spectra were recorded at an ionizing voltage of 6 kEv on a VG 70-70 EQ. ESI mass spectra were recorded on FT-ICR APEXII. Specific rotations were measured with a P-1030-Jasco polarimeter with 10 cm optical path cells and 1 ml capacity (Na lamp, λ = 589 nm). Microwave assisted reaction were performed with Emrys Creator single-mode (power range 0-400 W from magnetron at 2.45 GHz).

Synthesis of 5

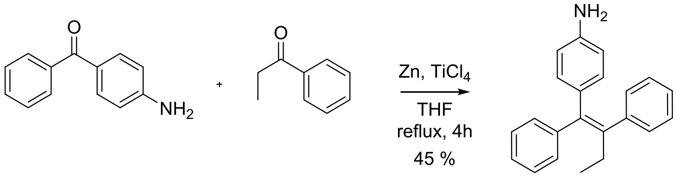

5

To a cold (-10°C) suspension of Zn (1.204 g, 18.124 mmol) in THF (18 mL), $TiCl_4$ (0.82 mL, 7.502 mmol) is dropwise added and the mixture is stirred for 10 min and then it is refluxed for 2 h. Then, a solution of 4-aminobenzophenone (0.371 g, 1.911 mmol) and propiophenone (0.281 g, 2.103 mmol) in THF (37 mL) is added to the cooled suspension of the titanium reagent at 0°C, and the reaction mixture is refluxed for 2.5 h. After the completion of the reaction, the reaction mixture is cooled to rt and poured into a 10% aq K_2CO_3 solution (15 mL). Vigorous stirring is maintained for 5 min, and the dispersed insoluble material is removed by vacuum filtration on celite. The organic layer is separated and the aqueous layer is extracted with AcOEt. The organic layers are washed with water and brine, dried with Na_2SO_4, filtered and evaporated. The residue is purified by flash column chromatography (Hex/AcOEt 8:2) and after evaporation of the solvent, product **5** is obtained as white amorphous solid (45% yield).

^{1}H-NMR ($CDCl_3$, 300 MHz): δ(ppm)= 7.37 (t, *J*=7.2 Hz, 2H), 7.31-7.27 (m, 3H), 7.23-7.13 (m, 5H), 6.69 (d, *J*=8.8 Hz, 2H), 6.40 (d, *J*=8.8 Hz, 2H), 2.48 (q, *J*=7.6 Hz, 2H), 0.950 (t, *J*=7.6 Hz, 3H).

^{13}C-NMR ($CDCl_3$, 75 MHz): δ(ppm)= 144.7, 144.0, 143.5, 141.4, 139.4, 134.7, 132.3, 130.4, 130.1, 128.6, 128.4, 127.0, 126.5, 115.2, 29.55, 13.99;

ESI-MS: m/z 300.42 $(M + H)^+$.

Anal. Calcd for $C_{22}H_{21}N$: C, 88.25; H, 7.07; N, 4.68. **Found**: C, 87.35; H, 6.87; N, 4.50.

Synthesis of 6

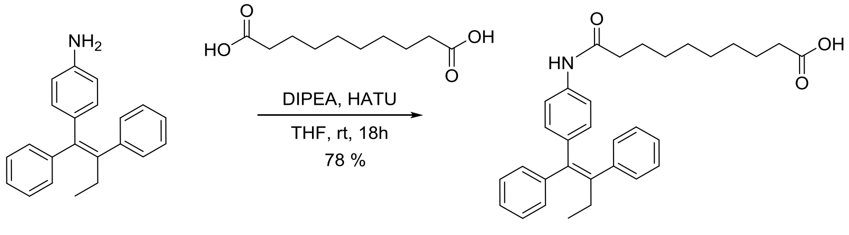

5 **6**

To a solution of sebacic acid (0.255 g, 1.263 mmol) in dry THF (20 mL) HATU (0.527 g, 1.386 mmol) and DIPEA (0.326 g, 2.523 mmol) are added and the reaction mixture is stirred for 30 minutes. Then **5** (0.378 g, 1.265 mmol) is added and the reaction mixture is stirred at rt overnight. The solvent is removed under reduced pressure, AcOEt is added and it is washed with water and brine. The organic layer is then dried over Na_2SO_4 and concentrated under reduced pressure. The crude is purified by flash chromatography (AcOEt/Hex 4:6) to obtain pure **6** (0.476 g, Yield: 78%).

^{1}H-NMR(CDCl$_3$, 300 MHz): δ(ppm)= 7.33-7.02 (m, 12H), 6.80 (d, *J*=7.8, 2H), 4.78 (bs, 1H), 2.43 (q, *J* = 7.6 Hz, 2H), 2.30 (t, *J*=7.7 Hz, 2H), 2.25 (t, *J*=7.5 Hz, 2H), 1.75-1.55 (m, 4H), 1.40-1.25 (m, 8H), 0.92 (t, *J* =7.7 Hz).

^{13}C-NMR (CDCl$_3$, 75 MHz): δ(ppm)= 175.3, 174.6, 145.1, 143.2, 143.1, 141.3, 139.7, 135.4, 131.9, 129.6, 129.4, 128.2, 127.7, 127.3, 126.3, 116.1, 37.58, 34.98, 31.80, 30.81, 26.96, 26.22, 13.60.

Synthesis of 1

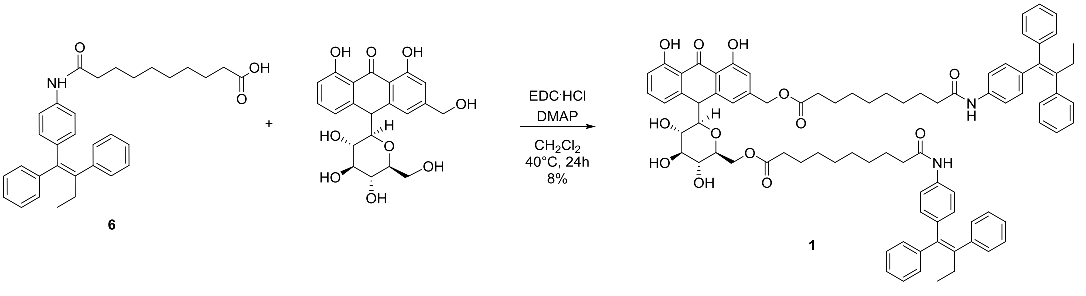

To a solution of **6** (0.085 g, 0.176 mmol) in CH_2Cl_2 (10 mL) DMAP (0.032 g, 0.262 mmol) and EDC·HCl (0.050 g, 0.262 mmol) are added and the reaction mixture is stirred for 30 minutes. Then aloin (0.091 g, 0.269 mmol) is added and the reaction mixture is stirred at 40°C overnight. The solvent is removed under reduced pressure to give **1** without further purification (0.021 g, Yield: 8%).

^{1}H-NMR (CD_3OD, 400 MHz): δ(ppm)= 7.58-7.47 (m, 2H), 7.37-7.34 (m, 3H), 7.30-6.95 (m, 24H), 6.89-6.87 (m, 1H), 6.81-6.79 (m, 3H), 5.16-5.13 (m, 2H), 4.90-4.86 (m, 1H), 4.67-4.64 (m, 1H), 3.68-3.41 (m, 4H), 3.13-3.04 (m, 2H), 2.51-2.25 (m, 12H), 1.74-1.52 (m, 8H), 1.31-1.25 (m, 16H), 0.92 (t, *J*=7.3 Hz, 6H).

^{13}C-NMR (CD_3OD, 100 MHz): δ(ppm)= 194.0, 174.5, 173.8, 173.1, 162.0, 161.8, 145.2, 144.9, 144.7, 143.4, 142.2, 141.9, 138.8, 138.4, 136.2, 135.9, 130.8, 130.4, 129.4, 129.1, 127.9, 127.6, 127.5, 127.0, 126.4, 125.9, 119.7, 118.7, 117.3, 116.9, 85.25, 85.06, 80.33, 79.31, 68.80, 64.79, 61.49, 44.40, 33.74, 33.58, 28.76, 28.52, 25.42, 24.62, 24.43, 12.42.

ESI-MS = 1372.3 $(M+Na^+)^+$

Synthesis of 8

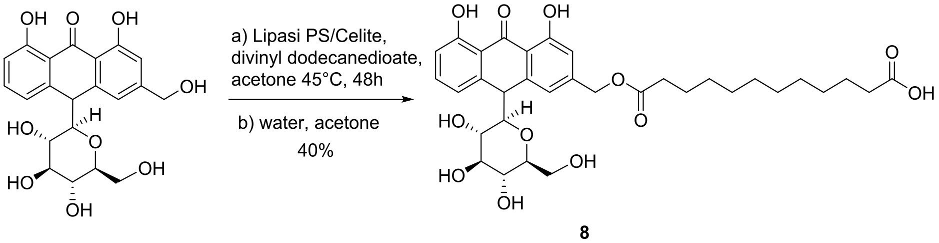
8

To a solution of aloin (100 mg, 0.24 mmol) in dry acetone (15 mL) divinyl dodecanedioate (101 mg, 0.36 mmol) and Novozyme 435 (30 mg) are added. The resulting heterogeneous mixture is incubated at 45 °C and 210 rpm for 48h. After that, 5 µL water are added to the mixture which is incubated again for additional 2 h, checking the formation of the target acid by TLC ($CHCl_3$/MeOH/HCOOH = 8:2:0.1, UV). The crude mixture is then filtered, concentrated *in vacuo* and purified by flash column chromatography on silica gel (AcOEt/MeOH/H_2O = 9.5:0.5:0.1) affording the purified product **8** as a yellow oil (60 mg, 40%).

^{1}H-NMR (CD_3OD, 400 MHz): δ(ppm)= 7.50 (ddd, *J*=8.3, 7.5, 6.3 Hz, 1H), 7.06 (q, *J*=6.0 Hz, 2H), 6.89-6.84 (m, 2H), 5.16 (d, *J*=3.7 Hz, 2H), 4.59 (d, *J*=1.5 Hz, 1H), 3.58 (dd, *J*=11.7, 1.9 Hz, 1H), 3.43-3.39 (m, 2H), 3.33 (dt, *J*=3.3, 1.6 Hz, 2H), 3.28 (t, *J*=8.6 Hz, 1H), 3.03-2.97 (m, 1H), 2.94-2.89 (m, 2H), 2.47-2.37 (m, 4H), 1.70-1.58 (m, 4H), 1.29 (bs, 12H).

^{13}C-NMR (CD_3OD, 100 MHz): δ(ppm)= 194.1, 173.68, 173.60, 170.9, 161.84, 161.75, 161.62, 161.59, 145.5, 145.08, 145.04, 144.4, 142.1, 135.8, 135.0, 119.9, 118.60, 118.59, 117.5, 117.24, 117.22, 116.88, 116.70, 115.8, 115.5, 114.1, 113.9, 85.0, 80.30, 80.20, 78.55, 78.53, 70.62, 70.53, 70.46, 64.74, 64.71, 61.89, 61.85, 44.5, 33.6, 33.2, 29.08, 29.03, 28.91, 28.88, 28.74, 28.65, 24.7, 24.3.

ESI-MS = 653.3 $(M+Na^+)^+$.

Synthesis of 3

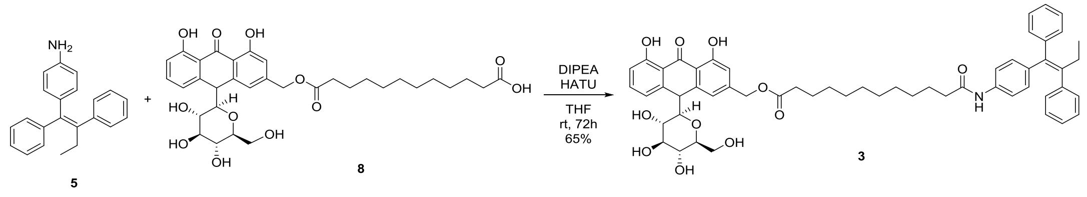

To a solution of **8** (0.080 g, 0.130 mmol) in THF (30 mL) HATU (0.050 g, 0.130 mmol) and DIPEA (0.034 g, 0.266 mmol) are added and the reaction mixture is stirred for 30 minutes. Then **5** (0.039 g, 0.130 mmol) is added and the reaction mixture was stirred at rt for 72h. The solvent is removed under reduced pressure to obtain crude **3**. The crude is purified by flash chromatography (CH_2Cl_2/MeOH) to obtain pure **3** (0.077 g Yield: 65%).

^{1}H-NMR ($CDCl_3$, 300 MHz): δ(ppm)= 7.45-6.76 (m, 19H), 4.84-4.64 (m, 2H), 4.53 (m, 1H), 4.12-4.08 (m, 1H), 3.74-3.68 (m, 2H), 3.20-2.80 (m, 4H), 2.41 (q, *J*=7.4 Hz, 2H), 2.31-2.26 (m, 2H), 2.15-2.12 (m, 2H), 1.70-1.57 (m, 2H), 1.53-1.42 (m, 2H), 1.32-1.24 (m, 12H), 0.89 (t, *J*=7.4 Hz, 3H).

^{13}C-NMR ($CDCl_3$, 75 MHz): δ(ppm)= 195.8, 175.5, 174.9, 163.3, 163.0, 147.4, 145.1, 143.8, 143.6, 142.8, 140.5, 140.1, 137.9, 132.5, 132.2, 131.2, 130.8, 129.6, 129.3, 128.1, 127.6, 121.6, 120.4, 119.5, 118.8, 118.2, 114.9, 114.4, 86.31, 80.09, 79.29, 71.82, 71.47, 64.85, 45.83, 38.33, 35.12, 30.85, 30.51, 27.26, 26.16, 13.50.

Synthesis of 7

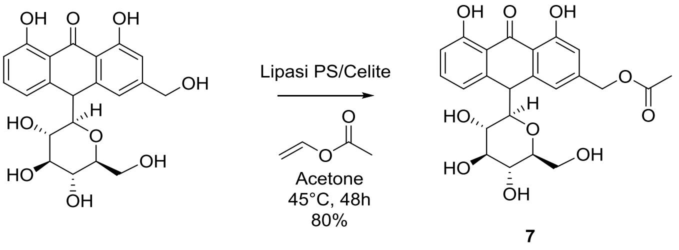

Aloin (100 mg, 0.24 mmol) and vinyl acetate (33 µL, 0.36 mmol) are dissolved in 15 mL of dry acetone under nitrogen atmosphere. Molecular sieves 4Å (30 mg) and lipase PS supported on Celite® (80 mg, 1 % w / w lipase / celite) are then added to the resulting solution which is incubated at 45 °C and 210 rpm for 48 h. After that, the formation of the desired product is checked by TLC ($CHCl_3$/MeOH/HCOOH = 8:2:0.1, UV) and the crude mixture filtered, concentrated *in vacuo* and purified by flash column chromatography on silica gel (AcOEt/MeOH/H_2O = 9.5:0.5:0.1), affording the purified product **7** as a yellow solid (85 mg, 80%).

^{1}H-NMR (CD_3OD, 400 MHz): δ(ppm)= 7.47 (ddd, *J*=8.3, 7.6, 5.8 Hz, 1H), 7.04-7.00 (m, 2H), 6.86-6.81 (m, 2H), 5.16 (d, *J*=3.6 Hz, 2H), 4.50 (d, *J*=1.9 Hz, 1H), 3.59-3.55 (m, 1H), 3.42-3.37 (m, 2H), 3.29-3.25 (m, 1H), 3.00-2.88 (m, 3H), 2.17 (s, 1H), 2.15 (s, 2H).

^{13}C-NMR (CD_3OD, 100 MHz): δ(ppm)= 194.0, 171.6, 171.13, 171.03, 161.77, 161.69, 161.55, 161.51, 145.4, 145.01, 144.88, 144.2, 142.0, 141.6, 135.7, 135.0, 119.9, 118.58, 118.51, 117.4, 117.2, 116.82, 116.63, 115.7, 115.5, 114.1, 113.8, 85.18, 85.01, 80.26, 80.17, 78.53, 78.50, 70.60, 70.58, 70.50, 70.46, 64.96, 64.91, 61.88, 61.83, 60.2, 44.45, 44.38, 19.50, 19.44, 13.1.

ESI-MS = 483.1 $(M+Na^+)^+$.

Synthesis of 2

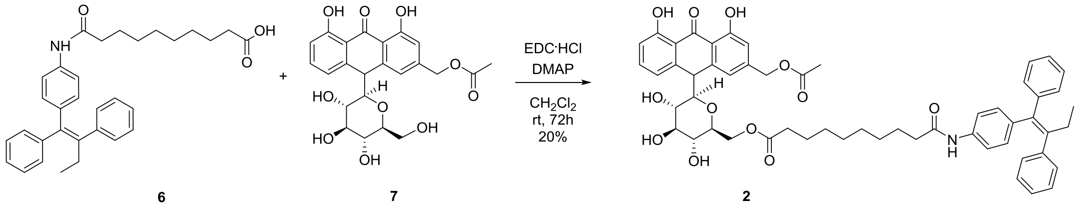

To a solution of **6** (0.080 g, 0.166 mmol) in CH_2Cl_2 (18 mL) are added EDC·HCl (0.038 g, 0.199 mmol) and DMAP (0.025 g, 0.199 mmol) and the reaction mixture is stirred for 30 minutes. Then **7** (0.076 g, 0.166 mmol) is added and the reaction mixture is stirred at rt for 72h. The solvent is removed under reduced pressure to obtain crude **2**. The crude is purified by flash chromatography (CH_2Cl_2/MeOH) to obtain pure **2** (0.030 g Yield: 20%).

^{1}H-NMR ($CDCl_3$, 300 MHz): δ(ppm)= 7.53-7.50 (m, 1H), 7.38-7.35 (m, 2H), 7.30-7.09 (m, 12H), 6.90-6.88 (m, 2H), 6.80 (d, *J*=8.4 Hz, 2H), 5.15 (d, *J*=3.6 Hz, 2H), 4.88 (m, 1H), 4.65 (s, 1H), 3.56 (d, *J*=12 Hz, 1H), 3.53 (d, *J*=9.6 Hz, 1H), 3.44 (dd, *J*=12, 5.2 Hz, 1H), 3.12-3.01 (m, 3H), 2.47 (q, *J*=7.6 Hz, 2H), 2.37 (t, *J*=7.2 Hz, 2H), 2.31-2.26 (m, 2H), 2.16 (s, 3H), 1.67-1.57 (m, 4H), 1.37-1.27 (m, 8H), 0.924 (t, *J*=7.2 Hz, 3H).

^{13}C-NMR ($CDCl_3$, 75 MHz): δ(ppm)= 194.7, 174.8, 173.9, 173.8, 162.3, 162.2, 145.8, 144.1, 142.8, 142.6, 142.0, 139.4, 139.1, 136.9, 135.8, 131.4, 130.1, 129.7, 128.5, 128.2, 127.0, 126.8, 119.4, 119.1, 117.9, 116.3, 114.6, 85.70, 81.06, 79.93, 69.60, 65.60, 62.13, 45.03, 37.19, 34.36, 29.42, 29.16, 26.08, 25.08, 20.03, 13.06.

Synthesis of 4

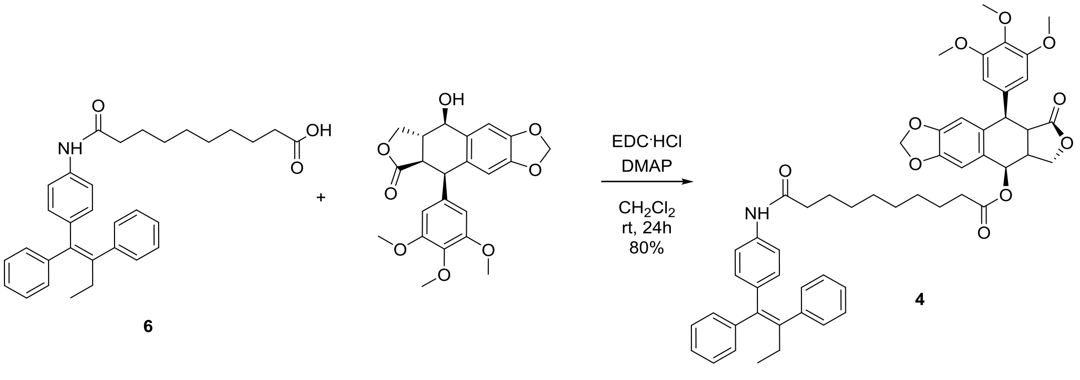

To a solution of **6** (0.059 g, 0.122 mmol) in dry CH_2Cl_2 (10 mL), EDC·HCl (0.028, g, 0.147 mmol) and DMAP (0.011 g, 0.086 mmol) are added. Then, aloin (0.051 g, 0.122 mmol) is added in the reaction mixture and stirred at rt for 5 h. HCl 1M (9 mL) is then added and the aqueous phase is washed with AcOEt (4 x 8 mL). The combined organic extracts are dried over Na_2SO_4 and evaporated under reduced pressure. The crude is purified by flash chromatography (AcOEt/Hex) to provide **4** (0.086 g, 80 %) as an orange solid.

^{1}H-NMR ($CDCl_3$, 300 MHz): δ(ppm)= 7.38-7.09 (m, 12H), 6.80 (d, *J*=8.5 Hz, 2H), 6.78 (s, 1H), 6.53 (s, 1H), 6.37 (s, 2H), 5.95 (d, *J*=4.5 Hz, 2H), 5.88 (d, *J*=8.9 Hz, 1H), 4.59 (d, *J*=4.0, 1H), 4.36-4.31 (m, 1H), 4.22-4.18 (m, 1H), 3.78 (s, 3H), 3.72 (s, 6H), 2.92 (dd, *J*=14, 4.5 Hz, 1H), 2.82-2.77 (m, 1H), 2.55-2.29 (m, 4H), 2.22 (t, *J*=7.5 Hz, 2H), 1.81-1.51 (m, 4H), 1.48-1.18 (m, 8H), 0.93 (t, *J*=7.7 Hz, 3H).

^{13}C-NMR ($CDCl_3$, 75 MHz): δ(ppm)= 174.9, 174.4, 171.8, 153.3, 148.8, 148.3, 144.1, 142.9, 142.7, 139.5, 138.8, 137.7, 136.4, 135.5, 133.0, 132.0, 130.3, 130.2, 129.0, 128.8, 128.6, 127.3, 126.8, 119.2, 110.4, 108.7, 107.8, 102.3, 74.06, 72.15, 61.43, 56.76, 46.30, 44.40, 39.53, 38.27, 35.03, 29.81, 26.16, 25.69, 14.22.

4. Design and Synthesis of a new Self-immolative Linker

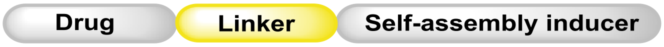
Drug
Linker
Self-assembly inducer

The need of improving the drug release of the systems described in the previous chapters prompted us to consider the synthesis of a new class of conjugates. These conjugates are characterized by the presence of a self-immolative linker able to improve the drug release in particular conditions.[149]

Self-immolative linkers

The strategy of the self-immolative linker consists of connecting the drug and the carrier in a cleavable way (**Figure 41 a**) or by attaching a triggering moiety that, upon specific conditions or in the presence of specific enzymes, is able to induce a cascade that ends with release of the drug (**Figure 41 b**). In the latter case, the linker forms a scissible bond with a protecting group and a stable bond with the drug unit, that becomes labile upon removal of the protecting group, resulting in a rapid disassembly of the three components (self-immolative elimination).

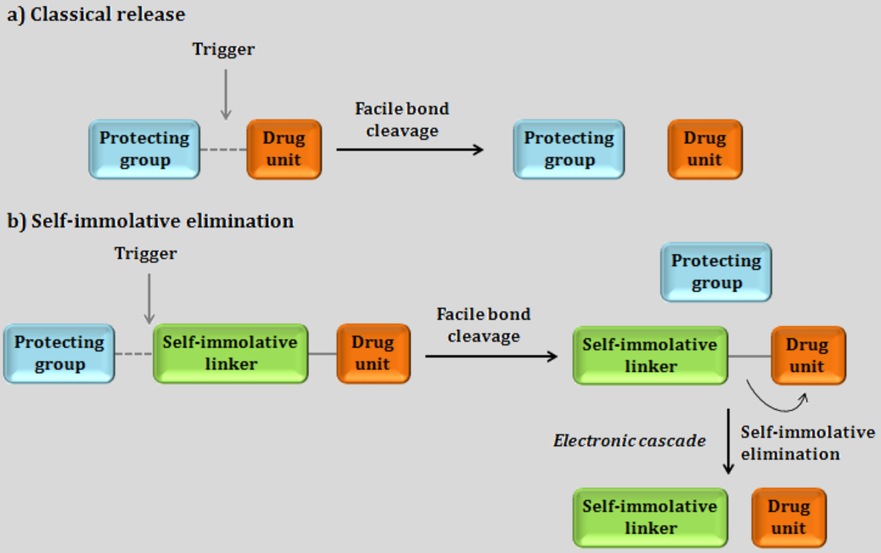
a) Classical release
Trigger
Protecting group
Drug unit
Facile bond cleavage
Protecting group
Drug unit
b) Self-immolative elimination
Trigger
Protecting group
Self-immolative linker
Drug unit
Facile bond cleavage
Protecting group
Self-immolative linker
Drug unit
Electronic cascade
Self-immolative elimination
Self-immolative linker
Drug unit

Figure 41. Different approaches for drug release.

Some examples of self-immolative linkers including their mechanism of drug release are summarized in **Table 12**:

Linker	Reaction type	Release mechanism
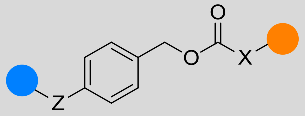	1,6-benzyl elimination	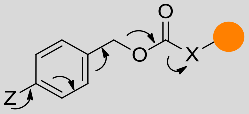
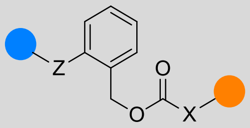	1,4-benzyl elimination	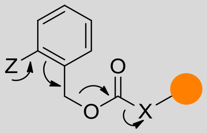
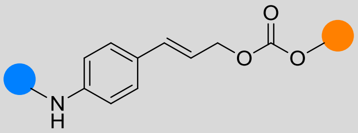	1,8-elimination	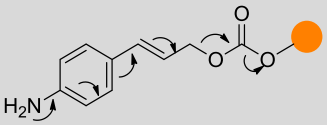
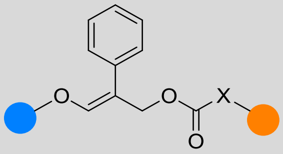	β-elimination	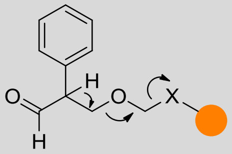
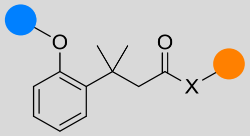	Cyclization (lactonization)	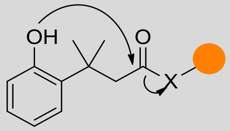
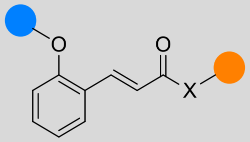	Cyclization (lactonization)	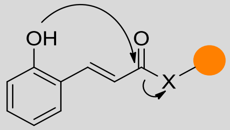
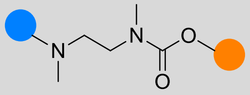	Cyclization	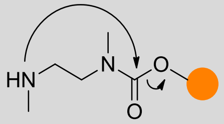

Table 12. Self-immolative linkers and their mechanism of drug release.
● = Protecting group; ● = Drug unit; X, Z = O, NH

The evolution of self-immolative linker technology has led to self-immolative systems capable of amplified release, such as dendrimers (**Figure 42 a**) and polymers (**Figure 42 b**).

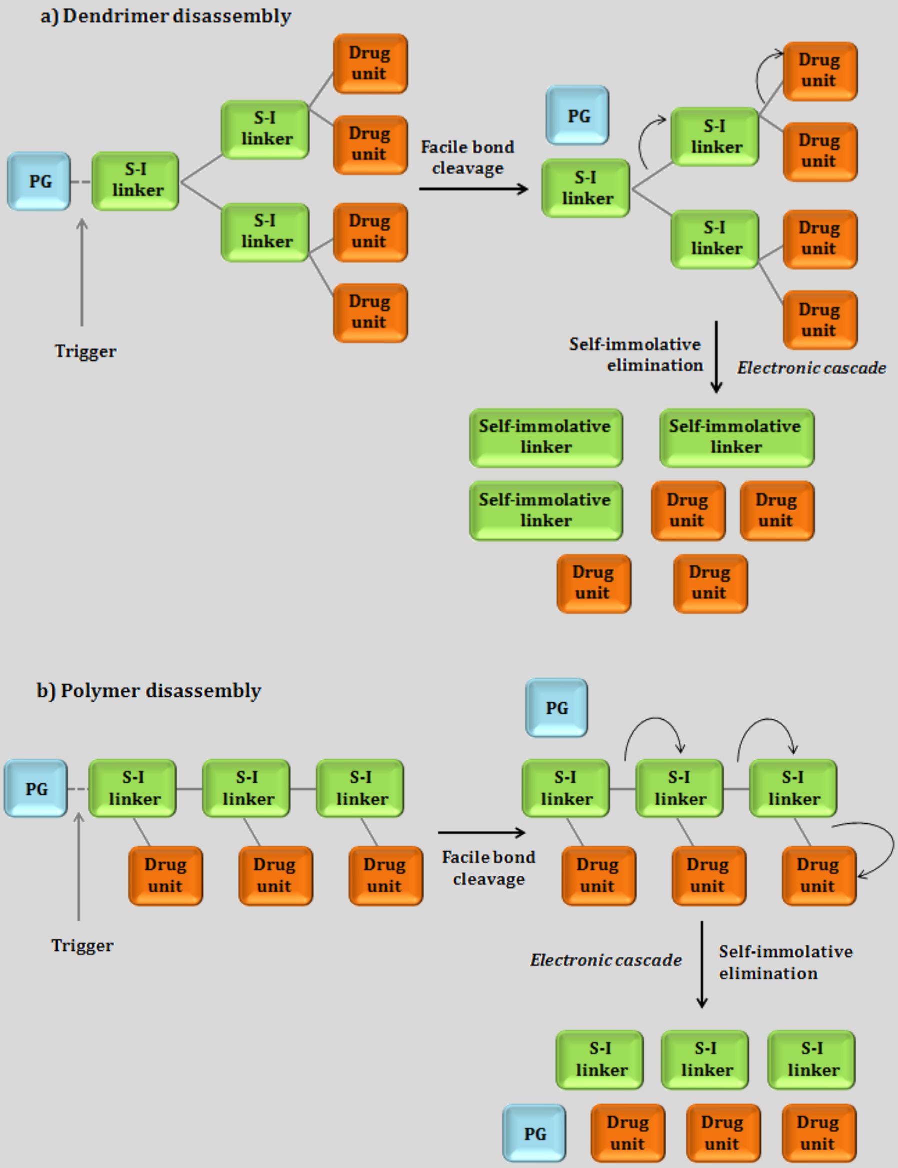
a) Dendrimer disassembly
PG
S-I linker
S-I linker
S-I linker
Drug unit
Drug unit
Drug unit
Drug unit
Trigger
Facile bond cleavage
Self-immolative elimination
Electronic cascade
Self-immolative linker
Self-immolative linker
Self-immolative linker
b) Polymer disassembly
Facile bond cleavage
Trigger
Electronic cascade
Self-immolative elimination

Figure 42. Dendrimer and polymer disassembly.

In order to guarantee the release of the drug inside the cell, we designed a new self-immolative linker.

This new linker is covalently bonded to a self-assembly (SA) inducer, able to cause the formation of nanoparticles, and it is characterized by the presence of a labile bond (**Scheme 9**). The labile bond is the one with the acetyl group on the phenolic oxygen and it is cleaved by a lipase inducing the release of the free drug.

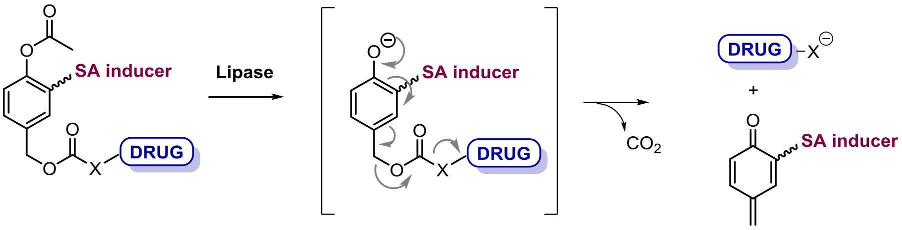

Scheme 9. Mechanism of drug release of the self-immolatice linker.

The general structure of the conjugates synthetized is reported is **Figure 43**: the self-assembly inducer is bonded to the self-immolative linker through a 10-atom chain. We decided to synthetized both the compound characterized by a simple carbon chain and the one characterized by the presence of a disulphide moiety, in order to study the role of both the parts of the molecule.

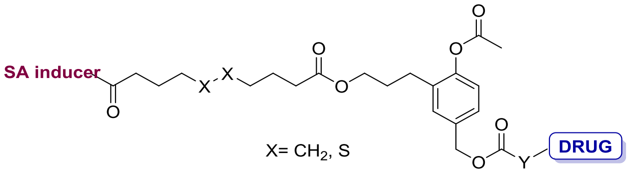

Figure 43. General structure of the conjugates.

The detailed structure of the conjugates synthetized is reported below (**Figure 44**).

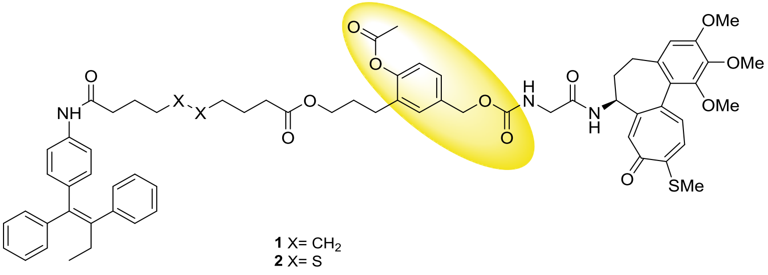

Figure 44. Structures of the conjugates characterized by the presence of the self-immolative linker.

We decided to prepare a class of bivalent compounds in which also the self-assembly inducer has some antiproliferative activity and we selected 4-(1,2-diphenylbut-1-en-1-yl)aniline (Chapter 4) as self-assembly inducer and desacetylthiocolchicine as anticancer drug.

Colchicine

Colchicine is a well-known alkaloid from *Colchicum autumnale* and *Gloriosa superba* (**Figure 45**). It interferes with microtubule growth and, therefore, affects mitosis and other microtubule dependent functions.[150]

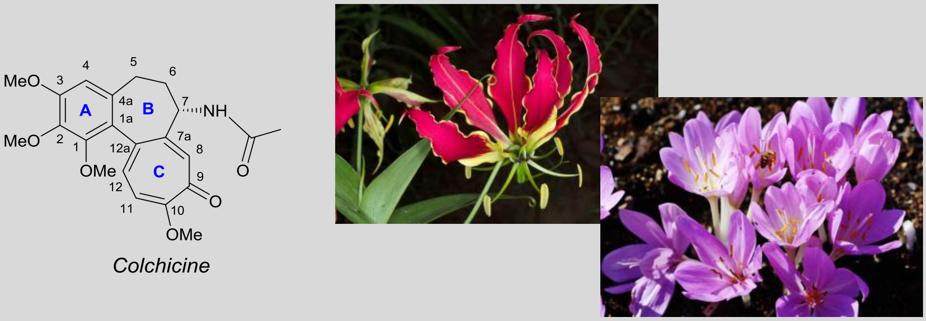

Figure 45. Structure of Colchicine and *Colchium autumnale* and *Gloriosa superba*.

Colchicine is one of the oldest drugs still in use for the treatment of gout and amyloidosis of familial Mediterranean fever.[151] Although colchicine is a potent antimitotic agent, its medicinal uses are limited due to its high toxicity. Virtually all of its therapeutic and toxic effects are believed to be a consequence of its interaction with tubulin. For these reasons, colchicine has become an attractive molecule for the medicinal chemists in pursuit of less toxic and more selective analogs which bind to tubulin.

Structurally, colchicine can be divided into three parts (**Figure 45**): a trimethoxybenzene ring moiety (A), a seven-membered ring with a side chain at C(7) (B), and a tropolone ring (C). Previous studies suggested that the interaction between colchicinoids and tubulin was stereoselective and mainly attributed to the configuration and conformation of the biaryl system composed of the trimethoxyphenyl ring and tropolonic ring.[152,153,154]

Colchicinoids with an a*S*-configured biaryl system[155] bind readily to tubulin, while those with an a*R* configuration bind poorly. Moreover, it has been proposed that in addition to the effect of the C(1) substituents on the biaryl configuration, the C(7) side chain could also influence the binding rate of colchicinoids to tubulin as well as the configuration of the colchicinoids through steric effects.[156]

Colchicine interaction with proteins

Colchicine interacts mainly with three known proteins: tubulin, cytochrome P450 3A4 (CYP3A4) and P-glycoprotein (P-gp).

Tubulin: Microtubules are composed of two structurally similar protein subunits, α-tubulin and β-tubulin, which are spherical proteins composed of ∼440 amino acids (50kDa).[157] Colchicine binds at the interface between the α and β subunits of tubulin within the heterodimer by H-bonding (with the Cys241 residue of β-tubulin) and hydrophobic interactions[158,159] (**Figure 46**). Colchicine binds with high affinity to tubulin that can become copolymerized into microtubules. The antiproliferative action of colchicine involves the capacity of the tubulin–colchicine complex to bind to the ends of microtubules and actually prevent the elongation of the microtubule polymer.[160] Because of this effect, colchicine effectively functions as a ‘mitotic poison’ or spindle poison as tubulin availability is essential to mitosis.

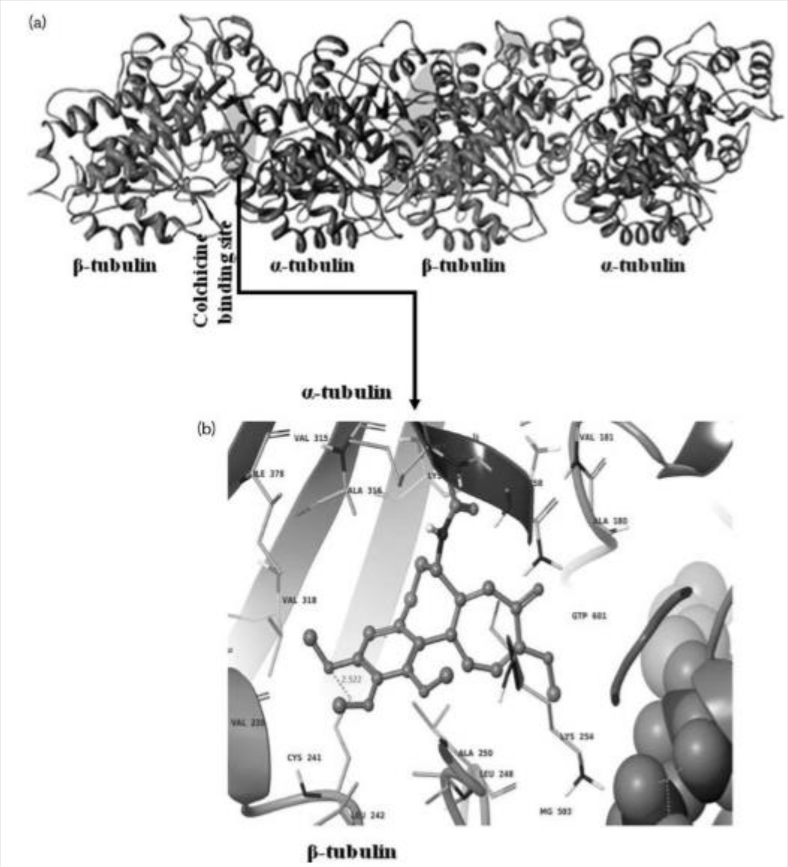
(a)
β-tubulin
Colchicine binding site
α-tubulin
β-tubulin
α-tubulin
α-tubulin
(b)
VAL 315
ILE 378
ALA 316
LYS
VAL 181
ALA 180
VAL 318
GTP 601
2.522
VAL 238
CYS 241
LEU 242
ALA 250
LEU 248
LYS 254
MG 503
β-tubulin

Figure 46. *(a)Crystal structure of αβ-tubulin heterodimers showing the binding sites of colchicine.(b) Interactions of colchicine with the colchicine-binding site of tubulin.*

To discover colchicine-based anticancer drugs, the tubulin–colchicine domain computational stimulation has been investigated using the crystal structures of colchicine and its semisynthetics.[161] The thiocolchicine (**Figure 47**) analogues were more potent than the colchicine analogues in the tubulin polymerization assay.[162] Different semisynthetic thiocolchicine hybrids such as paclitaxel–thiocolchicine, thiocolchicine–podophyllotoxin and vindoline–thiocolchicine as well as thiocolchicine dimers and were successfully tested as multifunctional tubulin inhibitors.[163,164,165]

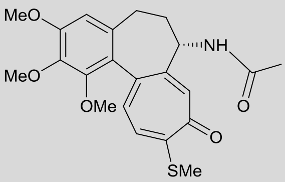

Thiocolchicine

Figure 47. *Structure of thiocolchicine.*

Cytochrome P450 3A4: In the occurrence of several drug–drug interactions, drug metabolism through the cytochrome P450 (CYP450) system has emerged as a significant determinant. CYP450 belongs to the hemethiolate class of enzymes that catalyse the oxidation of a wide variety of xenobiotics and pharmaceutical agents. CYP450 enzymes metabolize the majority of marketed drugs; thus, it is important to characterize the interactions of potential new therapies with members of this enzyme.

In humans, colchicine metabolism has not yet been investigated. *In vitro* experiments using primary human hepatocyte cultures or hepatic microsomes and *in vivo* animal studies are the only available data sources. Its metabolic clearance is chiefly dependent on the metabolic activity and free plasma fraction on the enzymes. However, the blood flow has a limited influence over it. It has been established by various authors that colchicine undergoes oxidative demethylation into 2-, 3- and 10-DMC.[166] Recently, colchicine derivatives have been tested for the inhibition of five major CYP450 isoenzymes. The results indicate that these compounds showed moderate or very low inhibition of CYP450 enzymes, and thus does not have CYP liability.[167]

P-glycoprotein: P-gp is an ATP-dependent phosphoglycoprotein that is located in the cell membrane and interacts with various drugs. P-gp affects the absorption, distribution and elimination of its substrates, including colchicine.[168]

Overexpression of P-gp decreases intracellular drug levels, as a result limiting drug cytotoxicity. In case of colchicine, the development of tumour resistance mainly occurs through its P-gp induction activity, causing its active efflux from tumour cells, and increase in the expression of βIII tubulin isotype.[169,170] Colchicine is a substrate of the P-gp efflux pump and it activates this pump by inducing conformational change. The P-gp substrate and induction liability of colchicine restricts its use in combination with other cytotoxic drugs that are P-gp substrates such as vinblastine, doxorubicin and paclitaxel.[171] To overcome P-gp-mediated resistance in colchicine, it has been shown that its N-benzylated derivative maintained similar levels of cytotoxic activity in resistant A2780AD ovarian carcinoma cells that are known to overexpress the ABCB1 (P-gp) drug transporter.[172]

The features described above provide promise for the rational design of colchicine analogs. Much work has been done with thiocolchicine, which acts similarly to colchicine[173] but it is stable toward acid and it is therefore a preferred compound in structure-activity studies.[174] Among thiocolchicine derivatives, N-deacetyl thiocolchicine was tested *in vitro* on human breast cancer cell line (MDR negative MDA-MB 231), showing a significant antiploriferative activity.[175]

Synthesis of the conjugates

We started the preparation of the conjugates by synthetizing the self-immolative moiety. The first synthetic pathway is reported in **Scheme 10**. The commercially available 4-hydroxybenzaldehyde was alkylated with allylbromide in the presence of potassium carbonate and potassium iodide to obtain ether **3** that was subsequently reduced to alcohol **4** using $NaBH_4$. The formation of carbonate **5** was achieved in good yield by treating compound **5** with 4-nitrophenylchloroformate. Unfortunately, the microwave-assisted Claisen rearrangement was not successful and we were not able to isolate the desired product.

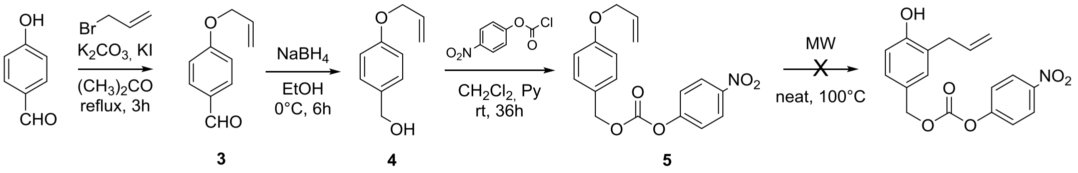

Scheme 10. First synthetic pathway for the self-immolative linker.

We decided to consider an alternative synthetic pathway (**Scheme 11**), changing the reactions sequence. Compound **4** was first submitted to a microwave-assisted Claisen rearrangement to obtain alcohol **6** in good yield. The following acylation with acetic anhydride and reduction with $NaBH_4$ led to the obtainment of compound **8**, which was reacted with 4-nitrophenylchloroformate to achieve carbonate **9**. Then, a hydroboration reaction, followed by a basic work up (aq. NaOH), was performed to achieve a formal anti-Markovnikov addition on the double bond and get the final self-immolative linker **10**.

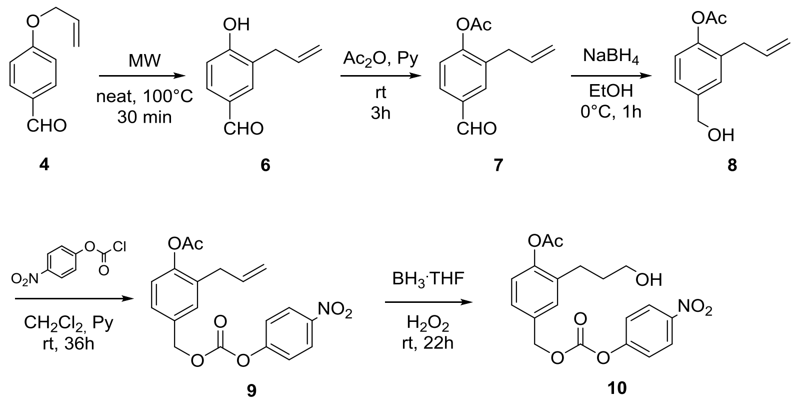
MW
neat, 100°C
30 min
Ac2O, Py
rt
3h
NaBH4
EtOH
0°C, 1h
CH2Cl2, Py
rt, 36h
BH3·THF
H2O2
rt, 22h
4
6
7
8
9
10

Scheme 11. Alternative synthetic pathway.

The self-immolative linker **10** is then reacted with the anticancer compound N-desacetylthiocolchicine which was previously synthetized (**Scheme 12**) following a reported procedure.[176]

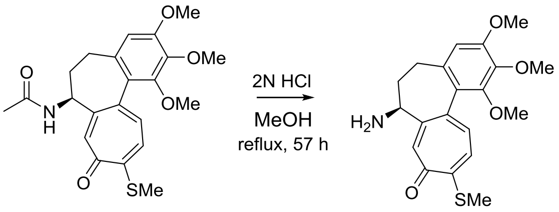
2N HCl
MeOH
reflux, 57 h

Scheme 12. Preparation of N-desacetylthiocolchicine.

Unfortunately, the reaction between the amino group of N-desacetylthiocolchicine and the carbonate moiety of compound **10** was not effective and we didn't manage to obtain the desired product (**Scheme 13**).

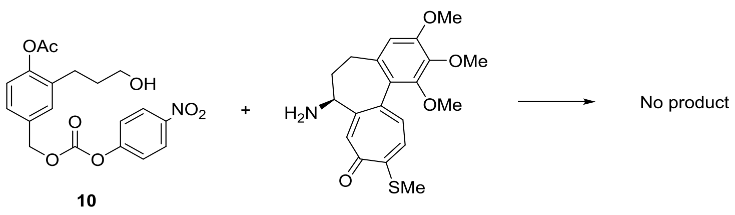
10
No product

Scheme 13. Drug-conjugation reaction.

Therefore, we decided to functionalize the amino moiety of the N-desacetylthiocolchicine with glycine in order to link the anticancer compound to our linker through a less hindered amine. For this aim, compound **11** was prepared according to **Scheme 14**.

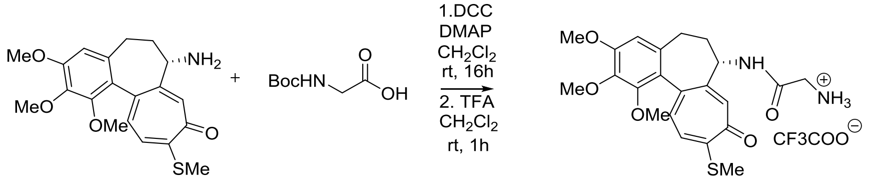
MeO
MeO
OMe
NH2
SMe
O
+
BocHN
O
OH
1.DCC
DMAP
CH2Cl2
rt, 16h
2. TFA
CH2Cl2
rt, 1h
MeO
MeO
OMe
NH
O
NH3
CF3COO
SMe
O

11

Scheme 14. Synthesis of compound **11**.

This approach was successful to obtain the desired intermediate **12** (**Scheme 15**).

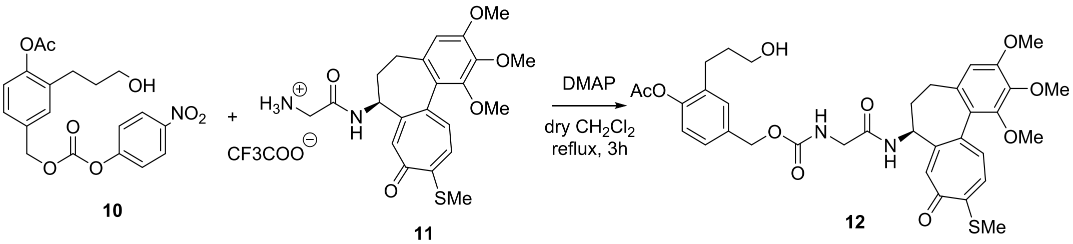
OAc
OH
O
O
O
NO2
+
H3N
O
N
H
CF3COO
OMe
OMe
OMe
O
SMe
DMAP
dry CH2Cl2
reflux, 3h
AcO
OH
O
H
N
O
N
H
O
OMe
OMe
OMe
O
SMe

10 **11** **12**

Scheme 15. Drug-conjugation reaction.

The final reaction between compound **12** and the acids **13a**,**b** (Chapter 4) in the presence of EDC and DMAP lead to the obtainment of the final esters **1** and **2** (**Scheme 16**).

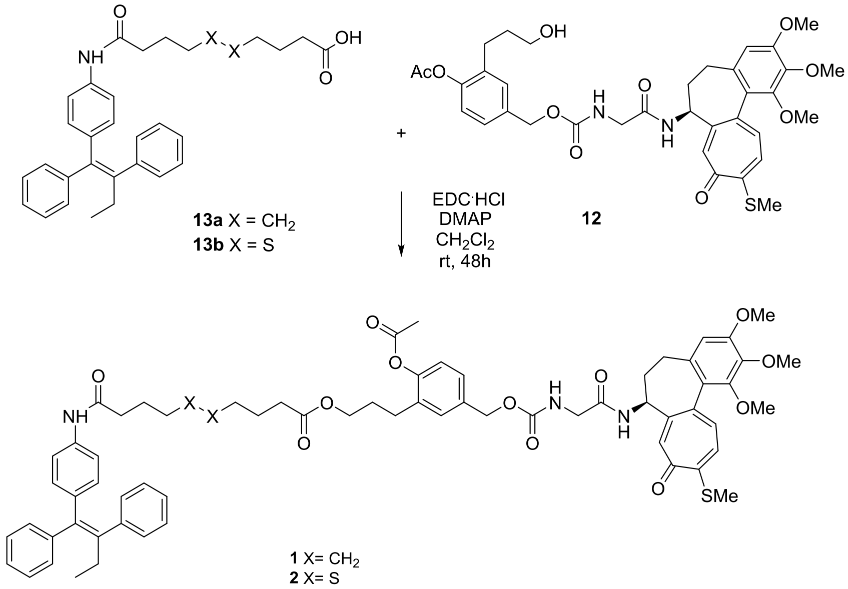
13a X = CH$_2$
13b X = S
+
12
EDC·HCl
DMAP
CH$_2$Cl$_2$
rt, 48h
1 X= CH$_2$
2 X= S
AcO
OH
OMe
SMe
NH

Scheme 16. Synthesis of conjugates **1** and **2**.

Lipase-induced drug release

The efficacy of the release of the parental drug has been evaluated incubating our final compounds in the presence of different types of lipases (**Scheme 17**) and analysing the reaction mixtures by reverse-phase HPLC.

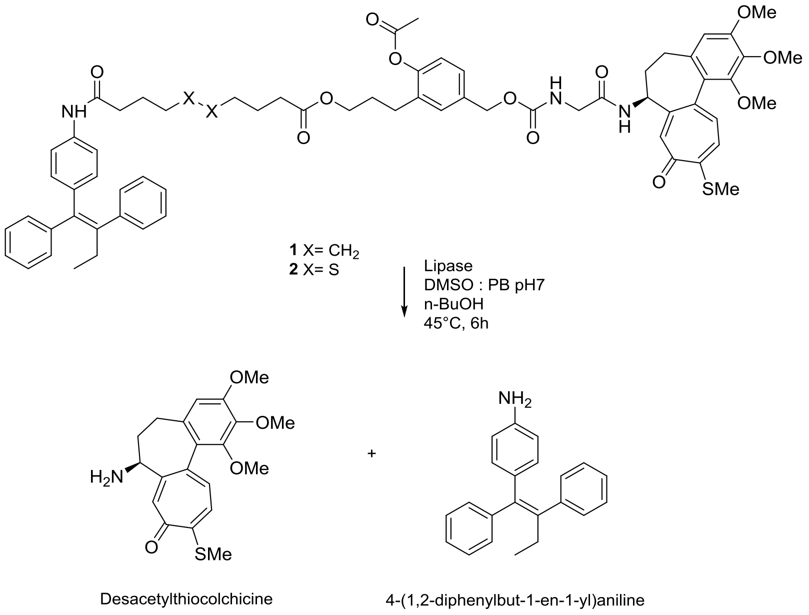
1 X= CH2
2 X= S
Lipase
DMSO : PB pH7
n-BuOH
45°C, 6h
Desacetylthiocolchicine
4-(1,2-diphenylbut-1-en-1-yl)aniline
OMe
SMe
NH2
H2N

Scheme 17. Lipase-mediated drug release.

In the case of compound **1**, the best result was obtained using porcine pancreatic lipase which gave 88% of hydrolysis and we were able to observe by HPLC-MS the peaks corresponding to the released desacetylthiocolchicine and the 4-(1,2-diphenylbut-1-en-1-yl)aniline.

The higher conversion of compound **2** was instead achieved using lipase PS @Celite and also in this case we confirmed by HPLC-MS the release of the two active compounds demonstrating the ability of the conjugates to release the two active moiety.

Nanoparticles characterization

Next, the ability of the obtained compounds **1** and **2** to form NPs was investigated. Two different nanosuspensions were prepared by a dropwise addition of an organic solution of the compounds to ultrapure water and by the subsequent removal of the organic solvent under reduced pressure. Both the conjugates seemed to self-assemble, and the resulting homogeneous suspensions were characterized by DLS.

DLS measurements (**Table 13**) gave a first confirmation of the success of the process: compounds **1** and **2** were able to give monodisperse suspensions of NPs, with hydrodynamic diameters in the range of 280–320 nm.

Zeta potential value was negative for compound **1** suggesting that the electrostatic repulsion contributes to the colloidal stability of the suspension.

Compound	Mean Diameter (nm)	Z potential (mV)
1	280.1 ± 13.8	-15.1 ± 2.24
2	312.8 ± 36.6	n.d.

Table 13. Nanoparticles characterization.

Currently the biological activity of the conjugates and the corresponding nanoparticles on different types of cancer cells is under investigation.

Experimental Procedures

General

Thin-layer chromatography (TLC) was performed on Merck precoated 60F254 plates. Reactions were monitored by TLC on silica gel, with detection by Uv light (λ = 254 nm) or by charring with 1% permanganate solution. Flash chromatography was performed using Silica gel (240-400 Mesh, Merck). NMR spectra were recordered with Brucker 300 and 400 MHz spectrometers. Chemical shifts are reported in parts per million (δ) downfield from tetramethylsilane (TMS). EI mass spectra were recorded at an ionizing voltage of 6 kEv on a VG 70-70 EQ. ESI mass spectra were recorded on FT-ICR APEXII. Specific rotations were measured with a P-1030-Jasco polarimeter with 10 cm optical path cells and 1 ml capacity (Na lamp, λ = 589 nm). Microwave assisted reaction were performed with Emrys Creator single-mode (power range 0-400 W from magnetron at 2.45 GHz).

Synthesis of 3

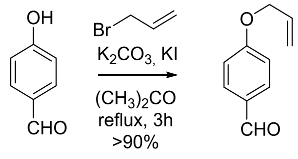

3

To a solution of 4-hydroxybenzaldehyde (2.005 g, 16.377 mmol) in acetone (100 mL) allybromide (3.950 g, 32.653 mmol), K_2CO_3 (4.502 g, 32.574 mmol) and KI (0.273 g, 1.644 mmol) are added and the reaction mixture is stirred at room temperature for 3h. Brine (70 mL) is added and extracted with AcOEt (5x15 mL). The organic layers are dried over Na_2SO_4 and the solvent is removed under reduced pressure to obtain **3** as a yellow oil (2.660 g, Yield: > 90%) without any further purification.

^{1}H-NMR ($CDCl_3$, 300 MHz): δ(ppm) = 9.98 (s, 1H), 7.82 (d, *J*=8.8 Hz, 2H), 7.01 (d, *J*=8.8 Hz, 2H), 6.09-5.99 (m, 1H), 5.45-5.43 (m, 1H), 5.35-5.31 (m, 1H), 4.61 (dt, *J*=5.2, 1.4 Hz, 2H).

^{13}C-NMR ($CDCl_3$, 100 MHz): δ (ppm) = 190.6, 163.6, 132.3, 131.9, 130.1, 118.2, 115.0, 69.0.

ESI-MS: *m*/*z* 185 (M + Na)$^+$.

IR (neat): 3076, 2925, 2837, 1686, 1596, 1575, 1507 cm^{-1}.

Anal. Calcd for $C_{10}H_{10}O_2$: C, 74.06; H, 6.21. **Found**: C, 73.95; H, 6.32.

Synthesis of 4

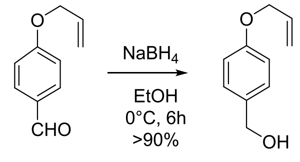

3 **4**

To a solution of **3** (0.308 g, 1.899 mmol) in EtOH (15 mL) at 0°C $NaBH_4$ (0.144 g, 3.798 mmol) is added and the reaction mixture is stirred at 0°C for 2.5 h. The solvent is the removed under reduced pressure, H_2O (20 mL) is added and extracted with CH_2Cl_2 (5x10 mL). The organic layers are dried over Na_2SO_4 and the solvent is removed under reduced pressure to obtain **4** as a yellow oil (0.303 g, Yield: > 90%) without any further purification.

^{1}H-NMR ($CDCl_3$, 300 MHz): δ(ppm): 7.13 (d, *J*=8.5 Hz, 2H), 6.89 (d, *J*=8.5 Hz, 2H), 5.96 (ddt, *J*=17.1, 10.5, 5.7 Hz, 1H), 5.40 (dd, *J*=17.1, 1.2 Hz, 1H), 5.28 (dd, *J*=10.5, 1.2 Hz, 1H), 4.51 (d, *J*=5.7 Hz, 2H), 4.20 (s, 2H).

^{13}C-NMR ($CDCl_3$, 100 MHz): δ(ppm) = 153.4, 133.7, 128.8, 126.2, 118.3, 114.5, 69.1, 63.2.

Synthesis of 5

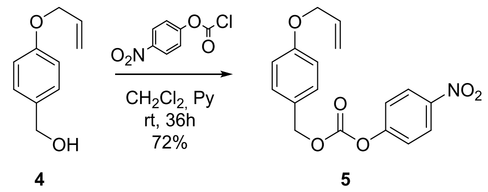

To a solution of **4** (0.303 g, 1.843 mmol) in dry CH_2Cl_2 (26 mL) 4-nitrophenyl chloroformate (0.743 g, 3.694 mmol) and dry pyridine (0.582 g, 7.365 mmol) are added and the reaction mixture is stirred at room temperature for 18 h. The solvent is then removed under reduced pressure. The crude is purified by flash chromatography (Hex/AcOEt 9:1) to obtain **5** (0.449 g, Yield: 72%).

^{1}H-NMR ($CDCl_3$, 300 MHz): δ(ppm): 8.27 (d, *J*=9.4 Hz, 2H), 7.40 (d, *J*=9.4 Hz, 2H), 7.36 (d, *J*=8.5 Hz, 2H), 6.93 (d, *J*=8.5 Hz, 2H), 6.09-6.01 (m, 1H), 5.40 (dd, *J*=17.1, 1.2 Hz, 1H), 5.28 (dd, *J*=10.5, 1.2 Hz, 1H), 5.22 (s, 2H), 4.51-4.47 (m, 2H).

Synthesis of 6

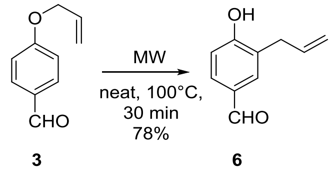

Compound **3** (3.492 g, 21.011 mmol) is exposed to microwave radiation in a microwave oven at 190°C for 30 minutes. The crude is purified by flash chromatography (Hex/AcOEt 8:2) to obtain **6** (2.657 g, Yield: 78%).

^{1}H-NMR (CDCl$_3$, 300 MHz): δ(ppm): 9.85 (s, 1H), 7.69-7.62 (m, 2H), 6.92 (d, *J*=8.5 Hz, 1H), 6.01-5.96 (m, 1H), 5.25-5.19 (m, 2H), 3.49-3.41 (m, 2H).

Synthesis of 7

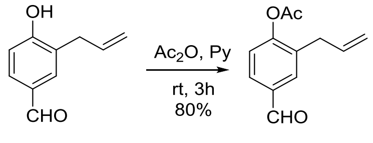

6 **7**

To a mixture of Ac_2O/Pyridine 1:1 (40 mL) **6** (2.003 g, 12.301 mmol) is added and the reaction mixture is stirred at room temperature for 2 h. At 0°C solid $NaHCO_3$ is added. The reaction mixture is extracted with AcOEt (3x20 mL) and organic layers are washed with H_2O. The organic layers are dried over Na_2SO_4 and the solvent is removed under reduced pressure. The crude is purified by flash chromatography (Hex/AcOEt 85:15) to obtain **7** (2.302 g, Yield: 80%).

^{1}H-NMR ($CDCl_3$, 300 MHz): δ(ppm): 9.85 (s, 1H), 7.77-7.73 (m, 2H), 7.23 (d, *J*=11.1 Hz, 1H), 5.94-5.84 (m, 1H), 5.14-5.09 (m, 2H), 3.38-3.34 (m, 2H), 2.33 (s, 3H).

Synthesis of 8

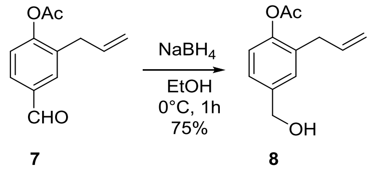

To a solution of **7** (0.203 g, 0.984 mmol) in EtOH (10 mL) at 0°C NaBH$_4$ (0.074 g, 1.965 mmol) is added and the reaction mixture is stirred at 0°C for 30 minutes. The solvent is the removed under reduced pressure, H$_2$O (20 mL) is added and extracted with CH$_2$Cl$_2$ (5x10 mL). The organic layers are dried over Na$_2$SO$_4$ and the solvent is removed under reduced pressure. The crude is purified by flash chromatography (CH$_2$Cl$_2$/MeOH 98:2) to obtain **8** (0.151 g, Yield: 75%).

^{1}H-NMR (CDCl$_3$, 300 MHz): δ(ppm): 7.22-7.18 (m, 2H), 7.02 (d, *J*=8.5 Hz, 1H), 5.91-5.81 (m, 1H), 5.11-5.03 (m, 2H), 4.65 (s, 2H), 3.32-3.28 (m, 2H), 2.31 (s, 3H).

Synthesis of 9

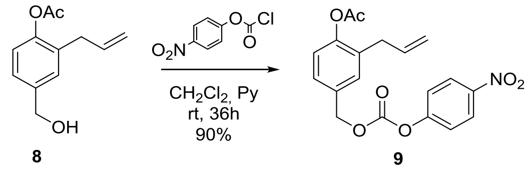

To a solution of **8** (1.194 g, 5.791 mmol) in dry CH_2Cl_2 (80 mL) 4-nitrophenyl chloroformate (2.343 g, 11.594 mmol) and dry pyridine (0.917 g, 11.594 mmol) are added and the reaction mixture is stirred at room temperature for 36 h. The solvent is then removed under reduced pressure. The crude is purified by flash chromatography (Hex/AcOEt 8:2) to obtain **9** (2.101 g, Yield: 90 %).

^{1}H-NMR (300 MHz, $CDCl_3$): δ(ppm): 8.27 (d, *J*=9.4 Hz, 2H), 7.37 (d, *J*=9.4 Hz, 2H), 7.32-7.28 (m, 2H), 7.07 (d, *J*=8.8, 1H), 5.93-5.89 (m, 1H), 5.25 (s, 2H), 5.11-5.03 (m, 2H), 3.32-3.28 (m, 2H), 2.31 (s, 3H).

Synthesis of 10

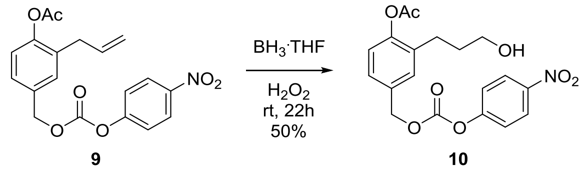

To a solution of **9** (1.106 g, 5.654 mmol) in dry THF (50 mL) BH_3·THF (7.771 mL, 3.885 mmol) is added and the reaction mixture is stirred at rt for 22 h. At 0°C H_2O_2 (0.166 mL, 7.079 mmol) is added and the reaction mixture is stirred at rt for 30 minutes. Solid NaCl and H_2O (50 mL) are added and extracted with Et_2O (3x40 mL). The organic layers are washed with brine, dried over Na_2SO_4 and the solvent is removed under reduced pressure. The crude is purified by flash chromatography (Hex/AcOEt 1:1) to obtain **10** (1.221 g, Yield: 50 %).

^{1}H-NMR ($CDCl_3$, 300 MHz): δ(ppm): 8.27 (d, *J*=9.4 Hz, 2H), 7.37 (d, *J*=9.4 Hz, 2H), 7.33-7.28 (m, 2H), 7.07 (d, *J*=8.8, 1H), 5.25 (s, 2H), 3.64 (t, *J*=6.1, 2H), 2.65 (t, *J*=7.1, 2H), 2.31 (s, 3H), 1.89-1.80 (m, 2H).

Synthesis of 11a

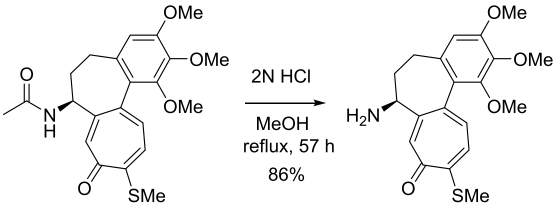

11a

To a solution of (-)-thiocolchicine (500 mg, 1.205 mmol) in MeOH (20 mL), HCl 2N (9.650 mL, 19.312 mmol) is added and the reaction mixture is stirred at reflux at 90 °C for 57 h. The solvent is removed under reduced pressure. H_2O (20 mL) is added and extracted with CH_2Cl_2 (3x15 mL). The aqueous layer is neutralized with NaOH, extracted with CH_2Cl_2. The organic layers are washed with brine and dried over Na_2SO_4. The solvent is removed under reduced pressure. The crude is purified by flash chromatography (CH_2Cl_2/MeOH 9:1) to obtain **11a** (0.387 g, Yield: 86 %).

^{1}H-NMR ($CDCl_3$, 300 MHz, detected signals): δ (ppm): 9.52 (bs, 2H), 7.58 (s, 1H), 7.19 (d, *J*=10.5 Hz, 1H), 7.03 (d, *J*=10.5 Hz, 1H), 6.54 (s, 1H), 4.25-4.20 (m, 1H), 3.91 (s, 6H), 3.66 (s, 3H), 2.43 (s, 3H), 2.41-2.28 (m, 4H).

Anal. calcd for ($C_{20}H_{23}NO_4S$): C, 64.32, H, 6.21, N, 3.75, S, 8.58; **Found**: C, 64.27, H, 6.35, N, 3.68, S, 8.47.

$[\alpha]_D^{20}$**:** -160.6 ° (c 0.35; MeOH).

Synthesis of 11b

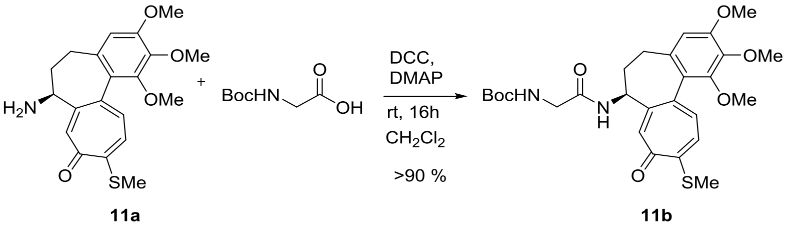

To a solution of **11a** (0.303 g, 0.812 mmol) in CH_2Cl_2 (30 mL), N-Boc-glycine (0.312 g, 0.59 mmol), DCC (1.009 g, 4.862 mmol) and DMAP (0.198 g, 1.624 mmol) are added. The reaction mixture is stirred at rt for 16 h, then filtered through Celite. The solvent is removed under reduced pressure. The crude is purified by flash chromatography (CH_2Cl_2/MeOH 95:5) to afford **11b** (0.420 g, > 90%).

^{1}H-NMR ($CDCl_3$, 300 MHz): δ (ppm): 8.20 (bs, 1H), 7.54-7.47 (m, 1H), 7.44-7.40 (m, 1H), 7.25 (s, 1H), 6.56 (s, 1H), 4.72-4.65 (m, 1H), 3.93-3.71 (m, 8H), 3.63 (s, 3H), 2.54-2.39 (m, 5H), 2.13-1.94 (m, 2H), 1.45 (s, 9H).

^{13}C-NMR ($CDCl_3$, 100 MHz, detected signals): δ (ppm): 182.3, 169.6, 158.2, 156.3, 154.5, 151.0, 141.8, 139.1, 135.5, 131.4, 128.1, 107.2, 80.6, 61.5, 61.3, 56.1, 52.1, 45.0, 36.4, 29.9, 28.3, 15.3.

Anal. Calcd for $C_{27}H_{34}N_2O_7S$: C, 61.11; H, 6.46; N, 5.28. **Found**: C, 61.14; H, 6.41; N, 5.30.

Synthesis of 11

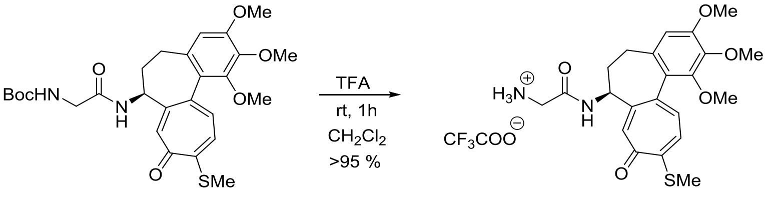
BocHN
O
N
H
OMe
OMe
OMe
O
SMe
TFA
rt, 1h
CH_2Cl_2
>95 %
$H_3N^{\oplus}$
$CF_3COO^{\ominus}$
O
N
H
OMe
OMe
OMe
O
SMe

11b **11**

To a solution of **11b** (0.420 g, 0.812 mmol) in dry CH_2Cl_2 (20 mL) at 0°C TFA (2.418 g, 21.085 mmol) is added and the reaction mixture is stirred at rt for 1 h. The solvent is removed under reduced pressure to obtain **11** (0.430 g, Yield: > 95%) without any further purification.

^{1}H-NMR ($CDCl_3$, 300 MHz, detected signals): δ (ppm): 10.33 (bs, 1H), 8.14 (d, *J*=5.4 Hz, 1H), 7.87 (d, *J*=11.4 Hz, 1H), 7.69 (d, *J*=11.4 Hz, 1H), 6.62 (s, 1H), 4.59-4.65 (m, 1H), 4.13-4.07 (m, 3H), 3.93 (s, 6H), 3.59 (s, 3H), 3.48-3.44 (m, 2H), 2.43-2.34 (m, 1H), 2.25 (s, 3H), 2.12-2.01 (m, 1H), 1.94-1.73 (m, 2H).

^{13}C-NMR ($CDCl_3$, 100 MHz, detected signals): δ (ppm): 182.3, 158.2, 156.3, 154.5, 151.0, 141.8, 139.1, 135.5, 131.4, 128.1, 107.2, 61.5, 61.3, 56.1, 52.1, 45.0, 36.4, 29.9, 15.3.

Anal. Calcd for $C_{22}H_{26}N_2O_5S$: C, 61.38; H, 6.09; N, 6.51. **Found**: C, 61.42; H, 6.08; N, 6.48.

Synthesis of 12

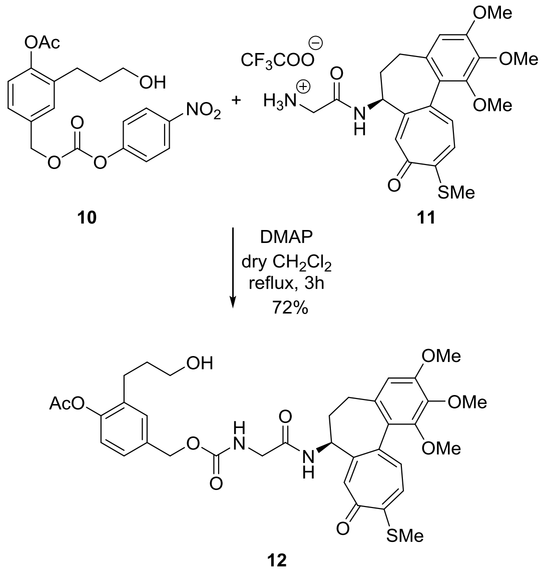
OAc
OH
NO2
10
CF3COO
H3N
11
OMe
SMe
DMAP
dry CH2Cl2
reflux, 3h
72%
AcO
12

To a solution of **11** (0.438 g, 0.812 mmol) in dry CH_2Cl_2 (10 mL) DMAP (0.247 g, 2.015 mmol) and a solution of **10** (0.315 g, 0.812 mmol) are added and the reaction mixture is stirred at reflux at 40°C for 3 h. The solvent is removed under reduced pressure. The crude is purified by flash chromatography (CH_2Cl_2/MeOH 95:5) to afford **12** (0.399 g, 72%).

^{1}H-NMR ($CDCl_3$, 300 MHz, detected signals): δ (ppm): 8.14-8.01 (m, 1H), 7.59-7.87 (m, 2H), 7.30 (s, 1H), 7.16-7.06 (m, 1H), 6.98-6.92 (m, 1H), 6.53 (s, 1H), 5.01 (s, 2H), 4.68-4.62 (m, 1H), 3.93-3.87 (m, 8H), 3.62 (s, 3H), 3.59-3.54 (m, 2H), 2.61-2.54 (m, 4H), 2.41 (s, 3H), 2.29 (s, 3H), 1.91-1.76 (m, 4H).

Synthesis of 13a

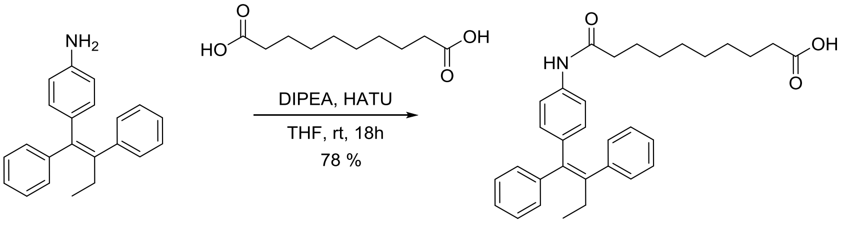

13a

To a solution of sebacic acid (0.255 g, 1.263 mmol) in dry THF (20 mL) HATU (0.527 g, 1.386 mmol) and DIPEA (0.326 g, 2.523 mmol) are added and the reaction mixture is stirred for 30 minutes. Then 4-(1,2-diphenylbut-1-en-1-yl)aniline (0.378 g, 1.265 mmol) is added and the reaction mixture is stirred at rt overnight. The solvent is removed under reduced pressure, AcOEt is added and it is washed with water and brine. The organic layer is then dried over Na_2SO_4 and concentrated under reduced pressure. The crude is purified by flash chromatography (AcOEt/Hex 4:6) to obtain pure **13a** (0.476 g, Yield: 78%).

^{1}H-NMR ($CDCl_3$, 300 MHz): δ(ppm)= 7.33-7.02 (m, 12H), 6.80 (d, *J*=7.8, 2H), 4.78 (bs, 1H), 2.43 (q, *J* = 7.6 Hz, 2H), 2.30 (t, *J*=7.7 Hz, 2H), 2.25 (t, *J*=7.5 Hz, 2H), 1.75-1.55 (m, 4H), 1.40-1.25 (m, 8H), 0.92 (t, *J* =7.7 Hz).

^{13}C-NMR ($CDCl_3$, 75 MHz): δ(ppm)= 175.3, 174.6, 145.1, 143.2, 143.1, 141.3, 139.7, 135.4, 131.9, 129.6, 129.4, 128.2, 127.7, 127.3, 126.3, 116.1, 37.58, 34.98, 31.80, 30.81, 26.96, 26.22, 13.60.

Synthesis of 13b

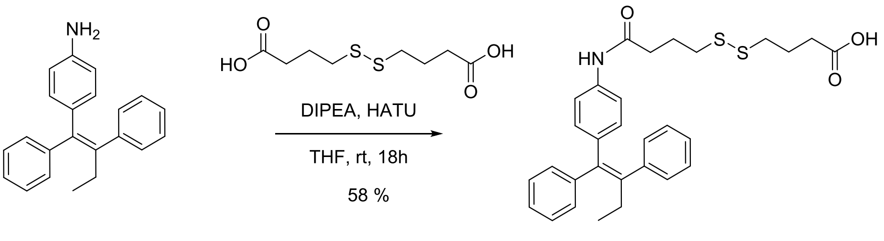

13b

To a solution of 4,4'-dithiobutyric acid (0.228 g, 0.958 mmol) in dry THF (15 mL) HATU (0.401 g, 1.054 mmol) and DIPEA (0.248 g, 1.921 mmol) are added and the reaction mixture is stirred for 30 minutes. Then 4-(1,2-diphenylbut-1-en-1-yl)aniline (0.827 g, 0.958 mmol) is added and the reaction mixture is stirred at rt overnight. Then, the solvent is removed under reduced pressure. H_2O (20 mL) is added, acidified with HCl and extracted with CH_2Cl_2 (3x15 mL). The combined organic layers are dried over Na_2SO_4 and evaporated under reduced pressure. The crude is purified by flash chromatography (Hex/EtOAc 6:4 + 1% of glacial acetic acid) to provide **13b** (0.289 g, Yield: 58%).

^{1}H-NMR ($CDCl_3$, 300 MHz) δ(ppm): 7.30-7.05 (m, 12H), 6.80 (d, *J*=8.5 Hz, 2H), 2.75 (q, *J*=7.6 Hz, 2H), 2.45 (t, *J*=7.5 Hz, 4H), 2.07-1.96 (m, 4H), 1.35-1.25 (m, 4H), 0.95 (t, *J*=7.7 Hz, 3H).

Synthesis of 1

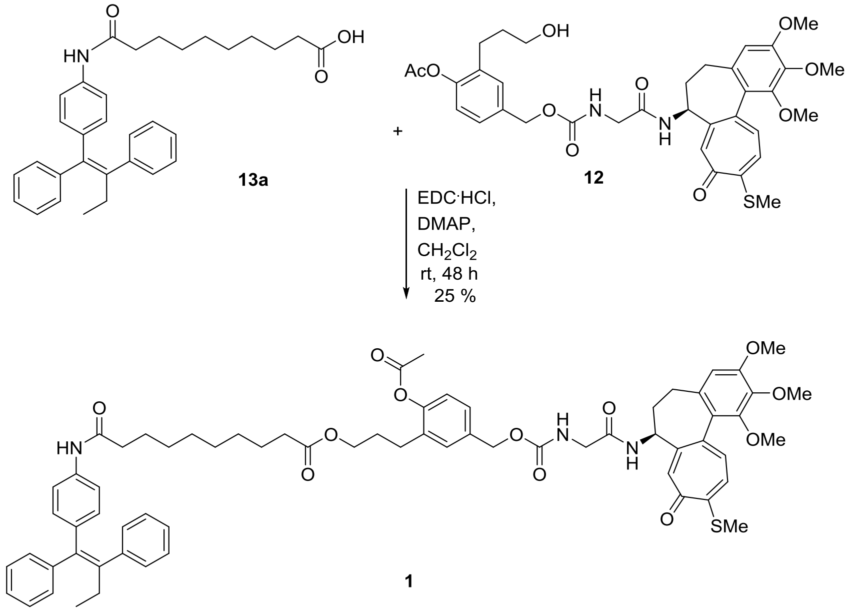

To a suspension of **13a** (0.106 g, 0.221 mmol) in dry CH_2Cl_2 (5 mL) EDC·HCl (0.050 g, 0.262 mmol), DMAP (0.019 g, 0.154 mmol) are added and the reaction mixture is stirred for 30 minutes. Then **12** (0.150 g, 0.221 mmol) is added and the reaction mixture is stirred at rt for 48 h. The solvent is removed under reduced pressure. The crude is purified by flash chromatography (CH_2Cl_2/MeOH 98:2) to afford **1** (0.063 g, 25%).

^{1}H-NMR ($CDCl_3$, 300 MHz, detected signals): δ (ppm): 7.47-6.79 (m, 20H), 6.53 (s, 1H), 5.01 (s, 2H), 4.68-4.62 (m, 1H), 4.07-4.02 (m, 2H), 3.93-3.87 (m, 8H), 3.62 (s, 3H), 2.61-2.42 (m, 6H), 2.39 (s, 3H), 2.23-2.17 (m, 7H), 1.89-1.85 (m, 2H), 1.70-1.59 (m, 6H), 1.36-1.22 (m, 8H), 0.92 (t, *J* =7.7 Hz, 3H).

^{13}C-NMR (400 MHz, $CDCl_3$, detected signals): δ (ppm): 172.02, 170.08, 169.49, 159.11, 157.33, 154.38, 151.84, 149.39, 144.14, 143.69, 142.86, 142.71, 142.36, 139.94, 139.45, 139.10, 138.84, 137.38, 136.49, 135.60, 135.00, 134.87, 133.82, 131.98, 131.46, 130.70, 130.34, 130.14, 129.11, 128.79, 128.56, 128.44, 127.99, 127.89, 127.44, 127.28, 126.84, 126.39, 126.27, 123.15, 120.10, 119.24, 115.24, 114.73, 108.13, 67.20, 64.25, 62.23, 62.06, 56.80, 52.87, 45.21, 38.30, 37.20, 34.99, 34.49, 32.59, 30.54, 30.35, 29.73, 29.65, 29.42, 27.42, 26.16.

ESI-MS: m/z 1168.8 $[M+Na]^+$.

Synthesis of 2

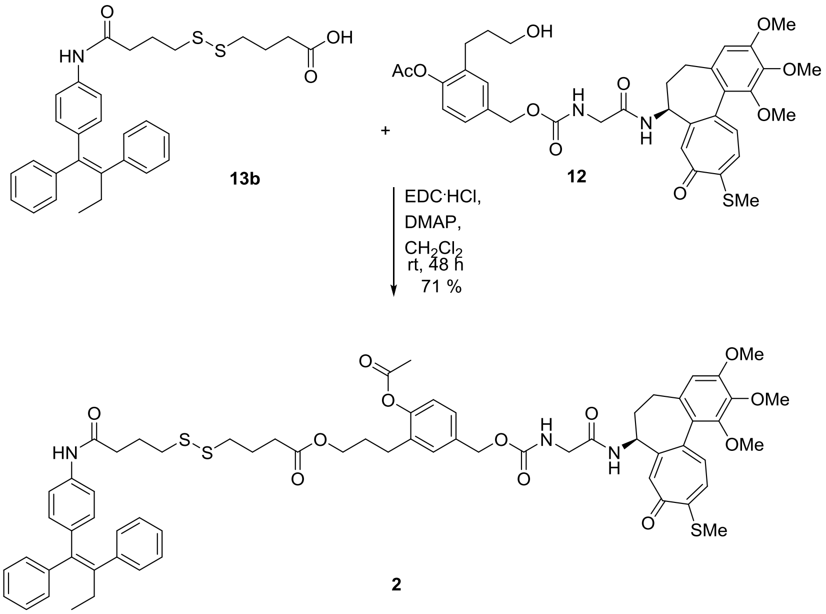

To a suspension of **13b** (0.114 g, 0.221 mmol) in dry CH_2Cl_2 (5 mL) EDC·HCl (0.050 g, 0.262 mmol), DMAP (0.019 g, 0.154 mmol) are added and the reaction mixture is stirred for 30 minutes. Then **12** (0.150 g, 0.221 mmol) is added and the reaction mixture is stirred at rt for 48 h. The solvent is removed under reduced pressure. The crude is purified by flash chromatography (CH_2Cl_2/MeOH 95:5) to afford **2** (0.184 g, 71%).

^{1}H-NMR (300 MHz, $CDCl_3$, detected signals): δ (ppm): 7.47-6.75 (m, 20H), 6.53 (s, 1H), 4.95 (s, 2H), 4.68-4.62 (m, 1H), 4.07-4.02 (m, 2H), 3.93-3.87 (m, 8H), 3.62 (s, 3H), 2.69-2.25 (m, 20H), 2.09-1.82 (m, 8H), 0.92 (t, *J*=7.7 Hz, 3H).

^{13}C-NMR (400 MHz, $CDCl_3$, detected signals): δ (ppm): 182.91, 173.76, 171.08, 170.09, 169.61, 159.07, 157.34, 154.36, 151.84, 149.35, 144.13, 142.84, 142.73, 142.32, 139.50, 139.09, 138.83, 136.51, 135.52, 135.06, 134.93, 133.68, 131.96, 131.45, 130.67, 130.33, 130.13, 129.19, 128.80, 128.57, 127.83, 127.28, 126.85, 126.29, 123.12, 120.13, 119.26, 114.73, 108.14, 67.12, 64.52, 62.23, 62.06, 56.80, 52.90, 45.12, 38.65, 38.35, 37.09, 36.07, 33.26, 30.58, 30.35, 29.73, 29.29, 27.38, 25.14, 24.97, 21.59, 15.80, 14.20.

ESI-MS: m/z 1204.7 $[M+Na]^+$.

Lipase-incubation of 1

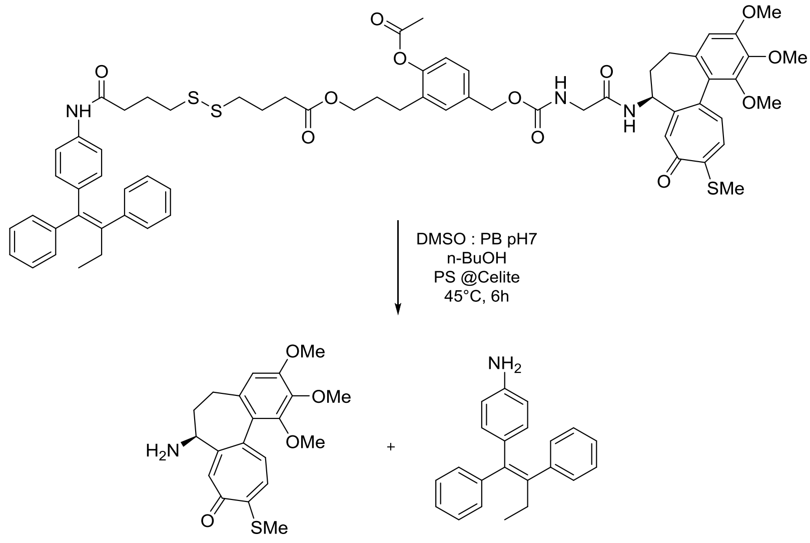
OMe
OMe
OMe
O
NH
S
S
O
O
O
O
H
N
O
N
H
O
SMe
DMSO : PB pH7
n-BuOH
PS @Celite
45°C, 6h
OMe
OMe
OMe
H2N
O
SMe
+
NH2

To a solution of **1** in DMSO : Posphate Buffer 20 mM pH7 (1 mg/mL), n-BuOH (0.010 mL, 0.1091 mmol) and the desired enzyme (PS @Celite, 10 mg) preparation are added. The mixture is incubated at 45°C for 6 hours, then half the reacting media is extracted with AcOEt. The organic layer is dried over Na_2SO_4, evaporated *in vacuo* and dissolved again in CH_3CN/ MeOH (2:1) in order to be analysed by reversed-phase HPLC (Kinetex 5µ EVO C18 100Å, λ= 256 nm, flow= 0.3 mL/min, A= H_2O milliQ + 0.01 TFA, B= CH_3CN + 0.01 TFA, gradient: t_0 A= 90%, 30 min A=20%, 35 min A=0%,).

Overnight reaction with PS @Celite gave the 85% of **1** hydrolysis on the bases of the total products area, in this case deacetylthiocolchicine and 4-(1,2-diphenylbut-1-en-1-yl)aniline.

Lipase-incubation of 2

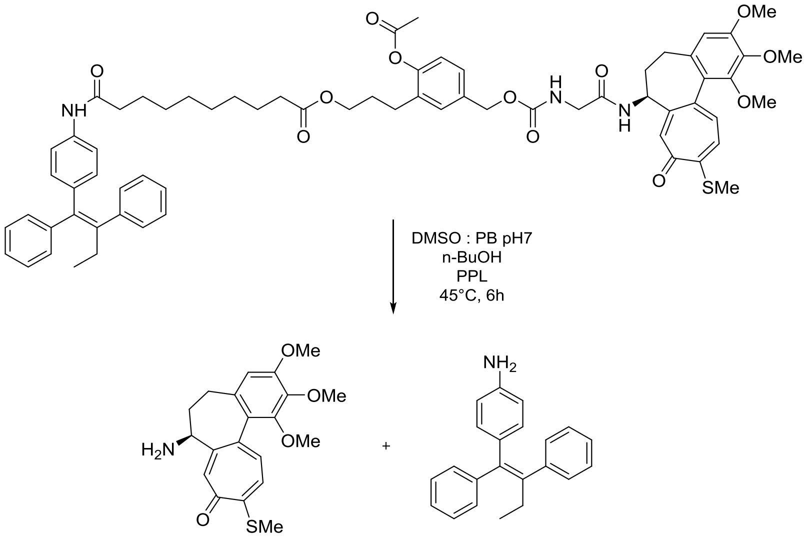

To a solution of **2** in DMSO : Posphate Buffer 20 mM pH7 (1 mg/mL), n-BuOH (0.010 mL, 0.1091 mmol) and the desired enzyme (PPL, Porcine Pancreatic lipase type II, 10 mg) preparation are added. The mixture is incubated at 45°C for 6 hours, then half the reacting media is extracted with AcOEt. The organic layer is dried over Na_2SO_4, evaporated in vacuo and dissolved again in CH_3CN/ MeOH (2:1) in order to be analysed by reversed-phase HPLC (Kinetex 5µ EVO C18 100Å, λ= 256 nm, flow= 0.3 mL/min, A= H_2O milliQ + 0.01 TFA, B= CH_3CN + 0.01 TFA, gradient: t_0 A= 90%, 30 min A=20%, 35 min A=0%,).

Overnight reaction with PPL gave the 85% of **2** hydrolysis on the bases of the total products area, in this case deacetylthiocolchicine and 4-(1,2-diphenylbut-1-en-1-yl)aniline.

5. Dual-drug conjugates

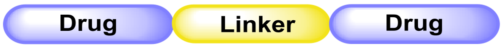
Drug
Linker
Drug

In this chapter, a different class of self-assembling conjugates is described. These compounds are characterized by a homodimeric structure: two molecule of the same drug are connected through a disulphide-containing linker (**Figure 48**).

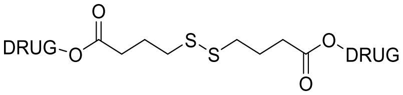

Figure 48. General structure of the homodimeric conjugates.

The publication of a recent paper regarding the spontaneous formation of nanoparticles by self-assembly of homodimeric compounds, which are not characterized by the presence of a self-assembly inducer tail,[177,178] moved us to reconsider the synthesis of disulphide-containing bivalent compounds, previously reported by our research group and able to release active drugs inside tumor cells.[179]

As a linker, we selected 4,4'-dithiodibutyric acid based on our previous studies, and we used paclitaxel (Chapter 2), podophyllotoxyn (Chapter 3), epothilone A and camptothecin as anticancer drugs.

Epothilone A

The epothilones are a class of natural cytotoxic macrolides first isolated by Gerhard Höfle of the National Biotechnology Research Institute in Braunschweig, Germany from a cultured strain of the myxobacterium *Sorangium cellulosum* in the late 1980s.[180,181] The chief components of the fermentation process are epothilone A and B, with epothilone C and D found in smaller amounts. Trace amounts of other epothilones are also detected (**Figure 49**).

The structures of epothilones A and B include a 16-membered macrocyclic lactone that differs only in the presence of a hydrogen or methyl group, while epothilones C and D lack of the epoxide ring.

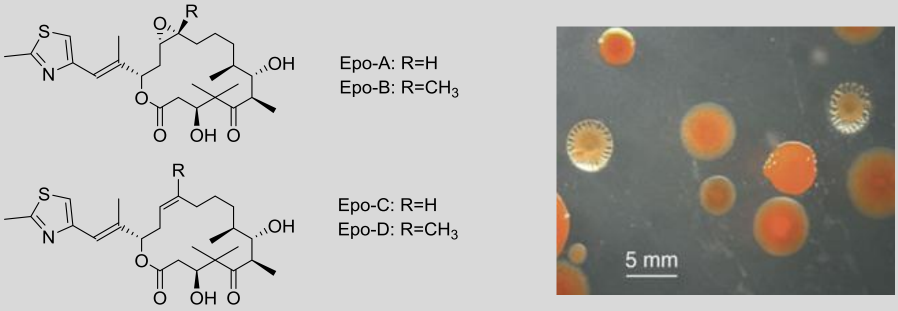

Figure 49. Epothilones and *Sorangium Cellulosum*.

Although the epothilones can already be made by fermentation, several research groups have reported methods for their total synthesis.[182]

Epothilones, like paclitaxel, induce tubulins to form microtubules at low temperatures and without guanosine triphosphate or microtubule-associated proteins.[183]

Epothilones exhibit kinetics similar to those of paclitaxel in inducing tubulin polymerization into microtubules *in vitro* (filtration, light scattering, sedimentation, and electron microscopy) and in producing enhanced microtubule stability and bundling in cultured cells. Furthermore, these 16-membered macrolides are competitive inhibitors of paclitaxel binding, exhibiting a 50% inhibitory concentration almost identical to that of paclitaxel in displacement competition assays.

Epothilone A has been shown to be 2000 to 5000 times more active than paclitaxel *in vitro* against *P*-glycoprotein– expressing MDR tumors and cell lines as well as tumors resistant to the taxanes based on tubulin mutations.

Unfortunately, epothilones showed to be unstable in mouse plasma, resulting in metabolites with a mass 18 units higher than the parent drugs, and it was subsequently demonstrated that administration of the esterase inhibitor bis(4-nitrophenyl)-phosphate produced an active result in the A2780 ovarian carcinoma tumor model.

For these reasons many efforts have been made in order to synthetize epothilone analogues with the goal of improving metabolic stability.

Camptothecin

Camptothecin (CPT) is a pentacyclic quinoline-containing alkaloid isolated in 1958 from *Camptotheca Acuminata*[184] (**Figure 50**) that acts as a selective inhibitor of the nuclear enzyme Topoisomerase I (TOP I).

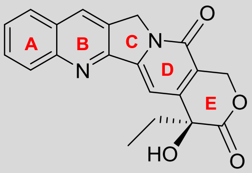

Figure 50. Camptothecin and *Camptotheca Acuminata.*

Unfortunately, therapeutic application of unmodified CPT is hindered by very low water solubility in aqueous medium, high toxicity and rapid inactivation through lacone hydrolysis *in vivo*.

To overcome the solubility and stability issues, various derivatives have been developed. Although a number of small and large molecule compounds are currently in clinical trials, only two CPT derivatives, irinotecan and topotecan, are approved for clinical use (**Figure 51**).[185]

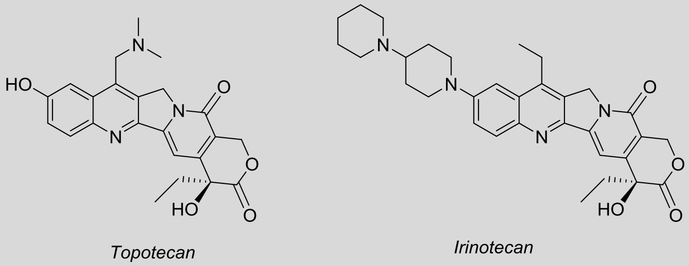

Figure 51. Structures of camptothecin analogues.

Irinotecan is currently used for metastatic colorectal cancer, while topotecan has been approved for ovarian cancer, cervical cancer and small-cell lung cancer.

These derivatives employ tertiary amine cations to improve solubility and subsequently improve lactone stability.

Substituted camptothecins

To summarize the SAR studies, the A and B rings are the most tolerant to modification with substitutions at positions 7, 9, 10, and 11 improving or retaining activity.[186] Interestingly, von Hoff has provided evidence that substitutions that increase hydrogen bonding at the 7-position improve binding to TOP I, thus increasing activity over CPT.[187]

On the other hand, altering the C and D rings or substituting positions 12 and 14 inactivates the molecules.

Finally, the E-ring lactone is necessary for activity by binding to TOP I: Hydrolysis or removal of the lactone leads to loss of all activity. The equilibrium between the closed, active lactone and the open, inactive carboxylate form is influenced by both the affinity of the carboxylate for human serum albumin and the local pH *in vivo* (**Figure 52**).

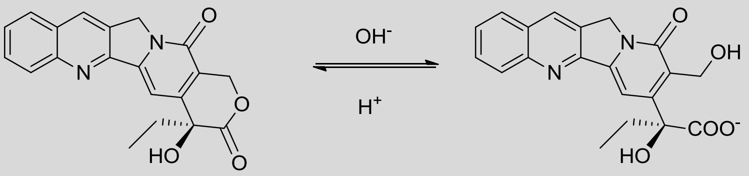

Figure 52. Lactone hydrolysis.

Since it is the site where binding to TOP I occurs, the E ring tolerates only minor modifications without dramatic, negative effects. For example, enlargement of the ring to form the betahydroxy lactone improves stability and drug activity. Interestingly, modification of the C20 hydroxyl group through alkylation or acylation has been shown to stabilize the lactone. Acylation is the favoured method for linking CPT covalently to macromolecules.

In addition, different kinds of CPT formulations have been prepared in order to accomplish CPT delivery to tumour cells by passive targeting, including micelles,[188] liposomes,[189] chitosan nanoparticles[190] and hydrogels.[191]

Synthesis of the conjugates

The general reaction for the synthesis of the homodimeric conjugates is reported in **Scheme 18**.

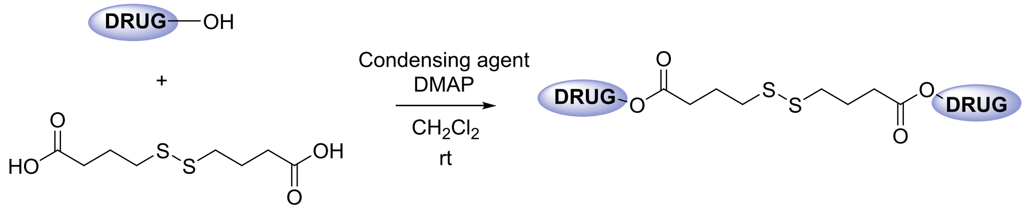

Scheme 18. General reaction for the synthesis of homodimeric compounds **1**-**4**.

All the conjugates were synthetized through a condensation reaction mediated by a condensing agent in the presence of DMAP. As condensing agent, it was used EDC·HCl for the drugs podophyllotoxyn, paclitaxel and camptothecin and DCC in the case of epothilone A (**Table 14**).

Drug	Condensing agent	Reaction time (h)	Yield (%)
Podophyllotoxyn (**1**)	EDC·HCl	72	85
Paclitaxel (**2**)	EDC·HCl	96	29
Epothilone-A (**3**)	DCC	96	16
Camptothecin (**4**)	EDC·HCl	96	27

Table 14. Reaction conditions and yields for the synthesis of dimers **1**-**4**.

^{1}H-NMR analysis of the isolated products confirmed the formation of the ester bond: for the derivatives of podophyllotoxyn, paclitaxel and epothilone A we were able to observe a downshift of the hydrogen on the carbon bearing the hydroxylic functionalized group (**Table 15**).

For the homodimeric conjugate of camptothecin, the ^{1}H-NMR was not crucial for the product characterization because the derivatized hydroxylic group is on a quaternary carbon.

Drug	Signal	Parental drug (ppm)	Product (ppm)
Podophyllotoxin	EDC·HCl	4.61	5.85
Paclitaxel	H-2’	4.78	5.51
Epothilone-A	H-7	3.80	5.44-5.37

Table 15. ^{1}H-NMR signal shift.

The definitive confirmation of the homodimeric structure of the products was achieved using mass spettrometry analysis. For conjugates 1-3 it was verified the presence of two molecule of the drugs bound to the 4,4’-dithiodibutyric acid, but for conjugate 4 it was demonstrated the formation of the product shown below (**Figure 53**).

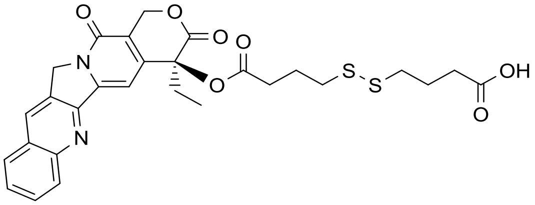

Figure 53. Structure of the obtained product.

Nanoparticles characterization

Next, the ability of the obtained compounds **1**-**3** to form NPs was investigated. Three different nanosuspensions were prepared by a dropwise addition of an organic solution of the compounds to ultrapure water and by the subsequent removal of the organic solvent under reduced pressure. All the conjugates seemed to self-assemble, and the resulting homogeneous suspensions were characterized by DLS.

DLS measurements (**Table 16**) gave the confirmation of the success of the process: compounds **1**, **2** and **3** were able to give monodisperse suspensions of NPs, with hydrodynamic diameters in the range of 200-300 nm.

Zeta potential values were negative for both the nanoassemblies suggesting that the electrostatic repulsion contributes to the colloidal stability of the suspension.

Compound	Mean Diameter (nm)	Z potential (mV)
1	298.5 ± 11.21	-14.7 ± 3.16
2	198.1 ± 6.747	-32.1 ± 0.709
3	208.7 ± 2.205	-21.1 ± 0.635

Table 16. Nanoparticles characterization.

The next step is the biological evaluation of the activity on different types of cell lines of these conjugates and of the corresponding nanoparticles.

Experimental Procedures

General

Thin-layer chromatography (TLC) was performed on Merck precoated 60F254 plates. Reactions were monitored by TLC on silica gel, with detection by Uv light (λ = 254 nm) or by charring with 1% permanganate solution. Flash chromatography was performed using Silica gel (240-400 Mesh, Merck). NMR spectra were recordered with Brucker 300 and 400 MHz spectrometers. Chemical shifts are reported in parts per million (δ) downfield from tetramethylsilane (TMS). EI mass spectra were recorded at an ionizing voltage of 6 kEv on a VG 70-70 EQ. ESI mass spectra were recorded on FT-ICR APEXII. Specific rotations were measured with a P-1030-Jasco polarimeter with 10 cm optical path cells and 1 ml capacity (Na lamp, λ = 589 nm). Microwave assisted reaction were performed with Emrys Creator single-mode (power range 0-400 W from magnetron at 2.45 GHz).

Synthesis of 1

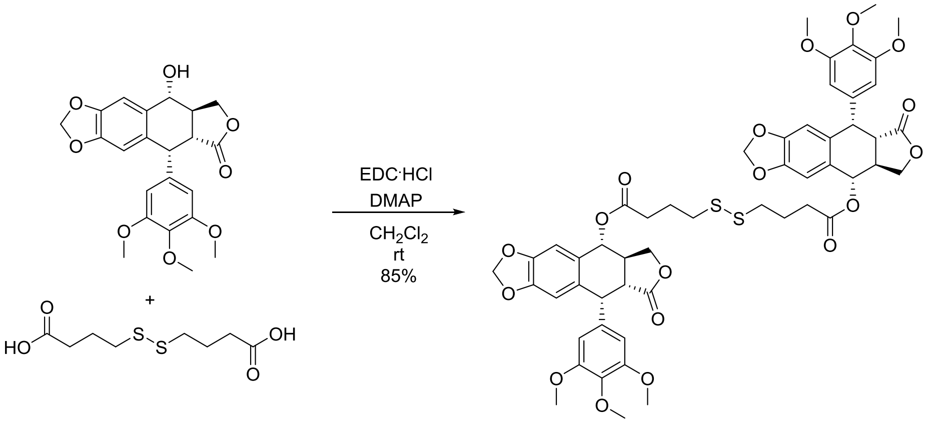

To a solution of 4,4′-dithiodibutyric acid (0.009 g, 0.0.041 mmol) in dry CH_2Cl_2 (3 mL) EDC·HCl (0.016 g, 0.082 mmol), DMAP (0.010 g, 0.082 mmol) and podophyllotoxin (0.050 g, 0.082 mmol) are added and the reaction mixture is stirred for 72 h. The solvent is removed under reduced pressure. The crude is purified by flash chromatography (CH_2Cl_2/MeOH 96:4) to afford **1** (0.036 g, 85%).

^{1}H-NMR ($CDCl_3$, 400 MHz): δ (ppm): 6.78 (s, 2H), 6.53 (s, 2H), 6.39 (s, 4H), 5.91 (d, *J*=4.2 Hz, 4H), 5.88 (d, *J*=8.1 Hz, 2H), 4.58 (d, *J*=3.6 Hz, 2H), 4.53-4.41 (m, 2H), 4.15-4.04 (m, 2H), 3.80 (s, 6H), 3.75 (s, 12H), 2.83-2.75 (m, 4H), 2.70-2.62 (m, 4H), 2.55-2.40 (m, 4H), 2.07-1.98 (m, 4H).

^{13}C-NMR ($CDCl_3$, 400 MHz): δ(ppm): 173.6, 173.4, 152.6, 148.2, 147.6, 137.1, 134.8, 132.4, 128.2, 109.8, 108.1, 107.0, 101.7, 73.8, 71.3, 60.7, 56.2, 45.5, 43.7, 38.7, 37.5, 32.5, 24.0.

ESI-MS: m/z 1053.46 $[M + Na^+]^+$.

$[\alpha_D^{22}]$= -89.11 (c = 0.365, $CHCl_3$).

Synthesis of 2

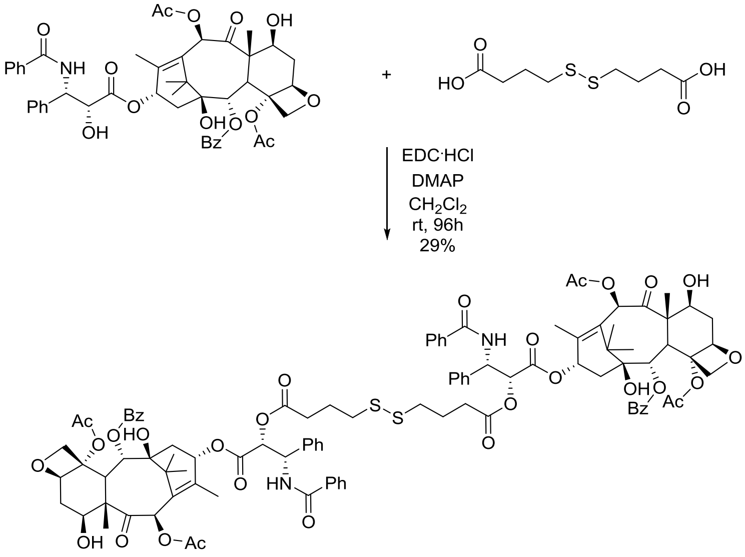

To a solution of 4,4′-dithiodibutyric acid (0.007 g, 0.0.029 mmol) in dry CH_2Cl_2 (2 mL) EDC·HCl (0.007 g, 0.058 mmol), DMAP (0.011 g, 0.058 mmol) and paclitaxel (0.050 g, 0.058 mmol) are added and the reaction mixture is stirred for 96 h. The solvent is removed under reduced pressure. The crude is purified by flash chromatography (CH_2Cl_2/MeOH 95:5) to afford **2** (0.016 g, 29%).

^{1}H-NMR ($CDCl_3$, 400M Hz): δ (ppm): 8.13 (d, *J*=7.9 Hz, 4H), 7.74 (d, *J*=7.8 Hz, 4H), 7.61 (t, *J*=7.8 Hz, 2H), 7.53-7.40 (m, 18H), 7.35 (s, 2H), 6.90 (d, *J*=6.7 Hz, 2H), 6.27 (s, 2H), 6.23-6.17 (m, 2H), 6.00-5.89 (m, 2H), 5.72 (d, *J*=6.9 Hz, 2H), 5.51 (d, *J*=3 Hz, 2H), 4.95 (d, *J*=8.4 Hz, 2H), 4.45-4.34 (m, 2H), 4.30 (d, *J*=14.4 Hz, 2H), 4.19 (d, *J*=14.4 Hz, 2H), 3.81 (d, *J*=6.9 Hz, 2H), 2.65-2.50 (m, 10H), 2.43 (s, 6H), 2.35-2.28 (m, 4H), 2.23 (s, 6H), 2.07-1.71(m, 18H), 1.24 (s, 6H), 1.14 (s, 6H).

^{13}C-NMR ($CDCl_3$, 400 MHz): δ(ppm): 204.43, 172.63, 171.89, 170.49, 168.72, 167.72, 143.32, 137.60, 134.36, 133.54, 132.70, 132.24, 130.91, 130.58, 130.40, 129.78, 129.42, 129.19, 128.48, 127.78, 127.20, 85.11, 81.77, 79.85, 76.26, 75.91, 74.74, 73.51, 72.53, 70.12, 59.20, 53.44, 46.29, 43.86, 37.59, 36.23, 32.60, 30.36, 27.48, 24.51, 23.38, 22.76, 21.48, 15.48, 10.28.

ESI-MS: m/z 1910.17 $[M + Na^+]^+$.

$[\alpha_D^{22}]$= -40.5077(c=0.65,$CHCl_3$).

Synthesis of 3

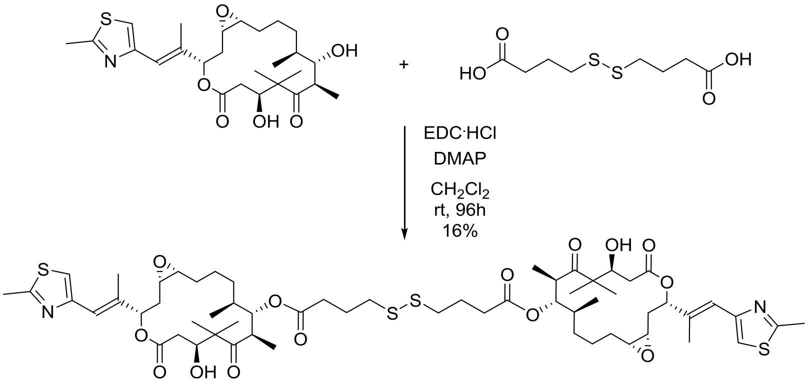

To a solution of 4,4′-dithiodibutyric acid (0.007 g, 0.0.030 mmol) in dry CH_2Cl_2 (2 mL) DCC (0.012 g, 0.061 mmol), DMAP (0.007 g, 0.061 mmol) and epothilone A (0.030 g, 0.061 mmol) are added and the reaction mixture is stirred for 96 h. The solvent is removed under reduced pressure. The crude is purified by flash chromatography (Hex/AcOEt 1:1) to afford **3** (0.006 g, 16%).

^{1}H-NMR (400 MHz, $CDCl_3$): δ(ppm): 7.05 (s, 2H), 6.63 (s, 2H), 5.51 (dd, *J*=2.3, 6.8 Hz, 2H), 5.38 (dd, J_1=1.9, 8.7 Hz, 2H), 4.14-4.11 (m, 2H), 3.42-3.38 (m, 2H), 3.10-3.06(m, 2H), 2.93-2.90 (m, 2H), 2.78 (t, *J*=7.0 Hz, 4H), 2.72 (s, 6H), 2.61-2.54 (m, 4H), 2.50 (t, *J*=7.3 Hz, 4H), 2.15 (s, 6H), 2.15-2.10 (m, 2H), 2.06 (t, *J*=7.1 Hz, 4H), 1.99-1.96 (m, 2H), 1.80-1.76 (m, 2H), 1.65-1.55 (m, 8H), 1.38 (s, 6H), 1.33-1.18 (m, 4H), 1.13 (s, 6H), 1.08 (d, *J*=6.9 Hz, 6H), 0.94 (d, *J*=6.8 Hz, 6H).

^{13}C-NMR (400 MHz, $CDCl_3$): δ(ppm): 216.2, 172.3, 170.4, 164.3, 152.2, 136.6, 120.0, 116.3, 78.4, 76.1, 73.9, 57.3, 53.8, 52.3, 43.7, 38.5, 38.0, 34.5, 32.6, 31.8, 29.4, 26.3, 24.4, 24.1, 22.1, 20.4, 19.0, 17.5, 15.5, 15.3.

ESI-MS: m/z 1211.50[M + Na$^+$]$^+$.

$[\alpha_D^{25}]$= -3.8 (c =0.554, $CHCl_3$).

Synthesis of 4

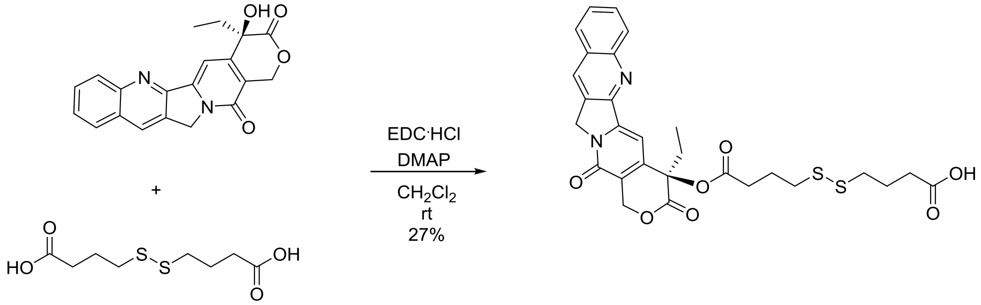

To a solution of 4,4′-dithiodibutyric acid (0.017 g, 0.0.072 mmol) in dry CH_2Cl_2 (3 mL) EDC·HCl (0.027 g, 0.143 mmol), DMAP (0.017 g, 0.143 mmol) and camptothecin (0.050 g, 0.143 mmol) are added and the reaction mixture is stirred for 96 h. The solvent is removed under reduced pressure. The crude is purified by flash chromatography (CH_2Cl_2/MeOH 96:4) to afford **4** (0.011 g, 27%).

^{1}H-NMR (DMSO, 300 MHz): δ(ppm): 8.71 (s, 1H), 8.21-8.13 (m, 2H), 7.89 (t, *J*=9.1, 6.3 Hz, 1H), 7.71 (t, *J*=9.1, 6.3 Hz, 1H), 7.03 (s, 1H), 5.51 (s, 2H), 5.27 (s, 2H), 2.76-2.66 (m, 8H), 2.16 (q, *J*=6.2 Hz, 4H), 2.0-1.85 (m, 2H), 0.94 (t, *J*=9.3 Hz, 3H).

^{13}C-NMR (DMSO, 300 MHz): δ(ppm): 171.62, 168.7, 156.61, 152.47, 147.94, 146.09, 145.42, 131.64, 130.46, 129.87, 128.99, 128.60, 128.06, 127.77, 118.84, 94.74, 75.91, 66.33, 50.31, 36.93, 36.23, 32.53, 31.74, 30.22, 24.14, 23.98, 7.62.

ESI-MS: m/z 591.28 [M + Na$^+$]$^+$.

6. Conclusions

The project developed in my three-year Ph.D is about the functionalization of known anticancer compounds to form bioconjugates, characterized by an enhanced pharmacokinetic profile. These conjugates were synthetized in order to have self-assembly properties and to form nanoparticles in an aqueous media.
In this thesis, we considered all the parts of these bioconjugates:

- the self-assembly inducer
- the linker moiety
- the active compound

We first illustrated the preparation and characterization of different squalene-conjugates: drug-squalene conjugates of paclitaxel, cyclopamine and doxorubicin and fluorescent squalene conjugates of fluorescin and tetramethylrhodamine, that resulted very promising for the study of nanoparticles internalization mechanisms by fluorescence spectroscopy.
Then we applied the approach of the co-nanoprecipitation of different drug-squalene conjugates to obtain hetero-nanoparticles, useful for combined chemotherapy. *In vitro* and *in vivo* evaluation of different combinations of these conjugates gave very promising results demonstrating the maintenance of the cytotoxic activity of the drugs and lowering their toxicity.

We next moved to the preparation of bivalent drug-conjugates, characterized by a cytotoxic moiety, the tamoxifen analog 4-(1,2-diphenylbut-1-en-1-yl)aniline, as self-assembly inducer, and aloin or podophyllotoxin as cytotoxic drugs. We demonstrated the ability of 4-(1,2-diphenylbut-1-en-1-yl)aniline to induce the formation of nanoparticles and this result open the possibility to prepare a wide collection of 4-(1,2-diphenylbut-1-en-1-yl)aniline based conjugates containing different anticancer drugs as building blocks and proper linkers to induce drug release after cell internalization.

Furthermore, we studied the synthesis of a new self-immolative linker able to improve the drug release from the conjugates and bearing a useful anchor point for the introduction of a self-assembly inducer. We employed this new linker in the preparation of two new conjugates containing thiocolchicine as anticancer compound and 4-(1,2-diphenylbut-1-en-1-yl)aniline as a cytotoxic self-assembly inducer. The ability of the self-immolative linker to release the two active part of the conjugates in the presence of a lipase was confirmed. We also demonstrated the ability of the conjugates to self-assemble in nanoparticles and in the future we are planning to test the maintenance of the antiproliferative activity of the two building blocks in the nanoformulated systems.

Finally we achieved the preparation of homodimeric compounds of the known anticancer compounds paclitaxel, podophyllotoxin and epothilone A. These conjugates were designed to be able to self-assemble in nanoparticles without the presence of a self-assembly inducer tail and to release the active units thanks to the presence of a disulphide containing linker. We verified the ability of the homodimeric compounds to self-assemble in nanoparticles by DLS and the biological evaluation of the nanoassemblies is in progress.

All together, the results here reported demonstrated that it is possible:

- to obtain, by simple modification, compounds that are able to self-assemble in nanoparticles;
- to obtain hetero-nanoparticles by mixing different compounds functionalized with the same self-assembly inducer;
- to obtain fluorescent hetero-nanoparticles by combining drug-conjugates with a dye-conjugate, functionalized with the same self-assembly inducer, with the aim to study cell internalization mechanism.

This approach can be applied for different types of diseases such as neurodegeneration and bacterial pathologies, and it could be useful for the implementation of a personalized medicine.

Acknowledgements

First, I would like to thank my supervisor Prof. Daniele Passarella for the enthusiastic encouragement and useful advice he has provided during these three years. I would also like to offer a special thank to the research group for the support and help.

Furthermore, the results obtained during this three-year project have been achieved thanks to a wide collaboration network including groups specialized in different research fields.

Nanoparticles characterization were made in collaboration with Dott. Barbara Stella and Prof. Franco Dosio of Università degli Studi di Torino and NanoBioLab (Dott. Benedetta Riva, Dott. Veronica Collico and Prof. Davide Prosperi) of Università degli Studi di Milano-Bicocca.

Biological evaluations were made in collaboration with Dott. Francesca Ricci and Dott. Giovanna Damia of IRCCS-Istituto di Ricerche Farmacologiche Mario Negri, Dott. Davide Cartelli and Prof. Graziella Cappelletti of Università degli Studi di Milano, Prof. Lisa Dalla Via of Università degli Studi di Padova and Dott. Panagiota A. Sotiropoulou of IRIBHM, Université Libre de Bruxelles.

Imaging analyses were made in collaboration with Dott. Davide Mazza of San Raffaele Scientific Institute.

Enzymatic reaction were made in collaboration with the group of Dr. Sergio Riva of the Institute of the Chemistry of Molecular Recognition of the Italian National Council of Research.

Finally I want to thank Prof. Maria Pérez Bosch and Prof. Joan Bosch of the group SINTEFARMA (Universitat de Barcelona, Spain) for my abroad period and the CM1106 COST Action ‘Chemical Approaches for Targeting Drug Resistance in Cancer Stem Cells’ for the financial support in this project.

Bibliography

---

[1] Song M, Liu, T, Shi C, Zhang X, Chen X, *ACS Nano* **2017**, *11*, 12−18.

[2] Haque N, Khalel R, Parvez N, Yadav S, Hwisa N, Al-Sharif M.S, Awen B.Z and Molvi K*, Chem. Pharm. Res* **2010**, *2(5*), 161-168.

[3]Mousaand S.A, Bharali D.J, *Cancers* **2011**, *3*, 2888–2903.

[4] Bildstein L, Dubernet C, Couvreur P, *Advanced Drug Delivery Reviews* **2011**, *63*, 3–23.

[5] Davis M. E, Chen Z and Shin D. M, *Nature Reviews Drug Discovery* **2008**, *7*, 771–782.

[6] Davidson RN, Croft SL, Scott A, Maini M, Moody AH, Bryceson AD, *Lancet* **1991**, *337*, 1061-1062.

[7] Guaglianone P, Chan K, DelaFlor-Weiss E, Hanisch R, Jeffers D, Sharma D, et al. *Invest New Drugs* **1994**, *12*, 103-10.

[8] Gabizon A, Peretz T, Sulkes A, Amselem S, Ben-Yosef R, BenBaruch N, et al. *Eur J Cancer Clin Oncol* **1989**, *25*, 1795-803.

[9] Krishnadas A, Rubinstein I, Onyuksel H, *Pharm Res* **2003**, 20, 297-302.

[10] Koo O, Rubinstein I, Onyuksel H, *Nanomedicine* **2005**, *1*, 77-84.

[11] Ashok B, Arleth L, Hjelm RP, Rubinstein I, Onyuksel H, *J Pharm Sci* **2004**, *93*, 2476-87.

[12] Danson S, Ferry D, Alakhov V, Margison J, Kerr D, Jowle D, et al., *Br J Cancer* **2004**, *90*, 2085-91.

[13] Kim TY, Kim DW, Chung JY, Shin SG, Kim SC, Heo DS, et al., *Clin Cancer Res* **2004**, *10*, 3708-16.

[14] Cavallaro G, Maniscalco L, Licciardi M, Giammona G, *Macromol Biosci* **2004**, *4*, 1028-1038.

[15] LeGarrec D, Gori S, Luo L, Lessard D, Smith DC, Yessine MA, et al., *J Control Release* **2004**, *99*, 83-101.

[16] Lee ES, Na K, Bae YH, *J Control Release* **2005**, *103*, 405 - 18.

[17] Matsumura Y, Hamaguchi T, Ura T, Muro K, Yamada Y, Shimada Y,et al., *Br J Cancer* **2004**, *91*, 1775 – 1781.

[18] Kakizawa Y, Harada A, Kataoka K, *Biomacromolecules* **2001***, 2*, 491 – 497.

[19] Kim SC, Kim DW, Shim YH, Bang JS, Oh HS, Wan Kim S, et al., *J Control Release* **2001**, *72*, 191 – 202.

[20] Shuai X, Ai H, Nasongkla N, Kim S, Gao J, *J Control Release* **2004**, *98*, 415 - 426.

[21] Yoo HS, Park TG, *J Control Release* **2004**, *96*, 273 – 283.

[22] Brime B, Frutos P, Bringas P, Nieto A, Ballesteros MP, Frutos G.J, *Antimicrob Chemother* **2003**, *52*, 103 - 109.

[23] He L, Wang GL, Zhang Q, *Int J Pharm* **2003**, *250*, 45 – 50.

---

[24] Seki J, Sonoke S, Saheki A, Fukui H, Sasaki H, Mayumi T, *Int J Pharm* **2004**, *273*, 75 - 83.

[25] Santos-Magalhaes NS, Pontes A, Pereira VM, Caetano MN, *Int J Pharm* **2000**, *208*, 71 – 80.

[26] Kayser O, Olbrich C, Yardley V, Kiderlen AF, Croft SL, *Int J Pharm* **2003**, *254*, 73 - 75.

[27] Merisko-Liversidge E, Sarpotdar P, Bruno J, Hajj S, Wei L, Peltier N, et al., *Pharm Res* **1996**, *13*, 272 - 278.

[28] Shenoy DB, Amiji MM, *Int J Pharm* **2005**, *293*, 261 - 270.

[29] Molpeceres J, Chacon M, Guzman M, Berges L, del Rosario Aberturas M, *Int J Pharm* **1999**, *187*, 101 - 113.

[30] Radwan MA, Zaghloul IY, Aly ZH, *Eur J Pharm Sci* **1999**, *8*, 95 - 98.

[31] Zara GP, Cavalli R, Bargoni A, Fundaro A, Vighetto D, Gasco MR, *J Drug Target* **2002**, *10*, 327 - 335.

[32] Yang SC, Lu LF, Cai Y, Zhu JB, Liang BW, Yang CZ, *J Control Release* **1999**, *59*, 299 - 307.

[33] Ibrahim NK, Desai N, Legha S, Soon-Shiong P, Theriault RL, Rivera E et al., *Clin Cancer Res* **2002**, *8*, 1038- 1044.

[34] Rhaese S, vonBriesen H, Rubsamen-Waigmann H, Kreuter J, Langer K, *J Control Release* **2003**, *92*, 199 - 208.

[35] Wartlick H, Spankuch-Schmitt B, Strebhardt K, Kreuter J, Langer K. J, *Control Release* **2004**, *96*, 483 - 495.

[36] Vinogradov SV, Batrakova EV, Kabanov AV, *Bioconjug Chem* **2004**, *15*, 50 - 60.

[37] Chauhan AS, Jain NK, Diwan PV, Khopade AJ, *J Drug Target* **2004**, *12*, 575 - 83.

[38] Tripathi PK, Khopade AJ, Nagaich S, Shrivastava S, Jain S, Jain NK, *Pharmazie* **2002**, *57*, 261 - 264.

[39] Hussain M, Shchepinov M, Sohail M, Benter IF, Hollins AJ et al., *J Control Release* **2004**, *99*, 139 - 155.

[40] Au JL, Jang SH, Zheng J, Chen CT, Song S, Hu L, et al., *J Control Release* **2001**, *74*, 31 - 46.

[41] Hoarau D, Delmas P, David S, Roux E, Leroux JC, *Pharm Res* **2004**, *21*, 1783 - 1789.

[42] TenTije AJ, Verweij J, Loos WJ, *Sparreboom Clin Pharmacokinet* **2003**, *42*, 665 - 685.

[43] Arnedo A, Irache JM, Merodio M, Espuelas M, Millan S, *J Control Release* **2004**, *94*, 217 - 227.

[44] Sethi V, Onyuksel H, Rubinstein I, *AAPS PharmSci* **2003**, *5*, M1045.

[45] Koo OM, Rubinstein I, Onyuksel H, *Nanomedicine: Nanotechnology, Biology, and Medicine* **2005**, *1*, 193–212

[46] Maeda H, *Adv. Enzyme Regul*. **2001**, *41*, 189–207.

[47] Maeda H, *J. Control. Release* **2012**, *164*, 138–144.

---

[48] Byrne JD, Betancourt T, Brannon-Peppas L, *Adv. Drug Deliv. Rev* **2008**, *60*, 1615–1626.

[49] Gmeiner W.H, Ghosh S, *Nanotechnol Rev* **2014**, *3*, 111–122.

[50] Weis SM, Cheresh DA, *Nat. Med* **2011**, *17*, 1359–1370.

[51] Rubin P, Casarett G, *Clinical Radiology* **1966**, *17*, 220–229.

[52] Shubik P, *Journal of Cancer Research and Clinical Oncology* **1982**, *103*, 211–226.

[53] Firth JA*, J Anat* **2002**, *200*, 541-548.

[54] Yu MK, Park J, Jon S, *Theranostics* **2012**, *2*, 3–44.

[55] Missailidis S, Thomaidou D, Borbas KE, Price MR. *J Immunol Methods* **2005**, *296*, 45-62.

[56] Dharap SS, Qiu B, Williams GC, Sinko P, Stein S, Minko T, *J Control Release* **2003**, *91*, 61-73.

[57] Ni S, Stephenson SM, Lee RJ, *Anticancer Res* **2002**, *22*, 2131-2135.

[58] Willis M, Forssen E, *Adv Drug Deliv Rev* **1998**, *29*, 249-271.

[59] Kularatne SA, Low PS, *Methods Mol. Biol.* **2010**, *624*, 249–265.

[60] Esmaeili F, Ghahremani MH, Ostad SN, Atyabi F, Seyedabadi M, Malekshahi MR, Amini M, Dinarvand RJ *Drug Target.* **2008**, *16*, 415–423.

[61] Huang RK, Steinmetz NF, Fu CY, Manchester M, Johnson JE. *Nanomedicine (Lond.)* **2011**, *6*, 55–68.

[62] Ishida O, Maruyama K. *Nihon Rinsho* **1998**, *56*, 657–662.

[63] Ding B, Wu X, Fan W, Wu Z, Gao J, Zhang W, Ma L, Xiang W, Zhu Q, Liu J, Ding X, Gao S, *Int. J. Nanomed.* **2011**, *6*, 1991–2005.

[64] Yang L, Mao H, Wang YA, Cao Z, Peng X, Wang X, Duan H, Ni C, Yuan Q, Adams G, Smith MQ, Wood WC, Gao X, Nie S, *Small* **2009**, 5, 235–243.

[65] El-Sayed IH, Huang X, El-Sayed MA, *Cancer Lett.* **2006**, *239*, 129–135.

[66] Yu C, Hu Y, Duan J, Yuan W, Wang C, Xu H, Yang XD, *PLoS One* **2011**, *6*, e24077.

[67] MacNaught AD, Wilkinson AR, (1997) "Compendium of chemical terminology: IUPAC recommendations" 2nd ed., Oxford, Blackwell Science.

[68] Faraji AH, Wipf P, *Bioorg. Med. Chem.* **2009**, *17*, 2950-2962.

[69] Wang YXJ, Hussain SM, Krestin GP, *Eur. Radiol.* **2001**, *11*, 2319-2331.

[70] Fumagalli G, Marucci C, Christodoulou MS, Stella B, Dosio F, Passarella D, *Drug Discov Today* **2016**, *21*, 1321-1329.

[71] Mura S, Bui DT, Couvreur P, Nicolas J, *J. Control. Release* **2015**, *208*, 25–41.

[72] Delplace V, Couvreur P, Nicolas J, *Polymer Chem.* **2014**, *5*, 1529–1544.

[73] Bildstein L, Dubernet C, Couvreur P, *Adv. Drug Deliv. Rev.* **2011**, *63*, 3–23.

---

[74] DeAssis DN, Mosqueira VC, Vilela JM, Andrade MS, Cardoso VN, *Int J Pharm*. **2008**, 349, 152–160.

[75] Jores K, Mehnert W, Drecusler M, Bunyes H, Johan C, MAder K, *J Control Release* **2004**, *17*, 217–227.

[76] Muhlen AZ, Muhlen EZ, Niehus H, Mehnert W. *Pharm Res.* **1996**, *13*, 1411–1416.

[77] Pangi Z, Beletsi A, Evangelatos K. *Adv Drug Del Rev.* **2003**, *24*, 403–419.

[78] Zambaux M, Bonneaux F, Gref R, Maincent P, Dellacherie E, Alonso M, Labrude P, Vigneron C. *J Control Release* **1998**, 50, 31–40.

[79] Song CX, Labhasetwar V, Murphy H, Qu X, Humphrey WR, Shebuski RJ, Levy RJ. *J Control Release* **1997**, *43*, 197–212.

[80] Couvreur P, Dubernet C, Puisieux F. *Eur J Pharm Biopharm.* **1995**, 41, 2–13.

[81] Allemann E, Gurny R, Doekler E. *Eur J Pharm Biopharm.* **1993**, *39*, 173–191.

[82] Fessi H, Puisieux F, Devissaguet JP, Ammoury N, Benita S, *Int J Pharm.* **1989**, *55*, R1–4.

[83] Dosio F, Reddy LH, Ferrero A, Stella B, Cattel L, Couvreur P, *Bioconjug. Chem.* **2010**, *21*, 1349-1361.

[84] Caron J, Maksimenko A, Wack S, Lepeltier E, Bourgaux C, Morvan E, Leblanc K, Couvreur P, Desmaele D, *Adv. Healthc. Mater.* **2013**, *2*, 172-185.

[85] Desmaele D, Gref R, Couvreur P, *J. Control. Release* **2012**, *161*, 609-618.

[86] Maksimenko A, Mougin J, Mura S, Sliwinski E, Lepeltier E, Bourgaux C, Lepetre S, Zouhiri F, Desmaele D, Couvreur P, *Cancer Lett.* **2013**, *334*, 346-353.

[87] Couvreur P, Stella B, Reddy LH, Hillaireau H, Dubernet C, Desmaele D, Lepetre S, Rocco F, Dereuddre N, Clayette P, Rosilio V, Marsaud V, Renoir JM, Cattel L, *Nano Lett.* **2006**, *6*, 2544-2548.

[88] Reddy LH, Khoury H, Paci A, Deroussent A, Ferreira H, Dubernet C, Decleves X, Besnard M, Chacun H, Lepetre S, Desmaele D, Rousseau B, Laugiern C, Cintrat JC, Vassal G, Couvreur P, *Drug Metab. Dispos.* **2008**, *36*, 1570-1577.

[89] Semiramoth N, Di Meo C, Zouhiri F, Saïd-HassaneF, Valetti S, Gorges R, Nicolas V, Poupaert JH, Chollet-Martin S, Desmaele D, Gref R, Couvreur P *ACS Nano* **2012**, *6*, 3820-3831.

[90] Sarpietro MG, Micieli D, Rocco F, Ceruti M, Castelli F *Int. J. Pharm.* **2009**, *382*, 73-79.

[91]Allain V, Bourgaux C, Couvreur , *Nucleic Acids Res.* **2012***, 40*, 1891-1903.

[92]Raouane M, Desmaele D, Gilbert-Sirieix M, Gueutin C, Zouhiri F, Bourgaux C, Lepeltier E, Gref R,

---

Ben Salah R, Clayman G, Massaadmassade L, Couvreur P *J. Med. Chem*. **2011**, *54*, 4067-4076.

[93] Arias JL, Reddy LH, Othman M, Gillet B, Desmaele D, Zouhiri F, Dosio F, Gref R, Couvreur P *ACS Nano* **2011**, *5,* 1513-1521.

[94] Dosio F, Stella B, Ferrero A, Garino C, Zonari D, Arpicco S, Cattel L, Giordano S, Gobetto R, *Int. J. Pharm.* **2013**, *440,* 221-228.

[95] Borrelli S, Christodoulou MS, Ficarra I, Silvani A, Cappelletti G, Cartelli D, Damia G, Ricci F, Zucchetti M, Dosio F, Passarella D *Eur. J. Med. Chem.* **2014**, *85*, 179-190.

[96] Ruedas-Rama MJ, Walters JD, Orte A, Hall EAH *Anal. Chim. Acta* **2012**, *751*, 1–23.

[97] Borrelli S, Cartelli D, Secundo F, Fumagalli G, Christodoulou MS, Borroni A, Perdicchia D, Dosio F, Milla P, Cappelletti G, Passarella D, *ChemPlusChem* **2015**, *80*, 47–49.

[98] Wani MC, Taylor HL, Wall ME, Coggon P, McPhail AT *J. Am. Chem. Soc.* **1971**, *93*, 2325-2327.

[99] Wang TH, Wang HS, Soong YK *Cancer* **2000**, *88*, 2619-2628.

[100] Gelderblom H, Verweij J, Nooter K, Sparreboom A *Eur. J. Cancer* **2001**, *37*, 1590-1598.

[101] Skwarczynski M, Hayashi Y, Kiso Y *J. Med. Chem.* **2012**, *49*, 7253-7269.

[102] Arpicco S, Dosio F, Stella B, Cattel L *Curr. Top. Med. Chem.* **2011**, *11*, 2346-2381.

[103] Zhang Z, Mei L, Feng SS *Expert Opin. Drug Deliv.* **2013**, *10*, 325-340.

[104] Scripture CD, Figg WD, Sparreboom A *Ther. Clin. Risk Manag.* **2005**, *1*, 107-114.

[105] Paik PK, James LP, Riely GJ, Azzoli CG, Miller VA, Ng KK, Sima CS, Heelan RT, Kris MG, Moore E, Rizvi NA *Cancer Chemother. Pharmacol.* **2011**, *68*, 1331-1337.

[106] Inbrahim NK, Desai N, Legha S, Soon-Shiong P, Theriault RL, Rivera E, Esmaeli B, Ring SE, Bedikian A, Hortobagyi GN, Ellerhrst JA *Clin. Cancer Res*. **2002**, *8*, 1038-1044.

[107] Ceruti M, Balliano G, Viola F, Cattel L, Gerst N, Schuber F *Eur. J. Med. Chem.* **1987**, *22*, 199-208.

[108] Bui DT, Nicolas J, Maksimenko A, Desmale D, Couvreur P *Chem. Commun.* **2014**, *50*, 5336–5338.

[109] Cappelletti G, Maggioni MG, Tedeschi G, Maci R *Exp. Cell Res.* **2003**, *288*, 9–20.

[110] Sotiropoulou PA, Christodoulou MS, Silvani A, Herold-Mende C, Passarella D *Drug Discovery Today* **2014**, *19*, 1547–1562.

[111] Zhou Y, Yang J, Rhim JS, Kopecek J *J. Controlled Release* **2013**, *172*, 946 – 953.

[112] Singh S, Chitkara D, Mehrazin R, Behrman SW, Wake RW, Mahato RI *PLoS One* **2012**, *7*, e40021.

[113] Ruch JM, Kim EJ *Drugs* **2013**, *73*, 613-622.

[114] Fumagalli G, Mazza D, Christodoulou MS, Damia G, Ricci F, Perdicchia D, Stella B, Dosio F, Sotiropoulou PA, Passarella D, *ChemPlusChem* **2015**, *80*, 1380 –1383.

[115] Whelan DR, Holm T, Sauer M, Bell TDM *Aust. J. Chem.* **2014**, *67*, 179 – 183.

---

[116] Tremblay MR, Nevalainen M, Nair SJ, Porter JR, Castro AC, Behnke ML, Yu LC, Hagel M, White K, Faia K, Grenier L, Campbell MJ, Cushing J, Woodward CN, Hoyt J, Foley MA, Read MA, Sydor JR, Tong JK, Palombella VJ, McGovern K, Adams J, *J. Med. Chem*. **2008**, *51*, 6646-6649.

[117] Isaacs AK, Xiang C, Baubet V, Dahmane N, Winkler J, *Org. Lett.* **2011**, *13*, 5140-5143.

[118] Renoux B, Legigan T, Bensalma S, Chadéneau C, Muller JM, Papot S, *Org. Biomol. Chem*. **2011**, *9*, 8459-8464.

[119] Hillaireau H, Couvreur P, *Cell. Mol. Life Sci.* **2009**, *66*, 2873–2896.

[120] Tremblay MR, Nevalainen M, Nair SJ, Porter JR, Castro AC, Behnke ML, Yu LC, Hagel M, White K, Faia K, Grenier L, Campbell MJ, Cushing CN, Woodward CN, Hoyt J, Foley MA, Read MA, Sydor JR, Tong JK, Palombella VJ, McGroven K, Adams, J *J. Med. Chem.* **2008**, *51*, 6646–6649.

[121] Ricci F, Bernasconi S, Perego P, Ganzinelli M, Russo G, Bono F, Mangioni C, Fruscio R, Signorelli M, Broggini M, Damia G, *Cell Cycle* **2012**, *11*, 1966–1976.

[122] Oliva CR, Moellering DR, Gillespie GY, Griguer CE, *PLoS One* **2011**, *6*, e24665.

[123] Heilemann M, Van De Linde S, Mukherjee A, Sauer M, *Angew. Chem. Int. Ed.* **2009**, *48*, 6903–6908.

[124] Klein T, Lçschberger A, Proppert S, Wolter S, Van De Linde S, Sauer M, *Nat. Methods* **2011**, *8*, 7–9.

[125] Fumagalli G, Stella B, Pastushenko I, Ricci F, Christodoulou MS, Damia G, Mazza D, Arpicco S, Giannini C, Morosio L, Dosio F, Sotiropoulou PA, Passarella D, *ACS Med. Chem. Lett.*, **2017**, *8*, 953–957.

[126] Maksimenko A, Dosio F, Mougin J, Ferrero A, Wack S, Reddy LH, Weyn AA, Lepeltier E, Bourgaux C, Stella B, Cattel L, Couvreur P, *Proc Natl Acad Sci U S A.* **2014**, *111*, E217- E226.

[127] Herman EH, El-Hage AN, Ferrans VJ, Ardalan B, *Toxicol Appl Pharmacol* **1985**, *78*, 202–214.

[128] Jain A, Agarwal A, Majumder S, Lariya N, Khaya A, Agrawal H, Majumdar S, Agrawal GP, *J Control Release* **2010**, *148*, 359–367.

[129] Liu D, Hu H, Zhang J, Zhao X, Tang X, Chen D, *Chem Pharm Bull* **2011**, *59*, 63–71.

[130] Gabizon A, Catane R, Uziely B, Kaufman B, Safra T, Cohen R, Martin F, Huang A, Barenholz Y, *Cancer Res* **1994**, *54*, 987–992.

[131] Gao ZG, Lee DH, Kim DI, Bae YH, *J Drug Target* **2005**, *13*, 391–397.

[132] Licciardi M, Cavallaro G, Di Stefano M, Fiorica C, Giammona G, *Macromol Biosci* **2011,** *11*, 445–454.

[133] Michimukai E, Kitamura N, Zhang Y, Wang H, Hiraishi Y, Sumi K, Hayashido Y, Toratani S,

---

Okamoto T, *In Vitro Cell Dev Biol Anim.* **2001**, *37*, 459-464.

[134] Christodoulou MS, Fokialakis N, Passarella D, García-Argáez AD, Gia OM, Pongratz I, Dalla Via L, Haroutounian SA, *Bioorg. Med. Chem.* **2013**, *21*, 4120– 4131.

[135] Christodoulou MS, Zarate M, Ricci F, Damia G, Pieraccini S, Dapiaggi F, Sironi M, Lo Presti L, García-Argáez AN, Dalla Via L, Passarella D, *Eur. J. Med. Chem.* **2016**, *118*, 79–89.

[136] Fumagalli G, Christodoulou MS, Riva B, Revuelta I, Marucci C, Collico V, Prosperi D, Riva S, Perdicchia D, Bassanini I, García-Argáez AN, Dalla Via L, Passarella D, *Org. Biomol. Chem.*, **2017**, *15*, 1106–1109.

[137] Fahim FA, Abd-Allah NM, Aboul-Ela F, Esmat AY, *J Tumor Marker Oncol.* **1993**, *8*, 27–33.

[138] Esmat AY, El-Gerzawy SM, Raafat A, *Cancer Biol Ther* **2005**, *4*, 108–112.

[139] Metenawy WH, Esmat AY, *Cancer Mol Biol* **1996**, *3*, 851–864.

[140] Esmat AY, Tomasetto C, Rio MC, *Cancer Biol Ther* **2006**, *5*, 97–103.

[141] Esmat AY, Said MM, Hamdy GM, Soliman AA, Khalil SA, *Drug Dev Res* **2012**, *73*, 154–165.

[142] Yousefzadi M, Sharifi M, Behmanesh M, Moyano E, Bonfill M, Cusido RM, Palazon J, *Eng. Life Sci.* **2010**, *10*, 281-292.

[143] Anand S, Penrhyn-Lowe S, Venkitaraman AR, *Cancer Cell* **2003**, *3*, 51-62.

[144] Ma Y, Fang S, Li H, Han C, Lu Y, Zhao Y, Liu Y, Zhao C, *Chem Biol Drug Des* **2013**, *82*, 12–21.

[145] Ettinger DS, Finkelstein DM, Ritch PS, Lincoln ST, Blum RH, *Lung Cancer* **2002**, *37*, 311-318.

[146] Bassanini I, Hult K, Riva S, *Beilstein J. Org. Chem.* **2015**, *11*, 1583–1595.

[147] Grossa J, Sayleb S, Karowb AR, Bakowskya U, Garidelb P, *Eur. J. Pharm. Biopharm.* **2016**, *104*, 30–41.

[148] Park MY, Kwon HJ, Sung MK, *Nutr. Res. Pract.* **2009**, *3*, 9–14.

[149] Blencowe CA, Russel AT, Greco F, Hayes W, Thorthwaite DW, *Polym. Chem.* **2011**, *2*, 773-790.

[150] Boye´O, Brossi A, "Tropolonic colchicum alkaloids and allo congeners. In The Alkaloids" (1992) Brossi A Ed., New York, Academic Press, Vol. 41, 125-176.

[151] Levy M, Spino M, Read SE, *Pharmacotherapy* **1991**, *11*, 196-211

[152] Yeh HJC, Chrzanowska M, Brossi A, *FEBS Lett.* **1988**, *229*, 82-86.

[153] Andreu JM, Timasheff SN, *Biochemistry* **1982**, *21*, 534-543.

[154] Andreu JM, Timasheff SN, *Biochim. Biophys. Acta* **1982**, *714*, 373-377.

[155] Prelog V, Helmchen G, *Angew. Chem. Int. Ed. Engl.* **1982**, *21*, 567-589.

[156] Maity SN, Ray K, Banerjee A, Mukhopadhyay K, Roychowdhury S, Chaudhuri GG, Biswas BB, Bhattacharyya B, *Indian J. Biochem. Biophys.* **1988**, *25*, 585-589.

---

[157] Downing KH, Nogales E, *Curr Opin Struct Biol* **1998**, *8*, 785–791.

[158] Ravelli RBG, Gigant B, Curmi PA, Jourdain I, Lachkar S, Sobel A, Knossow M, *Nature* **2004**, *428*, 198–202.

[159] Passarella D, Giardini A, Peretto B, Fontana G, Sacchetti A, Silvani A, Ronchi C, Cappelletti G, Cartelli D, Borlak J, Danieli B, *Bioorg Med Chem* **2008**, *16*, 6269–6285.

[160] Niel E, Scherrmann JM, *Joint Bone Spine* **2006**, *73*, 672–678.

[161] Bai R, Covell DG, Pei XF, Ewell JB, Nguyen NY, Brossi A, Hamel E, *J Biol Chem* **2000**, *275*, 40443–40452.

[162] Nakagawa-Goto K, Chen CX, Hamel E, Wu C, Bastow KF, Brossi A, Lee K. *Bioorg Med Chem Lett* **2005**, *15*, 235–238.

[163] Danieli B, Giardini A, Lesma G, Passarella D, Silvani A, Appendino G, Noncovich A, Fontana G, Bombardelli E, *Chem Biodivers* **2004**, *1*, 327–345.

[164] Cappelletti G, Cartelli D, Peretto B, Ventura M, Riccioli M, Colombo F, Snaith JS, Borrelli S, Passarella D, *Tetrahedron* **2011**, *67*, 7354–7357.

[165] Raspaglio G, Ferlini C, Mozzetti S, Prislei S, Gallo D, Das N, Scambia G, *Biochem Pharmacol* **2005**, *69*, 113–121.

[166] Schonharting M, Mende G, Siebert G, *Hoppe Seylers Z Physiol Chem* **1974**, *355*, 1391–1399.

[167] Singh B, Kumar A, Joshi P, Guru S, Kumar S, Wani ZA, Mahajan G, Hussain A, Qazi AK, Kumar A, Bharate SS, Gupta BD, Sharma PD, Hamid A, Saxena AK, Mondhe DM, Bhushan S, Bharate SB, Vishwakarma RA, *Org Biomol Chem* **2015**, *13*, 5674–5689.

[168] Ambudkar SV, Dey S, Hrycyna CA, Ramachandra M, Pastan I, Gottesman MM, *Annu Rev Pharmacol Toxicol* **1999**, *39*, 361–398.

[169] Druley TE, Stein WD, Ruth A, Roninson IB, *Biochemistry* **2001**, *40*, 4323–4331.

[170] Tateishi T, Soucek P, Caraco Y, Guengerich F, Wood A, *Biochem Pharmacol* **1997**, *53*, 111–116.

[171] Silva R, Carmo H, Vilas-Boas V, Barbosa DJ, Palmeira A, Sousa E, Carvalho F, Bastos Mde L, Remião F, *Chem Biol Interact* **2014**, *218*, 50–62.

[172] Cosentino L, Redondo-Horcajo M, Zhao Y, Santos AR, Chowdury KF, Vinader V, Abdallah QMA, Abdel-Rahman H, Fournier-Dit-Chabert J, Shnyder SD, Loadman PM, Fang W, Díaz JF, Barasoain I, Burns PA, Pors K, *J Med Chem* **2012**, *55*, 11062–11066.

[173] Kang GJ, Getahun Z, Muzaffar A, Brossi A, Hamel E, *J. Biol. Chem.* **1990**, *265*, 10255-10259.

[174] Muzaffar A, Brossi A, Lin CM, Hamel E, *J. Med. Chem.* **1990**, *33*, 567-751.

---

[175] Gelmi ML, Mottadelli S, Pocar D, Riva A, Bombardelli E, De Vincenzo R, Scambia G, *J. Med. Chem,* **1999**, 42, 5272-5276.

[176] Velluz L, Muller G, *Bull. Soc. Chim. Fr.* **1954**, 1072.

[177] Cheetham AG, Ou YC, Zhang P, Cui H, *Chem. Commun.* **2014**, *50*, 6039—6042.

[178] Ikuta Y, Koseki Y, Onodera T, Oikawa H, Kasai H, *Chem. Commun*. **2015**, *51,* 12835—12838.

[179] Danieli B, Giardini A, Lesma G, Passarella D, Peretto B, Sacchetti A, Silvani A, Pratesi G, Zunino F, *J. Org. Chem.***2006**, *71*, 2848-2853.

[180] Hofle G, Bedorf N, Seinmetz H, Schomburg D, Gerth K, Reichenbach H, *Angew. Chem. Int. Ed. Engl.* **1996**, *35*, 1567-1569.

[181] Altmann KH, Gertsch J, *Nat. Prod. Rep*. **2007**, *24*, 327-357.

[182] Cowden CJ, Paterson I, *Nature* **1997**, *387*, 238–239.

[183] Bollag DM, McQueney PA, Zhu J, Hensens O, Koupal L, Liesch J, Goetz M, Lazarides E, Woods CM, *Cancer Res* **1995**, *55,* 2325–2333.

[184] Wall ME, Wani MC, Cook CE, Palmer KH, MacPhail AT, Sim GA, *J. Am. Chem. Soc.* **1966**, *88*, 3888-3890.

[185] Creemers GJ, Lund B, Verweij J, *Cancer Treatment Rev.* **1994,** *20*, 73-96.

[186] Wadkins RM, Bearss D, Manikumar G, Wani MC, Wall ME, von Hoff DD, *Cancer Res*. **2004**, *64*, 6679-6683.

[187] Vladu B, Woynarowski JM, Manikumar G, Wani MC, Wall ME, von Hoff DD, Wadkins RM *Mol. Pharmacol.* **2000**, *57*, 243-251.

[188] Watanabe M, Kawano K, Yokoyama M, Opanasopit P, Okano T, Maitani Y, *Int. J. Pharm.* **2006**, *308*, 183–189.

[189] Emerson DL, *Pharm. Sci. Technol. Today* **2000**, *3*, 205–209.

[190] Min KH, Park K, Kim YS, Bae SM, Lee S, Jo HG, Park RW, Kim IS, Jeong SY, Kim K, Kwon IC, *J. Controlled Release* **2008**, *127*, 208–218.

[191] Chenite A, Chaput C, Wang D, Combes C, Buschmann M, Hoemann CD, Leroux JC, Atkinson BL, Binette F, Selmani A, *Biomaterials* **2000**, *21*, 2155–2161.